

**GEOLOGICAL AND STRUCTURAL  
INTERPRETATION OF THE BEPOSO AREA  
IN THE ASHANTI REGION OF GHANA,  
USING AEROMAGNETIC AND  
RADIOMETRIC DATA-SETS**

By

**Mariam Maku Quarshie**

**BSc Physics**

A Thesis submitted to the Department of Physics,  
Kwame Nkrumah University of Science and Technology, in  
partial fulfilment of the requirements for the degree of

**MASTER OF PHILOSOPHY(GEOPHYSICS)**

**College of Science**

**Supervisor: Prof. A. Menyeh**

**April 2015**



# KNUST

## Abstract

Aeromagnetic and radiometric data-sets, acquired over the Beposo area in the Ashanti region of Ghana, were used to come out with an integrated geological and structural map, that will help in delineating possible gold mineralisation zones. Important new information on the extent of the lithology and structure which led to a more comprehensive understanding of areas of poor outcrop or under cover were obtained through the use of magnetic enhancement transforms such as analytical signal, first vertical derivative, horizontal derivative and tilt derivative on the magnetic dataset. The first vertical derivative and tilt derivative together with the horizontal derivative map helped in tracing out geological structures such as the Ashanti shear and faults which probably served as conduits for hydrothermal fluids and their resulting gold concentration. A rose diagram of the strike of geological structures in the area indicated that most of these structures are striking between  $0^{\circ}$  and  $90^{\circ}$  in the NE-SW direction and dipping to the NE. Granitoid intrusions which probably caused isoclinal folds in the Birimian were clearly defined by the aeromagnetic and radiometric data-sets. The radiometric dataset provided geochemical (K, eTh, eU) information that helped in interpreting surface lithology and possible hydrothermal alteration zones. Potential zones representing structurally weak regions and serving as pathways for probable Au-mineralising hydrothermal fluids were mapped out using information from both data-sets. Results indicated that mineralisation in the area is controlled by lithology and structure, similar to what others discovered in surrounding

areas. It is envisaged that the geological structural information obtained from this study can assist the mining and mineral exploration companies in Ghana in their target generation.

# KNUST



# Contents

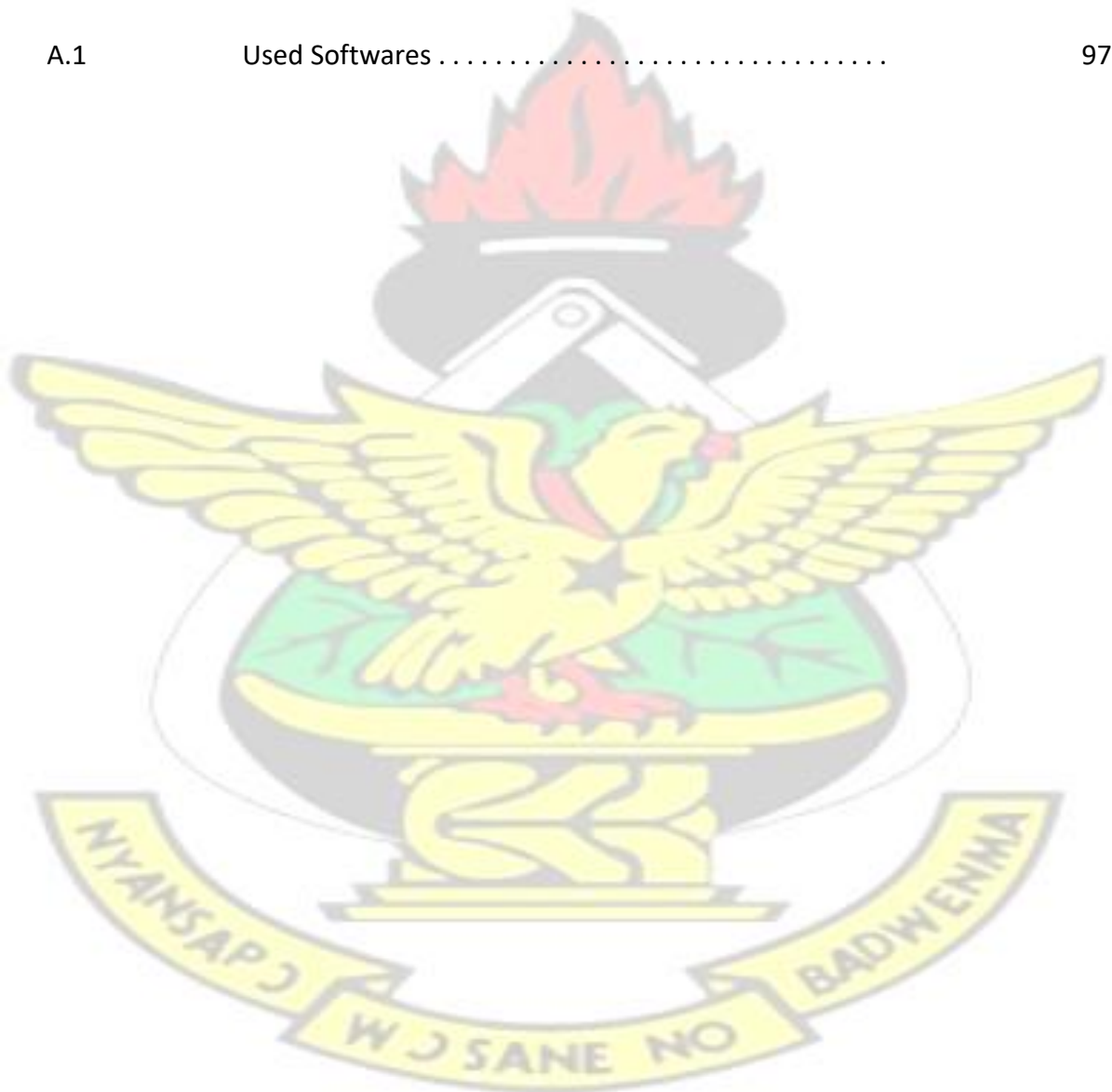
Declaration	i
Abstract	ii
List of Tables	viii
List of Figures	xi
List of Symbols and Acronyms	xii
Acknowledgement	xiii
1	1
1.1 INTRODUCTION	1
1.1.1 RESEARCH HYPOTHESIS	3
1.1.2 SIGNIFICANCE OF STUDY	3
1.1.3 PROBLEM STATEMENT	4
1.1.4 OBJECTIVES OF RESEARCH	4
1.1.5 JUSTIFICATION OF OBJECTIVES	5
1.1.6 FRAMEWORK OF THESIS	6
2	7
2.1 LITERATURE REVIEW	7
3	10
3.1 REGIONAL GEOLOGY	10
3.1.1 EBURNEAN OROGENY	11
3.1.2 GEOLOGY OF THE BEPOSO AREA	12
3.1.3 BIRIMIAN SERIES	14
3.1.4 TARKWAIAN SERIES	14
3.1.5 GRANITIDS	15
3.1.6 MINERALISATION	15
3.1.7 BIRIMIAN DEPOSITS	16
3.1.8 TARKWAIAN DEPOSITS	16

4		17
4.1	THEORY .....	17
4.1.1	The Magnetic Field of the Earth .....	17
4.1.2	The International Geomagnetic Reference Field (IGRF) .....	24
4.1.3	Magnetic Susceptibility .....	24
4.1.4	Magnetism of Rocks and Minerals .....	26
4.1.5	Remanent Magnetisation in Rocks .....	27
4.1.6	The Underlying Principle of the Magnetic Method .....	29
4.1.7	Application of Magnetic Enhancement Transforms .....	29
4.1.7.1	Reduction to the Magnetic Equator (RTE) .....	29
4.1.7.2	Analytic Signal Amplitude (AS) .....	30
4.1.7.3	First Derivative (FD) .....	30
4.1.7.4	Horizontal Derivatives (HDR) .....	30
4.1.7.5	Tilt Derivative (TD) .....	31
4.1.8	Airborne Radiometric (Gamma Ray Spectrometry) for Natural Radioelement Mapping .....	31
4.1.8.1	Basic Radioactivity .....	32
5		33
5.1	MATERIALS AND METHODS .....	33
5.1.1	Study area .....	33
5.1.1.1	Location .....	33
5.1.1.2	Climate .....	35
5.1.1.3	Physiography .....	35
5.1.1.4	Vegetation .....	35
5.1.1.5	Economic Activities .....	36
5.1.2	MATERIALS .....	36
5.1.2.1	Available Geophysical Data-Sets .....	36
5.1.2.2	Metadata .....	37
5.1.3	METHODOLOGY .....	37

5.1.3.1	Data Processing .....	37	
5.1.3.2	Pre-Processing .....	38	
5.1.3.3	Aeromagnetic Data.....	39	
5.1.3.4	Aeroradiometric Data .....	40	
5.1.3.5	Other Data-set .....	41	
6			42
6.1	RESULTS AND DISCUSSION .....	42	
6.1.1	Digital Elevation map .....	42	
6.1.2	Qualitative interpretation of Airborne Magnetic Data .....	44	
6.1.2.1	Residual Total Magnetic Intensity (RTMI) .....	44	
6.1.3	MAGNETIC ENHANCEMENT TRANSFORMS .....	46	
6.1.3.1	Reduction to Magnetic Equator (RTE) .....	46	
6.1.3.2	Analytical Signal (AS) .....	49	
6.1.3.3	First Vertical Derivative (1VD) .....	52	
6.1.3.4	Horizontal Derivative (HD) .....	55	
6.1.3.5	Tilt Derivative (TD) .....	57	
6.1.4	GEOLOGICAL STRUCTURES .....	59	
6.1.4.1	Deformation and Geological Structures .....	62	
6.1.5	LITHOLOGY FROM THE MAGNETIC DATA .....	64	
6.2	Airborne Radiometric Data Interpretation .....	67	
6.2.1	Potassium map .....	67	
6.2.2	Thorium map .....	70	
6.2.3	Uranium map .....	72	
6.3	RATIO MAPS .....	75	
6.3.1	eTh/K Ratio Map .....	77	
6.3.2	eU/ eTh Ratio Map .....	79	
6.4	LITHOLOGY FROM RADIOMETRICS .....	81	
6.4.1	Ternary map .....	81	
6.5	Hydrothermal Alteration and Potential Metal Ore Mineralisation Zones ..	84	

7		89
7.1	CONCLUSION AND RECOMMENDATION .....	89
7.1.1	Conclusion .....	89
7.1.2	Recommendation .....	89
Bibliography		90
A		97
A.1	Used Softwares .....	97

# KNUST



# List of Tables

5.1	Equipment Specification for data acquisition (Geological Survey of Ghana, 1998)	37
5.2	Survey specification for data acquisition (Geological Survey of Ghana, 1998)	37



# List of Figures

3.1	Geological outline map of West Africa showing basement outcrops and basins (Study area in black) (after (Boher et al., 1992)) .....	10
3.2	Geology of study area (modified after (Taylor et al., 1992)) .....	13
4.1	(A) The geomagnetic field (B) The Earth's field Inclination at different latitudes (Reeves, 2005) .....	18
4.2	Malformation of the geomagnetic field as a result of solar wind, causing bends in the ionosphere on the orbiting planets day side (Reeves, 2005) ..	19
4.3	Example of a magnetic storm noticed at a time when there is high solar activity. The storm is sudden at the initial stage and violent changes in F may be observed over several tens of hours (Reeves, 2005) .....	20
4.4	Elements of the geomagnetic field (Reeves, 2005) .....	23
5.1	The Beposo study area .....	34
5.2	Research methodology flow chart .....	38
6.1	Digital elevation model showing high and low lands in the Beposo area ..	43
6.2	Residual Total Magnetic Intensity (RTMI) of study area showing Birimian meta-volcanics (C1-C3), Birimian meta-sediments (A1, A3, B1 and B3), some Tarkwaian sediments (A2 and A4) and identified dykes (d1, d2 and d3) .....	45
6.3	Reduction to the Magnetic Equator transform map of the RTMI (inclination = -12.790 and declination = -4.620) of study area .....	48
6.4	Analytical signal transform map of study area showing main lithologies (G, B and T) with the boundary of one circled in black not clearly shown ....	51

6.5	First Vertical derivative map (calculated on RTP) of study area, showing deep (the Birimian and granitoids) and shallow seated (Tarkwaian) features and also areas of magnetic reversal . . . . .	53
6.6	Interpreted geological structures overlain on FVD of the study area in grey scale to enhance geological structures in the study area . . . . .	54
6.7	Horizontal derivative map (calculated using the RTE) of study area showing maximum ridge (magenta colour) over edges of magnetic basement blocks and linear features related to contacts in the data sets . . . . .	56
6.8	Tilt derivative map of the Beposo study area with improved fabric (e.g area circled in black compared with same area on Analytical Signal) . . . . .	58
6.9	Interpreted geological structures of study area from aeromagnetic data . . .	60
6.10	Rose diagram of geological structures in study area showing major strike direction and strike angles . . . . .	61
6.11	Interpreted geological structural map from aeromagnetic overlain with hydrothermal alteration zones . . . . .	66
6.12	Potassium map of study area overlain with identified lithology . . . . .	69
6.13	Thorium map of study area overlain with identified lithology . . . . .	71
6.14	Uranium map of study area overlain with identified lithology . . . . .	74
6.15	eU/K ratio map of study area overlain with identified lithology . . . . .	76
6.16	eTh/ K ratio map of study area overlain with identified lithology . . . . .	78
6.17	eU/eTh Ratio map of study area overlain with identified lithology . . . . .	80
6.18	Ternary image map of study area overlain with identified lithologies . . . .	82
6.19	Interpreted lithology from radiometric data of the study area . . . . .	83

6.20 RTE of the study area overlain with hydrothermal alteration zones . . . . .	86
6.21 Ternary map of study area overlain with identified lithology and hydrothermal alteration zones . . . . .	87
6.22 Proposed geological structural map of study area showing potential metal ore (gold) mineralisation zones . . . . .	88



# List of Symbols and Acronyms

AS	Analytical Signal
D	Declination
eTh	Equivalent Thorium
eU	Equivalent Uranium
F	Magnitude of total magnetic field
HD	Horizontal Derivative
I	Inclination
IGRF	International Geomagnetic Reference Field
J	Magnitude of magnetisation
K	Potassium
K	Magnetic Susceptibility
Z	Vertical component of the total magnetic field
$\phi$	Magnetic Latitude
RTE	Reduction to the magnetic equator
RTP	Reduction to the magnetic pole
RTMI	Residual Total Magnetic Intensity
TD	Tilt Derivative
VD	Vertical Derivative

# Acknowledgement

My first appreciation goes to the most high God who by his mighty power at work within us, is able to do far more than we would ever dare to ask or even dream of. Secondly, I gratefully acknowledge my supervisors, Prof. Aboagye Menyeh and Mr D.D. Wemegah for their support, friendship, motivation, interest in the project and the fatherly love they showed me. Special thanks go to Mr. Benjamin Boadi, a formal postgraduate student of KNUST, for the Oasis Montaj (Geosoft) and MapInfo training he gave me and also for his help and availability. This research work would not have been possible without the support of Ghana Geological Survey Department which made aero-magnetic and radiometric data-sets available for use for this research work. I would also like to thank Mr. Ernest Asare and all MPhil geophysics students (2013/2015 year group) at the Physics Department of K.N.U.S.T for their friendliness and diverse assistance. I am also grateful to all my family and friends for their encouragement and support. Finally, I thank all those who directly or indirectly contributed to the success of this project.



# CHAPTER 1

## 1.1 INTRODUCTION

With the depletion of mineral deposits near the surface, today it has become very important worldwide to search for mineral resources that are deep down within the Earth's crust to meet the growing demand of mankind. Although there may be many ways of obtaining minerals and metals from other countries, nations are now trying to secure and build up their resource base in order to face any unforeseen eventuality and for strategic reasons. For self-reliance in as much mineral commodities as possible, many developing countries like Ghana are now focusing on how to locate and develop deep seated metalliferous deposits.

Gold deposit is by far the most important exploration target in the Birimian unit of Africa. In Ghana, the prolific Ashanti belt located within this Birimian unit, has been exceedingly well endowed and contains world class potential gold reserves. Structural and hydrothermal alterations, which are critically important in controlling gold mineralisation throughout the Birimian units can usually, be observed directly in the magnetic and radiometric patterns (Armstrong and Rodeghiero, 2006).

Data from aero-magnetic surveys play key role in geophysics through the revealing of information from the subsurface. Magnetic data maps show changes in the geomagnetic field through magnetic mineral distribution in the Earth's crust. Interpreting the changes in the magnetic intensity of the crust due to the changes in the abundance of magnetic minerals in crustal rocks, has significantly helped in geophysical interpretation and

prospecting of minerals, especially in limited outcrop areas (Ghazala, 1993; Allek and Hamoudi, 2008).

The concentration of the common radioactive elements (eTh, eU and K), of the upper 30 cm of the Earth's crust is measured by the radiometric method (Telford et al., 1990) and interpreting the surface by using the distribution of these radioelement, relies on the fact that rocks are made of minerals containing specific amount of radio-elements. Also, the ability of surface materials to maintain valuable and detectable compositional difference between lithological units gives the efficiency of the gamma ray spectrometric method (Dickson and Scott, 1997; Wilford, 2002). Various publications have proved the usefulness of gamma ray data in mapping surface geology (Dickson and Scott, 1997; Gunn and Dentith, 1997; Johnson et al., 1979; Graham et al., 2013), looking out for altered areas related to mineralization (Jayawardhana and Sheard, 2000; Shives et al., 2000) and interpreting regolith activities and materials, particularly in highly weathered areas. Though factors like noticeable contrast in radio-elements between lithology units, vegetation cover, soil moisture and weathering affect gamma ray data for geological mapping, it has shown superiority over other geophysical data-sets in interpreting surface lithology in weathered and vegetated areas (Perrotta et al., 2008).

Also recent improvement in the analysis of geophysical data and enhancement transforms, have increased geophysical data-set resolution, so that very insidious changes in responses can be seen (Armstrong and Rodeghiero, 2006).

### 1.1.1 RESEARCH HYPOTHESIS

The following observations were tested in the study area:

- identification of potential mineralisation regions can be realised from the association between lithology, structure and metamorphism
- Geophysical data-sets (Airborne Magnetic and Radiometric) are useful for geophysical interpretation with varying ability in making distinction between geologic bodies with the help of geophysical enhancement transforms.
- lithology and structure control possible gold mineralisation in the study area

### 1.1.2 SIGNIFICANCE OF STUDY

One of the many areas in Africa where companies are exploring actively for gold, is the Ashanti Greenstone Belt of Ghana. As a result, many geophysical data-sets, over the years, have been collected, but has not always been subjected to synergistic interpretation (Perrouty et al., 2012). Integration and analysis of information from aeromagnetic, radiometric, and gravity surveys has become an advanced technique to ameliorate the geoscientific knowledge of densely forested areas (Bahiru et al., 2011). This is because when data-sets are analysed separately and finally integrated, useful information on lithology, structure and alteration can be derived. From the extracted information an integrated geological and structural map, where the individual data layers, are brought together, to resolve uncertainties can be developed. Geological inferences from this map can then be developed to serve as the basis for a more complete understanding of the geology of the Beposo area and its mineral potential.

### 1.1.3 PROBLEM STATEMENT

Due to several surficial factors and complex tectonic history in areas like the Beposo area, it is difficult to fully confirm the relating relationship between lithology, structure and metal ore mineralisation. This is because geophysical data-sets collected in the area over the years are not always subjected to a synergistic interpretation (Perrouty et al., 2012). As a consequence, a synergistic approach of interpretation was carried out believing that in-depth processes could partly and /or fully show on the surface, so that the interrelationship could be established.

The main objective of this research therefore is to perform a qualitative investigation by processing and interpreting geophysical (radiometric and aeromagnetic) data-sets acquired over the area. An integrated geological and structural map showing the main metal ore hosting structures (faults, folds, fracture systems etc.) in the Birimian unit and possible gold mineralisation zones will be developed. Geological and structural map because, they give reliable information of immense economic value. They also provide information about the thickness, distribution of rock units and relationship among structures and strata which gives insight into many aspects such as the mineral potential of an area.

### 1.1.4 OBJECTIVES OF RESEARCH

The primary objective is to obtain an integrated geological and structural map that will help in delineating possible gold mineralisation zones. A number of specific objectives to be addressed, include:

- To map the lithology of the study area
- To map the geological structures of the study area
- To map alteration regions associated with geological structures which may host possible mineralisation zones

### 1.1.5 JUSTIFICATION OF OBJECTIVES

Studies in surrounding areas (Obuasi and Konongo) within the Ashanti belt in South Western Ghana reveals that tectonic corridors which display complex structural features, notable as permeable zones for hydrothermal fluids, control gold mineralization (Milési et al., 1992). These structural and hydrothermal alterations, which control gold mineralisation, can usually be observed directly from the magnetic and radiometric patterns and also modern improvement in analysis of geophysical data-sets and enhancement transforms have improved the resolution of the geophysical datasets, have improved the resolution of geophysical data-sets so that very insidious changes in the geophysical reactions can be seen and mapped (Armstrong and Rodeghiero, 2006).

If surrounding areas within the belt are exhibiting similar signatures then it is possible that the area under study can exhibit similar signatures and a geological and structural map from integrating the two remotely sensed data (magnetic and radiometric) will provide a unique opportunity to answer exploration's ultimate goal to answer the following four questions:

- Where to mine? - That is the location and depth

- What to expect?- That is the amount of space occupied by the ore deposit
- How certain? - Chance of success (risk)
- How profitable?- Economics

#### 1.1.6 FRAMEWORK OF THESIS

The thesis work is presented in seven main chapters with each addressing main areas. Chapter one introduces the field of research and geophysical tools that were employed in the research. It also deals with the objectives, significance, justification and the problem the research seeks to address. Chapter two provides a general review of some available literature information. Chapter three gives an overview on geology of the south-western Ghana and the study area. It also deals with the gold mineralisation occurrences in Ghana. Chapter four outlines the theoretical background of radiometric, magnetic, magnetic image enhancement transform methods and alteration processes. Chapter five deals with the materials available for the study, the procedure used in collecting data and also outlines the data processing techniques that were used to visualise anomalies for data interpretation. Also, it describes the area under study. Chapter six presents the results obtained and discusses the results presented in the various maps obtained from the radiometric and magnetic data. It also contains a proposed integrated geological and structural map, deduced from the findings of both radiometric and magnetic data-sets, with possible zones of gold mineralization overlain on it. Chapter seven presents conclusions and recommendations.

## CHAPTER 2

### 2.1 LITERATURE REVIEW

In the 1980's, the value of high-resolution airborne geophysical data for geophysical mapping and mineral exploration was observed and effectively demonstrated in metal ore exploration. In all areas, including those where outcrop can be described as 'acceptable or good', high resolution airborne radiometric and magnetic data-sets have showed very well both geological structure and lithological boundaries than on previously published maps (Harris et al., 1994). Also valuable geophysical information not available in the enhanced products of the individual records can be obtained from the integrated enhancement of airborne geophysical data-sets (Harris et al., 1994).

In 1960, Haunting Survey Limited of United Kingdom undertook geophysical exploration for minerals in Ghana using airborne magnetic and radiometric survey in the South Western and South Eastern part of the country. Magnetic maps showing contrasts between rock units of high and low magnetic susceptibilities were produced and dikes, intrusive, fractured zones were clearly identified on the map (Kesse, 1985).

Also aeromagnetic data-sets are highly suited, to structural and lithological mapping, over wide range of scales due to its ability, of accurately mapping a single geological parameter, in a uniform manner over large areas (Boyle, 1979).

In the mid-1990s, Aerodat geophysical company (now High Sense/Fugro Airborne Survey) carried out a speculative survey (magnetic and radiometric) in the Kumasi Basin, Ashanti Belt and the Southern part of the Sefwi Belt. The Geology of areas with thick vegetation

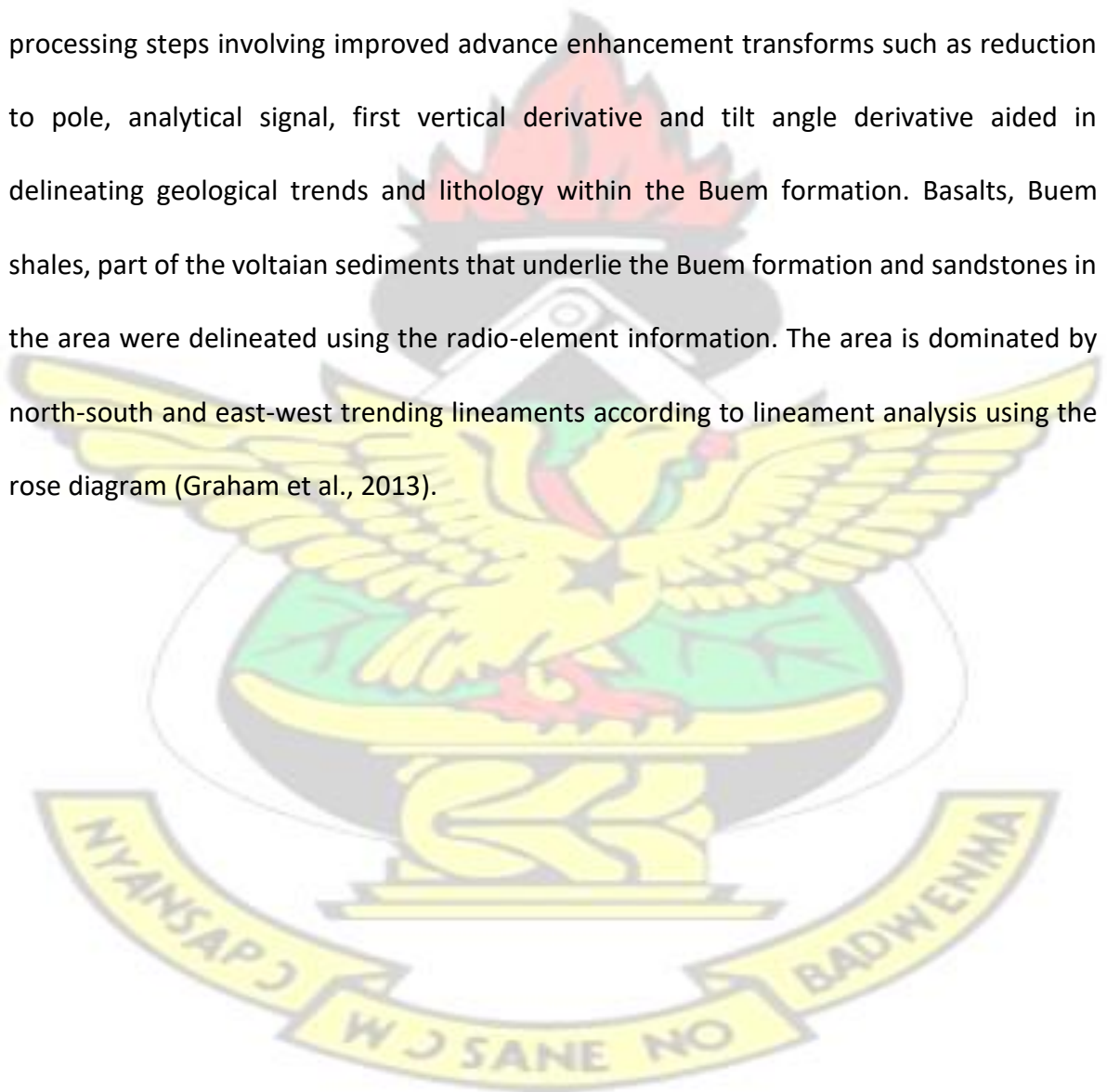
and very little outcrop were interpreted successfully. Important geological structures which control gold mineralisation throughout the Birimian were inferred through offsets in radiometric and magnetic patterns (Griffis et al., 2002).

New resolution Geophysics from South Africa (NRG) carried out high resolution aeroradiometric and magnetic survey for Goknet Mining Company Ltd from 18th June to 28th June, 2010. The objective was to identify structural trends to follow with soil geochemistry/auger drilling, ultimately ending up in the identification of targets for drilling. The radiometric data showed geochemical changes in the concentration of potassium, uranium and thorium. Additionally, the radiometric data was used directly to map zones that are altered, uranium mineralisation and discriminate Fe-oxide-Cu-Au, mafic targets and granophile deposits. The potassium map revealed important empirical indicator of gold mineralisation such as the monzonite which in certain mineralised belts hosts gold mineralisation (e.g. Edikan, Obotan, Obuasi etc.) and granites. Shear zones which are spatially related to the margins of the Akropong gold belt trending NE, were effectively mapped (Allen, 2011).

Aeromagnetic and radiometric data-sets were used to map the geology and geological structures in the Konongo area of Ghana. The application of magnetic enhancement transforms such as reduction to pole, analytical signal and first vertical derivative aided in tracing out fractures, folds, lithological boundaries and potential hydrothermal gold mineralisation zones within the area due to two main Birimian tectonic structural events. Gold mineralisation in the belt hosted by the contacts between Birimian metasedimentary and meta-volcanic rocks were also delineated. Data-sets from radiometric were used, to bring out geochemical records on the abundance of uranium (U), potassium (K) and

thorium (Th) within the study area, to delineate bedrock lithology as well as contact zones and alteration. The high resolution airborne radiometric and magnetic data resulted in better definition of lithological boundaries and geological structures (Boadi et al., 2013).

A similar work was carried out in the Nkwanta area of Ghana where airborne radiometric and magnetic data-sets were processed to interpret the geology of part of the Buem formation in the area and estimate the depth to basement of magnetic sources. Data processing steps involving improved advance enhancement transforms such as reduction to pole, analytical signal, first vertical derivative and tilt angle derivative aided in delineating geological trends and lithology within the Buem formation. Basalts, Buem shales, part of the voltaian sediments that underlie the Buem formation and sandstones in the area were delineated using the radio-element information. The area is dominated by north-south and east-west trending lineaments according to lineament analysis using the rose diagram (Graham et al., 2013).



## CHAPTER 3

### 3.1 REGIONAL GEOLOGY

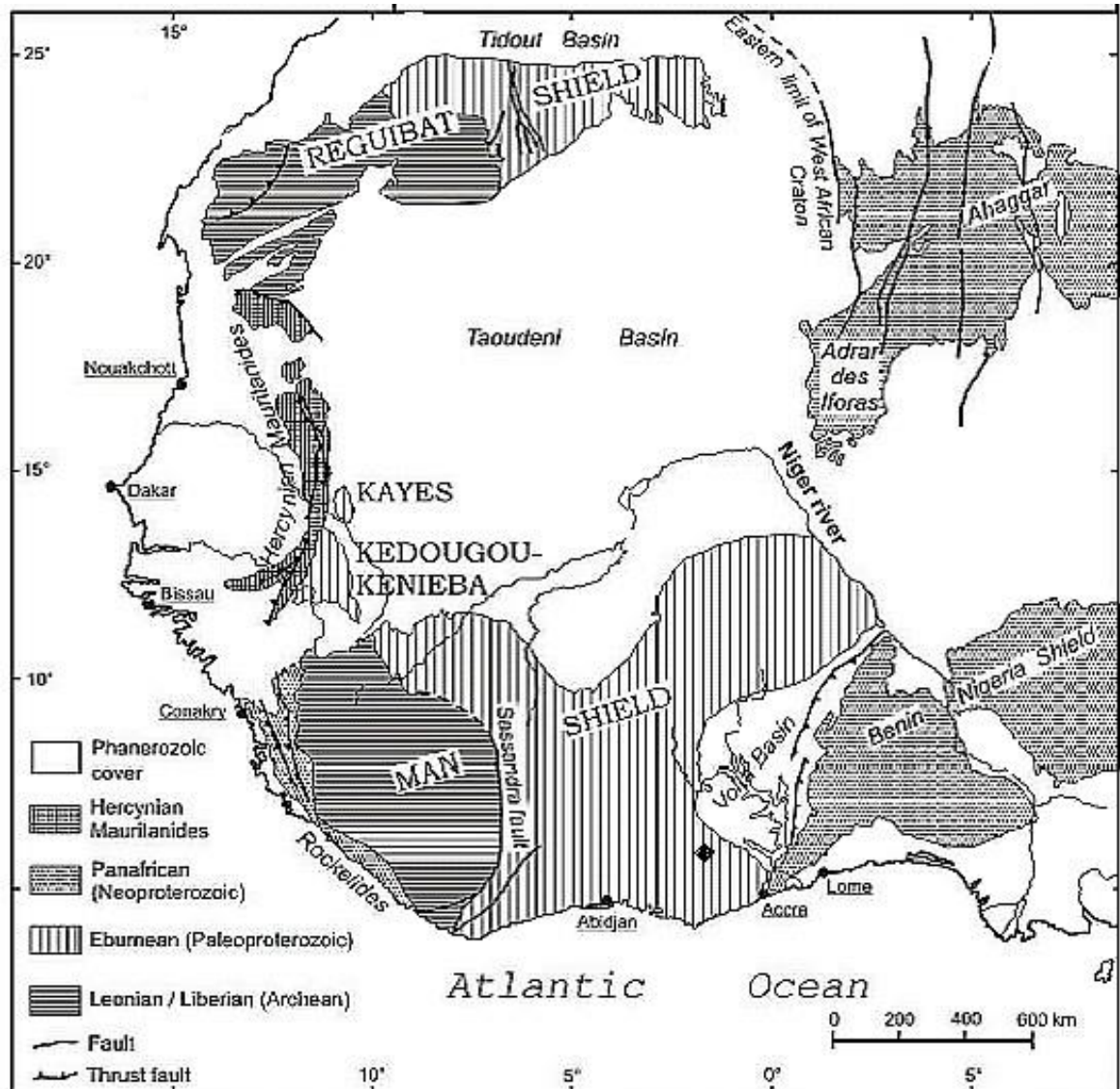


Figure 3.1: Geological outline map of West Africa showing basement outcrops and basins (Study area in black) (after (Boher et al., 1992))

Ghana's main gold mineralisation is mostly associated with Paleoproterozoic green stone belts trending NE-SW and separated by basins, together forming part of the Leo Man Craton. An Achaean nucleus that is tectonically bordering the Paleoproterozoic green stone belts forms part of the southern area of the Leo Man Craton (Fig 3.1).

Four of these greenstone belts occur in south western Ghana. These are the Sefwi, Bui, Kibi-Winneba and the Ashanti belt respectively. Their separating sedimentary basins are the Kumasi, Akyem or Cape Coast and Sunyani Basin (Duodu et al., 2009). These dividing sedimentary basins and greenstone belts were formed and deformed during intense tectonical events which affected the Birimian group (Bonhomme, 1962). The Birimian series, of age 2.17-2.18 billion years, and a marginally younger Tarkwaian series, of age 2.10-2.13 billion years are the various separations of Proterozoic rocks in Ghana.

### 3.1.1 EBURNEAN OROGENY

This corresponds to a time of plutonism and magmatic accretion between 2135 Ma and 2100 Ma that discontinued with the evolution of the Kumasi Basin (Feybesse et al., 2006) and a synchronous deformational event (2130-1980 Ma) which coincides with thrust tectonics, dominated by sinisterly trans-current Ashanti belt deformation. According to Allibone et al. (2002), this deformational event involve advancements, divided into the Eburnean I (2200-2150 Ma) and Eburnean II (2116-2088 Ma) and separated by the Birimian and Tarkwaian deposition.

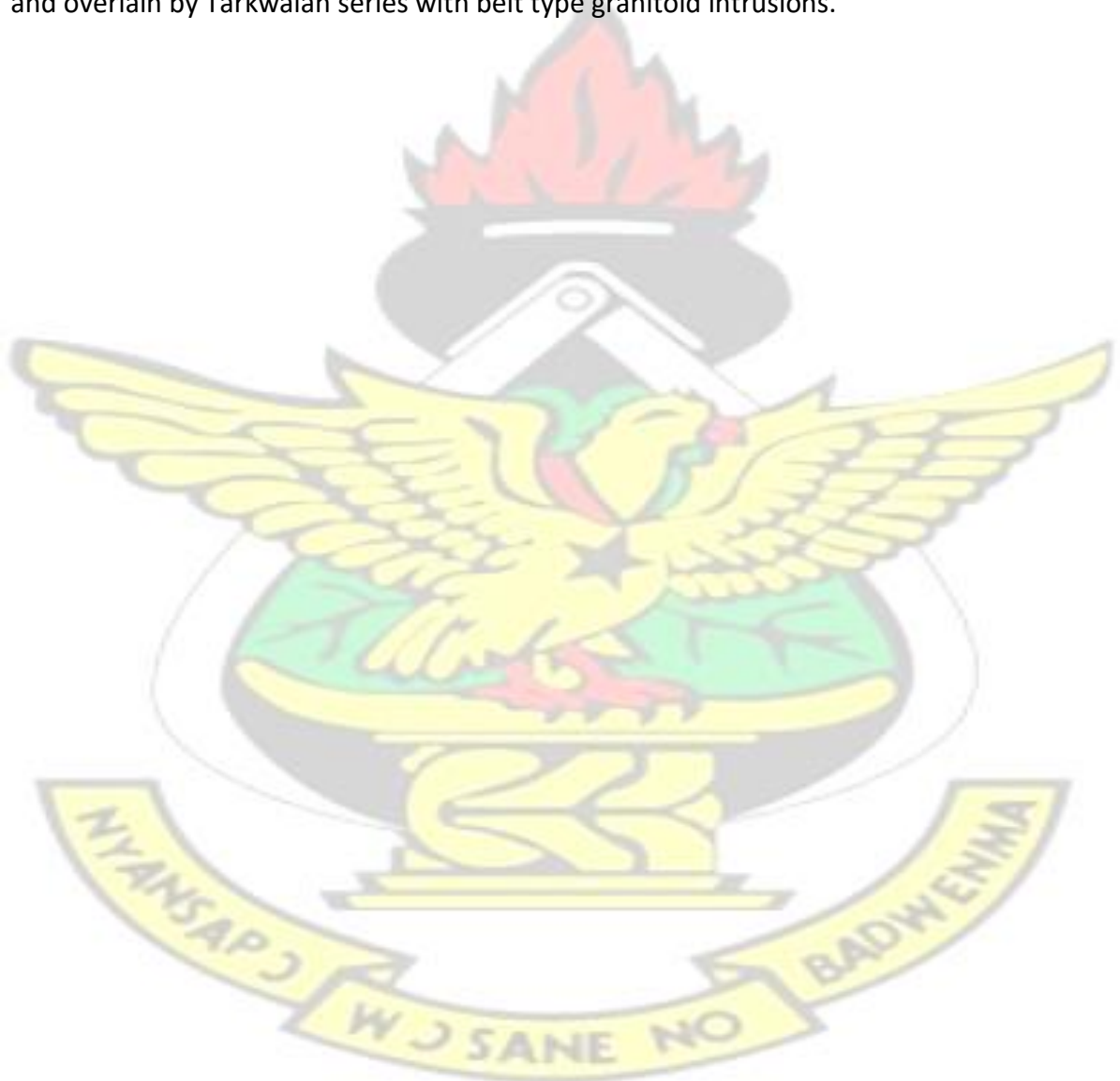
The Eburnean I event was associated with a time of magmatism and metamorphism which resulted in the emplacement of the Sefwi Group metavolcanics and granitoid. The Eburnean

II affected both the Birimian Supergroup and the Tarkwaian formation and is associated with major NW-SE shortening (Tunks et al., 2004; Allibone et al., 2002) that resulted in the formation of major thrust faults such as the Ashanti Fault together with isoclinal folds in the Birimian metasediments and Tarkwaian sediments. These features were imprinted by

thrusts faults that were reactivated during a phase of sinister transgression that utilised the existing thrust architecture (Tunks et al., 2004; Milési et al., 1991; Feybesse et al., 2006).

### 3.1.2 GEOLOGY OF THE BEPOSO AREA

Fig 3.2 shows the geology of the study area. The study area is underlain by Birimian series and overlain by Tarkwaian series with belt type granitoid intrusions.



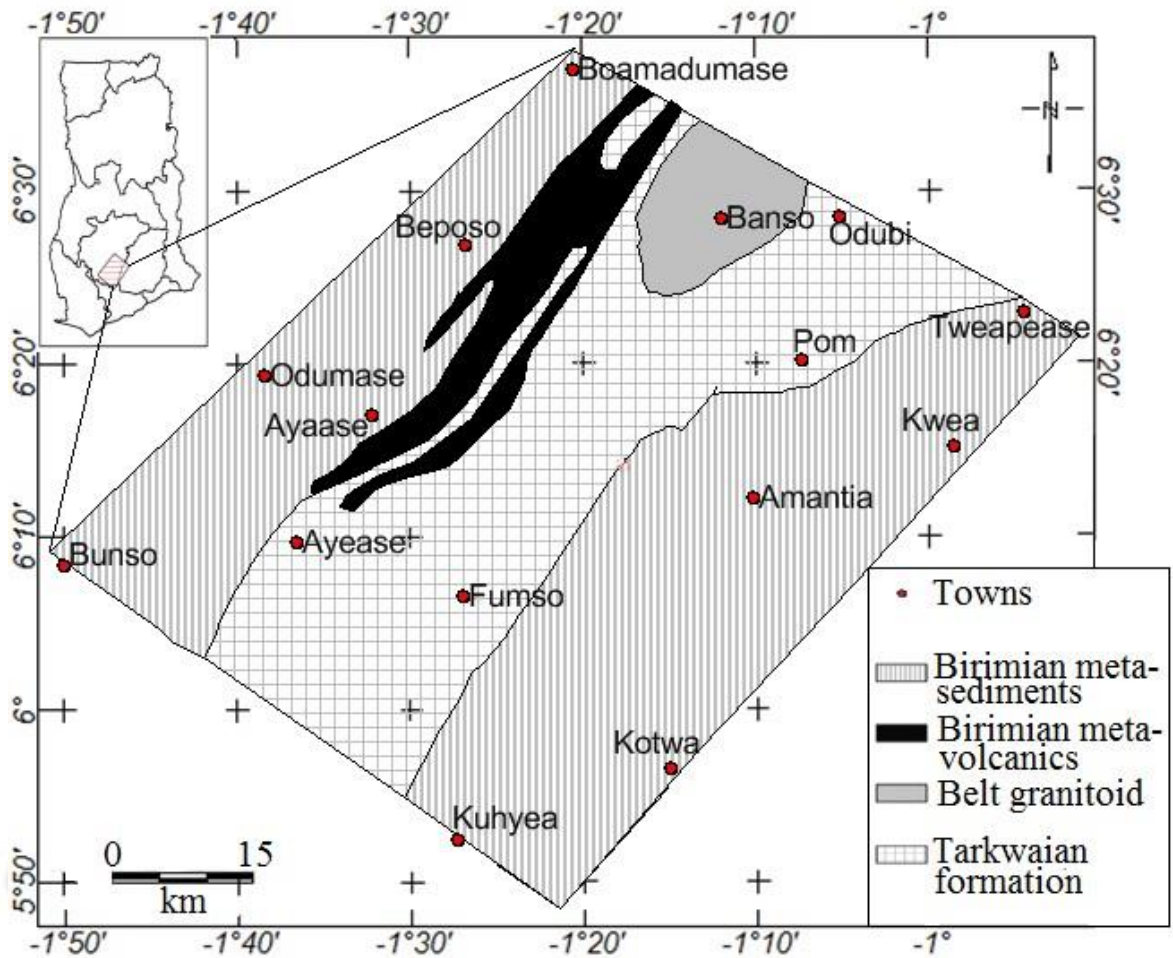


Figure 3.2: Geology of study area (modified after (Taylor et al., 1992))

### 3.1.3 BIRIMIAN SERIES

The Birimian series consist of metasediments and metavolcanics. The metasediments consists mainly of sediments, while the metavolcanics consists of rhyolitics and tuffs with minor sedimentary intercalations, andesitic and basaltic volcanics. Granites intrude both the metasediments and metavolcanics. The Birimian contains important gold occurrences.

### 3.1.4 TARKWAIAN SERIES

The Tarkwaian series is regarded to have been deposited in long intra-montane grabens, as shallow deltaic sediments, in part, at the same time with the Birimian. It consists of four groups of sediments (Junnor, 1935; Pigois et al., 2003; Whitelaw, 1929; Kesse, 1985).

The Kawere sediments, at the undermost of the Tarkwaian sediments and made up of conglomerates and sandstones between 250 m and 700 m thick and overlain by the Banket formation, which is made of conglomerates with interbedded local cross-bedded sandstone layers. The conglomerates are principally made of quartz pebbles of volcanic clast and Birimian origin (>90%) (Hirdes and Nunoo, 1994) that hold the Tarkwa Placer deposits. A zone that is less than 100 m thick hosts Gold within the conglomerate, while the Banket sequence is estimated to be 600 m thick.

The Banket sequence is overlain by approximately 400 m of Tarkwa Phyllites. The Huni Sandstone, which is the uppermost unit of the Tarkwa Group is made of alternating beds of quartzite and phyllite with minor dolerite sill intrusions, that form a package up to 1300 m thick (Pigois et al., 2003).

U/Pb and Pb/Pb dating of few detrital zircons indicated maximum depositional age of 2132.6

$\pm 3.4$  Ma for the Banket formation and  $2132 \pm 2.8$  Ma for the Kawere formation (Davis et al.,

1994; Hirdes and Nunoo, 1994). Intrusions of metagabbro sills and granitoids at  $2097 \pm 2$

Ma, within the Tarkwaian series at  $2102 \pm 13$  Ma constrains the Tarkwaian series (Adadey et al., 2009; Oberthür et al., 1998).

### 3.1.5 GRANITOIDS

During the paleoproterozoic, abundant granites intruded the Birimian and Tarkwaian series. A number of the granites interjected during both deformational phases corresponding to typical tonalite-trondhjemite-granodiorite suites. Granites from the first deformational phase sometimes show alignment of magmatic minerals (biotite and /or feldspar) but are generally unfoliated. Late deformation granites which are often K-feldspar rich, cross-cut major regional structures (Perrouty et al., 2012).

### 3.1.6 MINERALISATION

The Ashanti Belt of South Western Ghana hosts a gold district that contains a significant number of world class hydrothermal gold deposits. These deposits are spatially associated with the major shear zones and thrust faults along the contact between the Birimian and Tarkwaian units and in the Birimian Supergroup . 40 million ounces of gold is hosted by the overlying Tarkwa Basin which also hosts the Tarkwa Paleoplacer (Perrouty et al., 2012).

### 3.1.7 BIRIMIAN DEPOSITS

The main mineralisation in the Obuasi mine is associated with ductile shearing along the Ashanti Shear (Oberthür et al., 1994; Allibone et al., 2002) which describes secondary gold mineralisation that developed within quartz veins and carbonate-alteration zones in basaltic regions. Mumin and Fleet (1995) showed that for the Bogoso and Prestea deposits, gold mineralisation is as a result of the remobilisation of pre-existing gold along the Ashanti Shear. Shear zones that transect sediments, mafics or granitoids host Birimian

mineralisations (Klemd et al., 1992; 1993; Mumin and Fleet, 1995; Allibone et al., 2002; Mumin et al., 1996; Schmidt Mumm et al., 1997; Howell et al., 1990; Yao and Robb, 2000; Yao et al., 2001; Tunks et al., 2004; Griffis et al., 2002; Pigois et al., 2003).

### 3.1.8 TARKWAIAN DEPOSITS

The Tarkwa Group exhibits two styles of gold mineralisation. Those that occur within the Birimian and Tarkwaian contact due to hydrothermal alteration and Tarkwa Basin paleoplacers (e.g Tarkwa mine). The distribution of Gold grade in the Tarkwaian are parallel to bedding, supporting a sedimentary origin (Sestini, 1973). Paleochannels found within the Tarkwaian generally hosts the gold, along conglomerates and proximal to hematite rich areas within the Banket formation. Conditions (250-400°C and 0.5-3 kbar) of formation under greenschist facies were suggested by fluid inclusions studies of mineralised quartz pebbles (Klemd et al., 1993).

## CHAPTER 4

### 4.1 THEORY

#### 4.1.1 The Magnetic Field of the Earth

A dipolar magnetic source located at the center of the Earth generates about 90% of geomagnetic field aligned at  $11.5^{\circ}$  with the Earth's rotational axis. Convection current within the Earth's molten outer core, containing iron and nickel, is believed to be the originator of this geomagnetic field (Campbell, 1997). The geomagnetic field is studied and

tracked using global magnetic satellite and a network of magnetic observatories. The magnitude of the geomagnetic field varies between 20,000 nT at the equator and about 70,000 nT at the poles. This is called the main field of the Earth and it changes slowly with time. The geomagnetic field is believed to be diminishing on a time scale of the order of 100,000 years, followed by polar reversal (Cox, 1973).

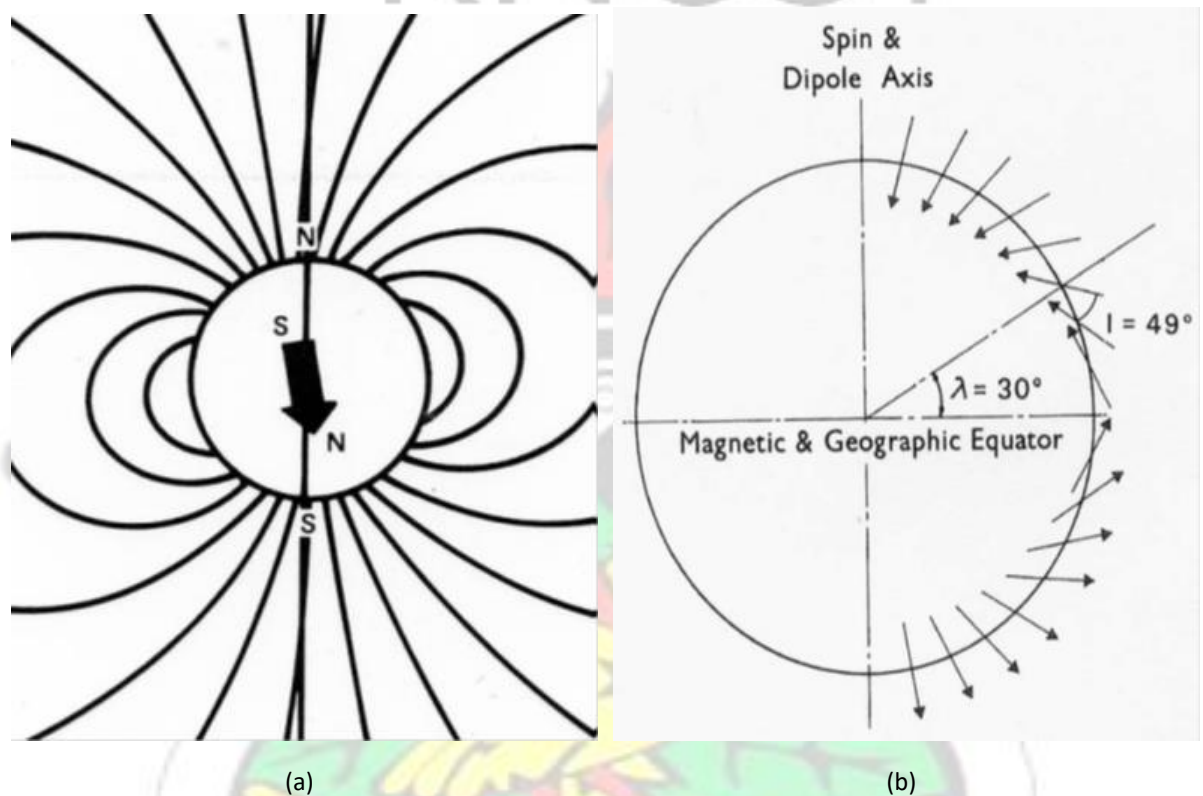


Figure 4.1: (A) The geomagnetic field (B) The Earth's field Inclination at different latitudes (Reeves, 2005)

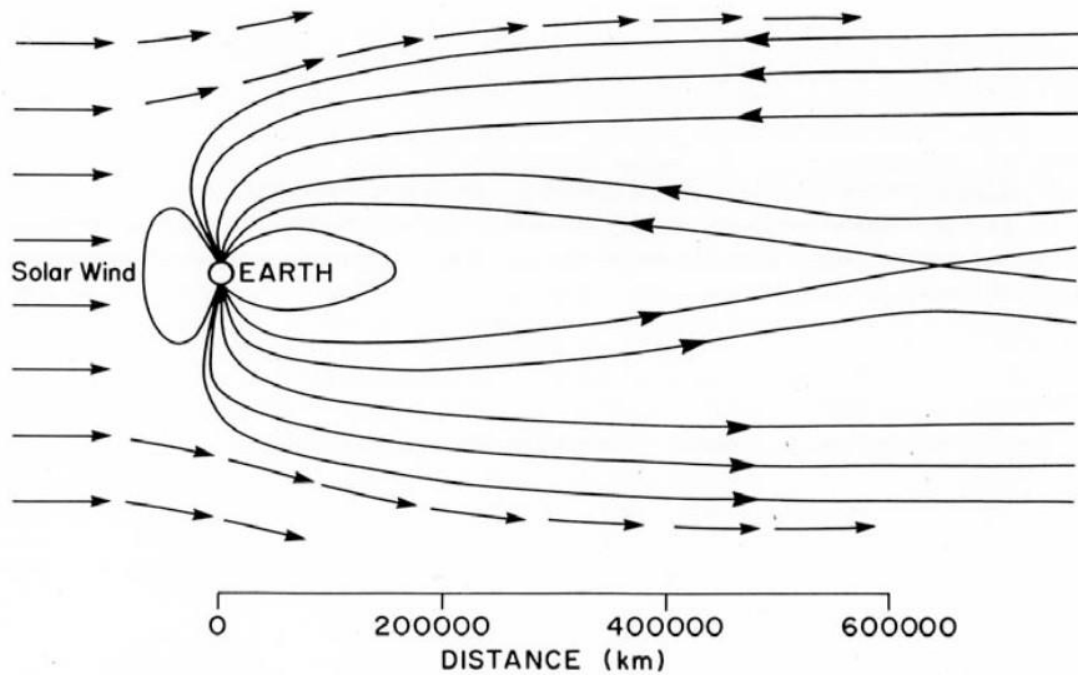


Figure 4.2: Malformation of the geomagnetic field as a result of solar wind, causing bends in the ionosphere on the orbiting planets day side (Reeves, 2005)

Iron bearing rocks near areas where temperatures are sufficiently low at the Earth's surface (i.e. < Curie temperature of the rocks) produce larger portion of the remaining 10% geomagnetic field. This region is restricted to the top 30 - 40 km of the Earth's crust and is the origin of the crustal field which constitutes induced field in remanent magnetism of the rocks and magnetically susceptible rocks. The remaining portion of the 10% originates from the upper atmosphere due to the interaction of the Earth's ionosphere with the solar wind.

Temporal changes (sometimes varying over a few hours at hundreds of nT or mostly varying over hours at tens of nT: the magnetic storm) are due to solar activity. The external constituents (except for magnetic storm) are separated out appropriately from field measurements in a procedure similar to the correction of drift in gravity surveys. Magnetic survey is most often halted, where magnetic storm is detected, until after the phenomenon

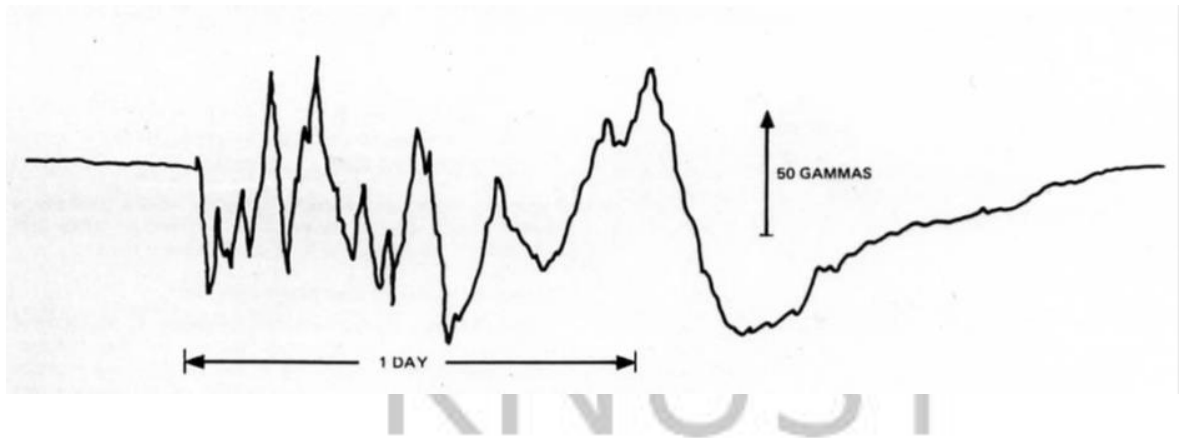


Figure 4.3: Example of a magnetic storm noticed at a time when there is high solar activity. The storm is sudden at the initial stage and violent changes in F may be observed over several tens of hours (Reeves, 2005)

has passed.

The relation of the crustal field to the distribution of magnetic minerals in the crust and the information this relation gives about exploration targets are the main subjects of the magnetic method. The magnetic induction,  $B$  whose magnitude is measured at a point in a magnetic survey, is the vector sum of four field components:

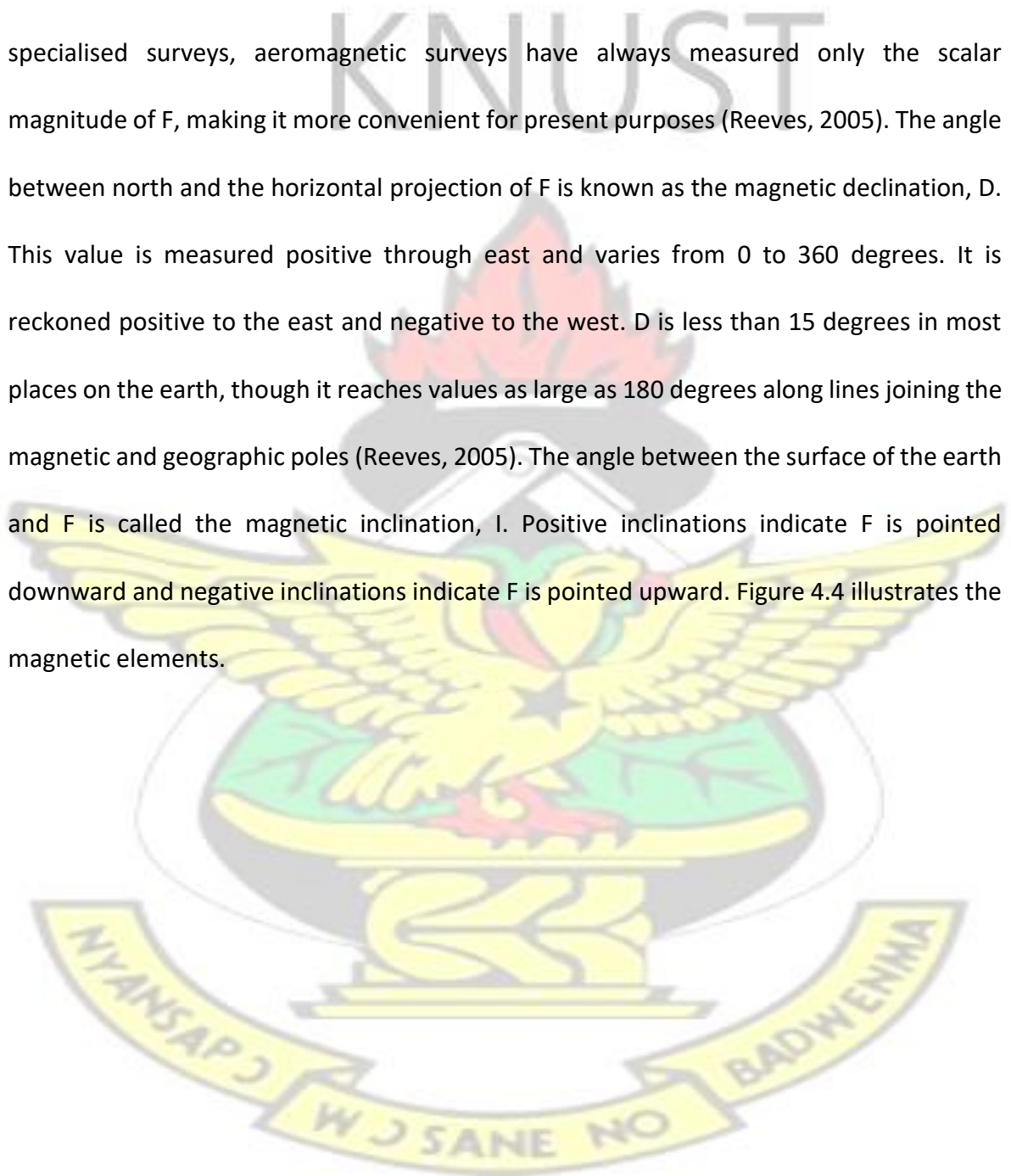
- the main geomagnetic field which originates from convection current in the Earth's outer core (Merrill, 2000);
- the induced magnetic field in magnetically susceptible earth materials polarised by the main geomagnetic field (Doell and Cox, 1967):
- remanent magnetism field of the earth materials (Doell and Cox, 1967); and,
- usually less important fields caused by atmospheric, cultural influences and solar activities (Telford et al., 1994).

In all, the induced and remanent fields are of particular interest to the geoscientist because the strength of these fields is directly related to the spatial distribution, magnetic susceptibility and concentration of the local crustal materials. Interestingly only a few minerals occur abundantly enough in nature to make valuable contribution to the induced and remanent fields. The most relevant of these is magnetite and to a lesser extent pyrrhotite and ilmenite (Clark, 1997; Telford et al., 1994).

Processed magnetic data-sets serve as indicators of the spatial distribution and concentration of magnetically significant minerals after the main field and minor source effects are removed from the observed magnetic field data through various data reduction and processing methods (Luyendyk, 1997). After, the data are enhanced and presented (Gunn, 1997) as maps for analysis. The analysis leads to the interpretation (Mackey et al., 2000; Gunn and Dentith, 1997) of lithology, structure, alteration, regolith and sedimentary processes, amongst other.

Units of measurement of the magnetic field are volt-seconds per square metre or Weber/m<sup>2</sup> or Teslas (T). This is because the magnetic field in SI units is defined in terms of the flow of electric current needed in a coil to generate that field. Since the magnitude of the earth's magnetic field is only about  $5 \times 10^5$  T, a more convenient SI unit of measurement in geophysics is the nanoTesla ( $\text{nT} = 10^{-9}$  T). The geomagnetic field then has an average value of about 50,000 nT. Magnetic anomalies as small as about 0.1 nT can be measured in conventional aeromagnetic surveys and may be often, hundreds and (less often) thousands of nT. 1 nT is numerically equivalent to the gamma ( $\gamma$ ) which is an old (cgs) unit of magnetic field. The gamma still has some use but should, strictly speaking, now be replaced by the nT (Reeves, 2005).

The definition of the main geomagnetic field at any point on the earth's surface as a vector quantity requires three values, normally expressed either as three orthogonal components (vertical, horizontal-north and horizontal-east components) or the magnitude of the total field vector ( $F$ ) and its orientation in dip and azimuth. With the exception of a few specialised surveys, aeromagnetic surveys have always measured only the scalar magnitude of  $F$ , making it more convenient for present purposes (Reeves, 2005). The angle between north and the horizontal projection of  $F$  is known as the magnetic declination,  $D$ . This value is measured positive through east and varies from 0 to 360 degrees. It is reckoned positive to the east and negative to the west.  $D$  is less than 15 degrees in most places on the earth, though it reaches values as large as 180 degrees along lines joining the magnetic and geographic poles (Reeves, 2005). The angle between the surface of the earth and  $F$  is called the magnetic inclination,  $I$ . Positive inclinations indicate  $F$  is pointed downward and negative inclinations indicate  $F$  is pointed upward. Figure 4.4 illustrates the magnetic elements.



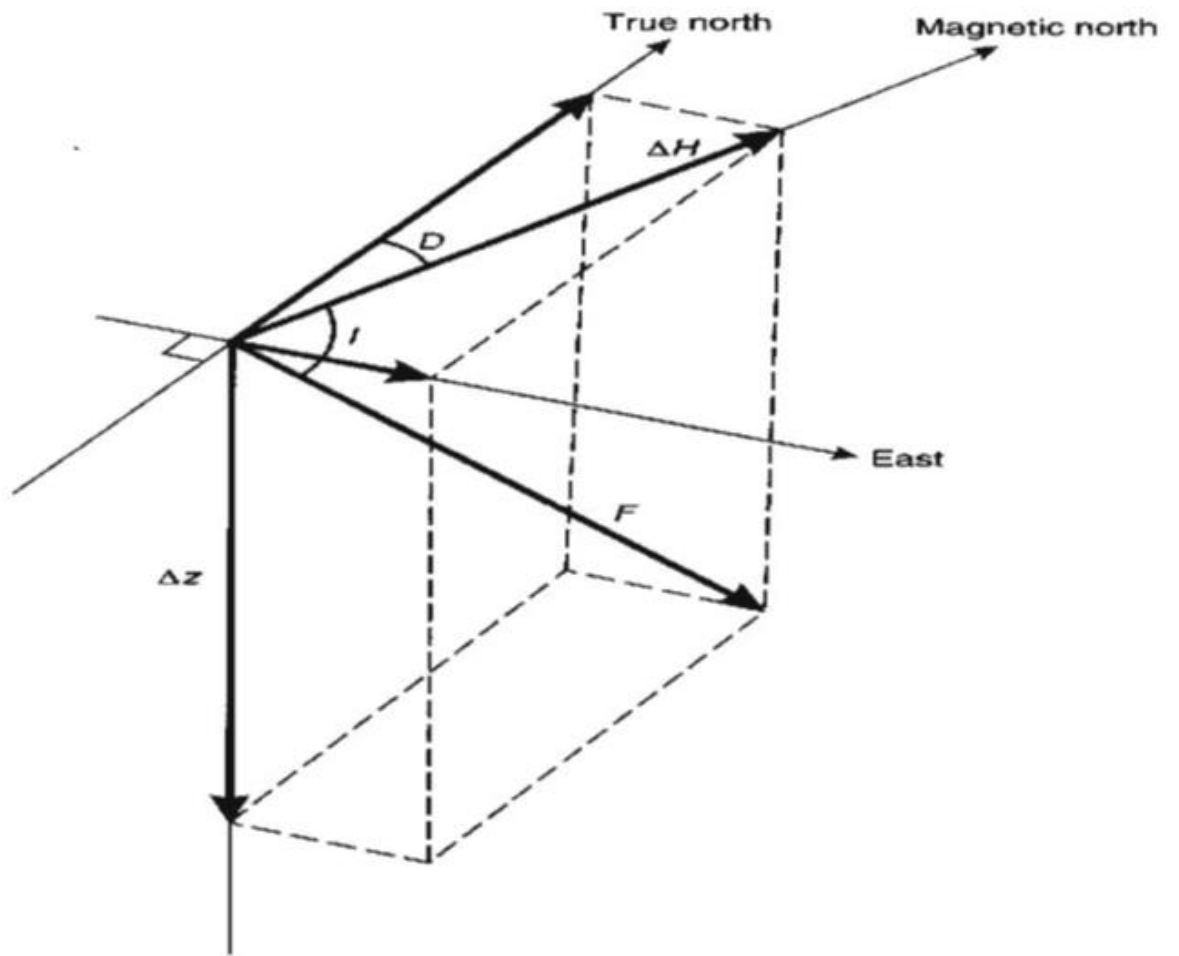


Figure 4.4: Elements of the geomagnetic field (Reeves, 2005)  $F$  is the total (Resultant) field:  $H^2 + Z^2 = F^2$

$$\Delta H = F \cos(I)$$

$$\Delta Z = F \sin(I)$$

$$\tan I = \Delta Z / \Delta H$$

Also,  $\tan I = 2 \tan \phi$  ( $\phi$  is magnetic latitude)

#### 4.1.2 The International Geomagnetic Reference Field (IGRF)

To leave anomalies that may be compared from one survey to another, even when surveys are conducted several decades apart (and when, the main field may have been subjected to considerable secular variation), the IGRF is calculated by subtracting on a rational basis the expected variations in the main field. Since the IGRF calculation involves the subtraction of about 99% of the value measured, it needs to be calculated with accuracy (Reeves, 2005). From exploration geophysics point of view, doubtlessly the major importance of the IGRF is the uniformity it presents, since the IGRF is universally accepted and freely available.

#### 4.1.3 Magnetic Susceptibility

When a Ferrous material is placed in the geomagnetic field, it becomes magnetised and the external geomagnetic field is reinforced by an induced magnetic field in the material. This is called the induced magnetisation. When the external geomagnetic field is removed, the induced magnetisation vanishes at once, but some materials acquire remanent or permanent magnetisation with fixed direction within the specimen in the direction of the inducing geomagnetic field. Crustal rocks inevitably lie within the influence of the geomagnetic field as it is now and hence are weakly magnetic. They can therefore exhibit both induced and remanent magnetisation and in some cases, they also record indications of how that field was in the past. The strength of the earth's field,  $F$ , is proportional to the magnitude of the magnetisation they acquire,  $J$ , in their vicinity, where  $k$ , the constant of proportionality is the magnetic susceptibility of the rock:

$$J = kF \quad (4.1)$$

$k$ , the magnetic volume susceptibility differs from the mass susceptibility and the molar susceptibility that are mostly not encountered in exploration geophysics (Reeves, 2005). The fundamental rock parameter of magnetic prospecting which plays similar role as density does in gravity interpretation is Susceptibility ( $k$ ) (Telford et al., 1990). It can take on positive or negative values and it is a numerical constant that is ascertained by the physical attributes of the magnetic material. Magnetic response of rocks is determined by the susceptibilities of constituent minerals which usually depends on its magnetite content. Acid igneous and Sediment rocks have small susceptibilities whereas serpentinites, gabbros, basalts and dolerites are usually strongly magnetic. Weathering mostly results in reduction of susceptibility because magnetite is oxidized to hematite, but because of the presence of maghemite and remanently magnetized hematite some laterites are magnetic (Milsom, 2003).

#### 4.1.4 Magnetism of Rocks and Minerals

Magnetically important minerals are surprisingly few in number though all materials are magnetic. They can be divided based on their behaviour when placed in an external geomagnetic field.

A substance is diamagnetic if its field is dominated by atoms with orbital electrons oriented to oppose the external magnetic field. That is, if it exhibits negative susceptibility. Diamagnetism will prevail only if the net magnetic moment of all the atoms is zero when  $H$  is zero, a situation characteristic of atoms with completely filled electron shells. The most

common diamagnetic earth materials are graphite, marble, quartz and salt. When the magnetic moment is not zero, when H is zero, the susceptibility is positive and the substance is paramagnetic. The effects of diamagnetism and paramagnetism are generally weak.

Certain elements, namely iron, cobalt and nickel, have such strong magnetic interaction that the moments align within fairly large regions called domains. This effect is called ferromagnetism and it is  $\sim 10^6$  times the effect of diamagnetism and paramagnetism (Telford et al., 1990). Ferromagnetism reduces with increasing temperature and disappears entirely above curie temperature. Naturally, ferromagnetic minerals do not exist (Telford et al., 1990).

The domains in some materials are subdivided into subdomains that align in opposite directions so that their moments nearly cancel; although they would otherwise be considered ferromagnetic, the susceptibility is comparatively low. Such a substance is antiferromagnetic. The only common example is hematite (Telford et al., 1990). In some materials, the magnetic subdomains align in opposition but their net moment is not zero, either because one set of subdomains has a stronger magnetic alignment than the other or because there are more subdomains of one type than of the other. These substances are ferrimagnetic. Examples of the first type are magnetite and titanomagnetite, oxides of iron and titanium. Pyrrhotite is a magnetic mineral of the second type. Practically all magnetic minerals are ferromagnetic (Telford et al., 1990).

#### 4.1.5 Remanent Magnetisation in Rocks

In many cases, the magnetisation of rocks depend mainly on the present geomagnetic field and the magnetic mineral content. Residual magnetism (called natural remanent magnetisation, NRM) often contributes to the total magnetisation, both in amplitude and direction. The effect is complicated because NRM depends on the magnetic history of the rock (Telford et al., 1990). Natural remanent magnetisation may be due to several causes.

The principal ones are:

- Thermoremanent magnetisation (TRM), which results when a magnetic material is cooled below the Curie point in the presence of an external geomagnetic field. Its direction relies on the direction of the field at the time and place where a rock cooled. Remanence acquired in this fashion is particularly stable. This is the main mechanism for the residual magnetisation of igneous rocks (Telford et al., 1990).
- Detrital magnetisation (DRM), which occurs during the slow settling of fine-grained particles in the presence of an external field. Varied clays exhibit this type of remanence (Telford et al., 1990).
- Chemical remanent magnetisation (CRM), which takes place when magnetic grains increase in size or are changed from one form to another as a result of chemical action at moderate temperatures, that is, below the Curie point. This process may be significant in sedimentary and metamorphic rocks (Telford et al., 1990).
- Isothermal remanent magnetisation (IRM), which is the residual magnetisation left following the removal of an external field. Lightning strikes produce IRM over very small areas (Telford et al., 1990).

- Viscous remanent magnetisation (VRM), which is produced by long exposure to an external field. Here the build-up of remanence is a logarithmic function of time and VRM is probably more characteristic of fine-grained than coarse-grained rocks. This remanence is quite stable (Telford et al., 1990).

Geomagnetic history studies indicate that the Earth's field has changed in magnitude and has a number of times, reversed its polarity. Furthermore, it appears that the reversals took place rapidly in geologic time, because there is no evidence that the Earth existed without a magnetic field for any significant period. Models studies of a self-excited dynamo show such a rapid turnover. Many rocks have remanent magnetism that is oriented neither in the direction of, nor opposite to, the present Earth field (Telford et al., 1990). Generally rocks are expected to have induced and remanent magnetisation. The induced,  $J_i$ , will be parallel to the present geomagnetic field, while the remanent component,  $J_r$ , may reasonably have any direction. They sum up vectorially to give the total magnetisation of the rock in situ since they are both vector quantities, (Reeves, 2005).

#### 4.1.6 The Underlying Principle of the Magnetic Method

The underlying principle of the magnetic method relies in the fact that when a ferrous body is placed within the geomagnetic field, An induced magnetic field is developed. The induced field is superimposed on the geomagnetic field at that location creating a magnetic anomaly. Detection depends on the distance from the sensor and the amount of magnetic material present.

## 4.1.7 Application of Magnetic Enhancement Transforms

Enhancement techniques are ways of cutting off signals of different wavelength to set apart and hence improve anomalous features with certain wavelength (GETECH, 2010).

### 4.1.7.1 Reduction to the Magnetic Equator (RTE)

The RTP takes the measured total magnetic field grid and transforms it into a magnetic grid that would result had the area been surveyed at the magnetic pole (MacLeod et al., 1993). This puts the limits of the magnetic anomalies directly over their sources, thus making magnetic interpretation easier and more reliable (Rajagopalan and Milligan, 1994). The filter is computed in the frequency domain by the operator (Cooper and Cowan, 2006). In practise, the standard RTP filter at very low geomagnetic latitude is difficult to apply. It produces variable-quality maps, sometimes dominated by declination-parallel artefacts (Rajagopalan and Milligan, 1994). To facilitate the interpretation of the anomalies at very low latitudes, the Reduction to Equator which was developed to solve the problem of the RTP was applied.

### 4.1.7.2 Analytic Signal Amplitude (AS)

This filter places magnetic anomalies on causative bodies and simplifies the fact that magnetic bodies mostly have a negative and positive peaks associated with it, which in many cases make interpretation of magnetic data difficult. The only assumptions made are uniform magnetisation and that the cross section of all causative bodies can be represented by polygons of finite or infinite depth extent. This function and its derivatives therefore, do

not depend on the magnetic declination, strike, dip, remanent magnetism and inclination (GETECH, 2010).

#### 4.1.7.3 First Derivative (FD)

This filter tends to reduce anomaly complexity by sharpening up anomalies over bodies, resulting in a clear visualisation of the underlying structures. Since it amplifies short wavelengths, this filter can be noisy (GETECH, 2010). Calculation of the first derivative in airborne magnetic surveys has the same advantage, thus the first derivative enhances anomalies over shallow magnetic bodies. It reaches its maximum values above magnetic units with zero cross-over at the edge of near vertical symmetrical bodies. Higher order (Second, third etc) vertical derivatives can also be used but usually they introduce unacceptable levels of noise (Reeves, 2005).

#### 4.1.7.4 Horizontal Derivatives (HDR)

The magnetic response is spatially more directly associated with the related magnetic body after the Reduction to the Equator correction. The maximum horizontal derivative is then situated over or near the edge of the body. Thus, the horizontal derivative map gives maximum ridges over edges of magnetic bodies (GETECH, 2010).

#### 4.1.7.5 Tilt Derivative (TD)

High frequency signatures may be overshadowed by low frequency signatures since the amplitude of magnetic anomalies rely on the magnetic field strength and to some extent

the depth of magnetic sources. For this reason, this filter is applied to delineate outlines of magnetic bodies without necessary diminishing anomalies of long-wavelength anomalies. The Tilt derivative filter, therefore reveals short wavelength and traces out magnetic lineaments.

The TD responds equally well to deep and shallow sources and to a range of amplitudes for sources at the same level (Cooper and Cowan, 2006). Subtle anomalies in magnetically quiet areas are thus enhanced relative to low frequency anomalies. The TD has the property of peaking over magnetic bodies with its zero-crossover close to the edge of the body. It is an excellent filter for fabric mapping, i.e. arising from shallow geological features, and shows better spatial resolution than the first vertical derivative (Naude, 2012). TD values are limited to  $+\pi/2$  and  $-\pi/2$  and is much simpler to interpret (Cooper and Cowan, 2006).

#### 4.1.8 Airborne Radiometric (Gamma Ray Spectrometry) for Natural Radioelement Mapping

Natural emanations from rocks and soils, called gamma rays, are detected by Radiometric surveys. These emanations come from the natural decay products of three elements, namely, uranium, thorium, and potassium (Urquhart, 2003). The spatial distributions of these three radioactive elements (namely potassium, thorium and uranium) are measured in a radiometric survey through gamma ray detection which is based on the abundance of the radioactive elements (IAEA, 2003).

#### 4.1.8.1 Basic Radioactivity

Surplus energy from atomic nuclei of some isotopes, are unstable, and therefore decay to form more stable nuclei of different isotope resulting in the emission of particles or energy, called nuclear radiation. The process is called nuclear disintegration or decay and nuclides with this feature are called radionuclides (IAEA, 2003). The law which expresses the reduction in the number of atoms of a radionuclide with time, known as the radioactivity decay law, is given by:

$$N_t = N_0 e^{-\lambda t} \quad (4.2)$$

where

## CHAPTER 5

### 5.1 MATERIALS AND METHODS

#### 5.1.1 Study area

##### 5.1.1.1 Location

The study area (fig 5.1) lies in the South Western part of the country with geographical coordinates of  $-1.333^{\circ}$  E and  $-0.874^{\circ}$  E to  $1.827^{\circ}$  E and  $-1.367^{\circ}$  E longitudes and  $-6.618^{\circ}$  N and  $5.818^{\circ}$  N to  $6.353^{\circ}$  N to  $6.141^{\circ}$  N latitude. Most parts of the study area falls within the Ashanti region of Ghana and it covers an area of  $4464.69 \text{ km}^2$ . The location encloses Adansi East, Assin, and Adansi West at the southern part, the Amansie East, Birim North,

Kwaebibirem, Ejisu Juabeng, East Akim, Asanti Akyem North, Asanti Akim South and the Bosomtwe/Atwima/Kwanhoma district at the northern part. It is approximately 34 km south east by road from the country's second largest city Kumasi, 133 km north west from Accra and 82 km north from Cape Coast. The area is drained by the Pra, Anum, Afram and Ofin rivers. Lake Bosomtwe which lies 28 km south-east of Kumasi occupies an area of 48 square kilometres at the northern part of the study area.

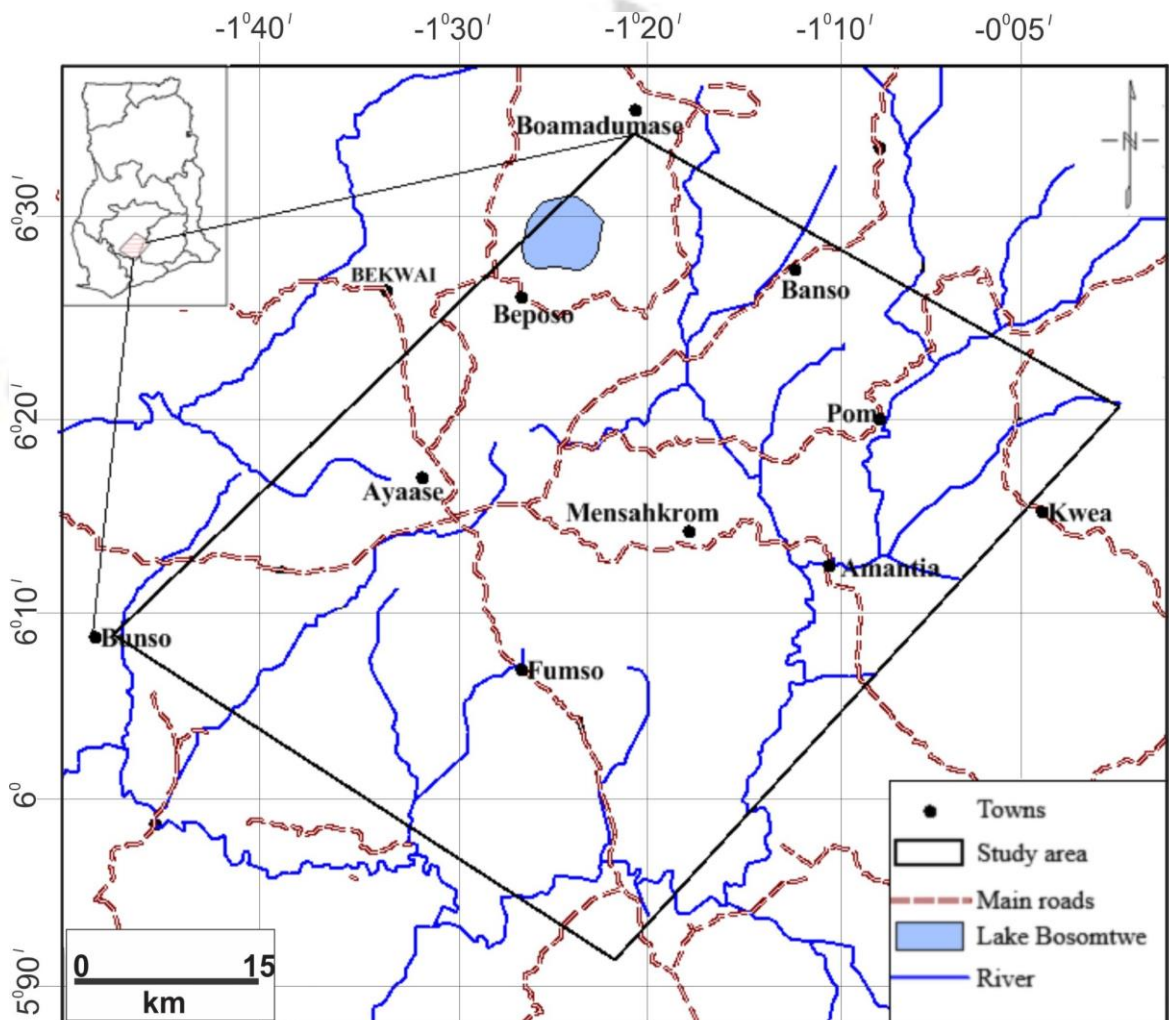


Figure 5.1: The Beposo study area

#### 5.1.1.2 Climate

Climatic data for the area within which location falls, gives 26 degree Celcius mean temperature with 1,465 mm average annual rainfall. The area is also subjected to tropical rainfall for most of the year with two rainy seasons, one between September to October averages 186 mm per month and the other between May and July averages 160 mm per month. When the dry and dusty Hamattan wind blows southwards off the Sahara desert, the area experiences the driest period from January to March. During the dry season daily temperature range from 22 degree Celcius to 30 degree Celcius and rainfall averages 54 mm per month, with humidity averaging 80 per cent (Griffis et al., 2002).

#### 5.1.1.3 Physiography

The area falls within the plateau of South Western Ghana. The general level of peneplanation varies between 152 to 305 meters and is broken by such hills as Atewa and Atewiredu (753 meters); Aya-Tinte (700 meters); Kwamisa (776 meters); Bonsa (643 meters); Wiawso (697 meters) and Banda (552 meters) (Kesse, 1985).

#### 5.1.1.4 Vegetation

The area is situated in the moist semi-deciduous forest zone which is characterized by thick canopy tall trees with a stratum of evergreen shrubs and shorter trees in the undergrowth. It is dominated by tropical hard woods such as odum, wawa, ofram, asamfra, mahogany, teak, bamboo and okyenkyen. Industrial crops such as cocoa, oil palm, coffee, mango and

citrus are also found in the area. However, the moist semi-deciduous forest zone is prone to disturbances by wild-fires and colonization of various grass species.

#### 5.1.1.5 Economic Activities

Agriculture is the dominant economic activity in the region. Other activities include timber processing and mining. The most important crop grown in the region for export is cocoa and the heaviest production areas are at Adansi and Ahafo-Ano. At the forest zone, Oil palms are grown with concentrations in the Asante Akim, Amansie, Adansi and Ejisu - Juabeng districts. Food crops grown include vegetables, maize, cocoyam, cassava, yam groundnuts and plantain. The next major foreign exchange earner after cocoa, Gold, is mined at Obuasi, the richest and largest gold mine in the country and it is still believed to have large reserves, though it has been mined for several years.

### 5.1.2 MATERIALS

#### 5.1.2.1 Available Geophysical Data-Sets

High quality airborne radiometric and magnetic data were acquired by the Geological Survey of Finland (GKT) in collaboration with Ghana Geological Survey Department and Ghana Minerals Commission in 1997-1998. Table 5.1 and Table 5.2 show survey specification and equipment for data acquisition.

### 5.1.2.2 Metadata

The Geophysical data-sets were collected with the following equipment specification (Table 5.1) and survey parameters (Table 5.2)

Table 5.1: Equipment Specification for data acquisition (Geological Survey of Ghana, 1998)

SURVEY EQUIPMENT	AIRCRAFT (FIXED WING)	MAGNETOMETER	SPECTROMETER
Equipment types	Cessna Titan 404 (C-FYAU)	cintrex Cesium SC-2	Exploranium GR 820-256 with 2048 in <sup>3</sup> NAI (TI) downward looking crystal and 256 in <sup>3</sup> upward looking crystal

Table 5.2: Survey specification for data acquisition (Geological Survey of Ghana, 1998)

SURVEY PARAMETER	PARAMETER SPECIFICATION
Year	1997-1998
Travel line spacing	400 m
Travel line direction	NW-SW
Tie line spacing	5000 m
Tie line direction	NE-SW
Nominal Terrain clearance	70 m
Navigation	Global Positioning System (GPS)
Sampling time	0.1 s (MAGNETICS), 1.0 s (RADIOMETRICS)
Air speed (nominal)	250-290 km/h, 70-80 m/s
Measurement spacing	8 m (MAGNETICS), 80 m (RADIOMETRICS)

### 5.1.3 METHODOLOGY

Fig 5.2 shows the research methodology.

#### 5.1.3.1 Data Processing

Sequential processes of editing, gridding, and Earth's background magnetic field removal were involved in the processing of the aero geophysical data set. Some corrections like

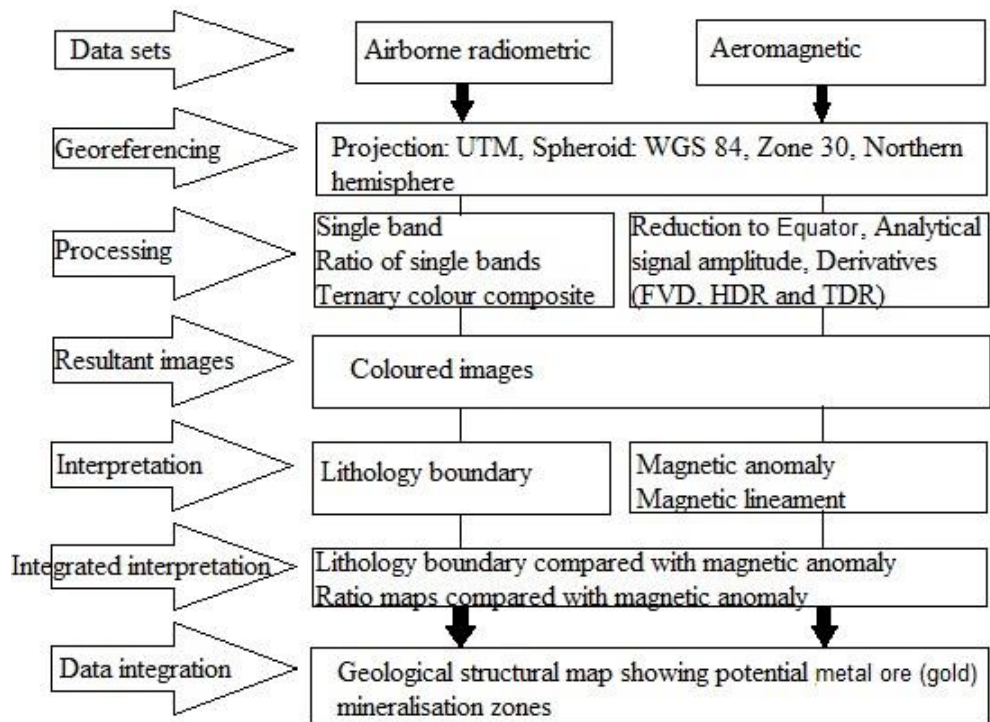


Figure 5.2: Research methodology flow chart

aircraft heading, lag error between aircraft and the sensor, instrument variation, removal of diurnal variation, background correction (Aircraft, Radon and Cosmic), stripping and inconsistencies between flight lines and tie lines were made by the Geological survey of Finland (GTK).

### 5.1.3.2 Pre-Processing

The data sets acquired from the Geological Survey of Ghana were geo-referenced to Universal Transverse Mercator Coordinate System, zone 30 of the northern hemisphere using GeoSoft software.

### 5.1.3.3 Aeromagnetic Data

The main processing phase here comprises three steps:

- calculating Residual magnetic intensity by subtracting the DGRF from the measured magnetic response,
- removing any apparent residual errors by micro-levelling the entire data set and
- gridding

# KNUST

The magmap tool (Oasis montaj, GeoSoft) which offers a number of tools was used to aid calculation of the residual grid (total magnetic response minus the IGRF at each station) for the right time of year. After, the following filters were applied to the magnetic anomaly grid calculated (Residual magnetic intensity):

- Reduction to Equator (RTE): The RTE was calculated using the Residual magnetic intensity grid to produce the RTE grid by utilizing an azimuthal transforms in the frequency range to reduce the directional noise introduced by the low geomagnetic latitude (Philips, 1997).
- Analytical Signal (AS): The residual magnetic intensity grid was again subjected to the AS transform. AS defined the position of magnetic body edges regardless of magnetic field inclination and or unusual magnetisation (GETECH, 2010).
- The First derivative(1VD) and Horizontal derivative (HD): The 1VD and HD were calculated using the RTE. The 1VD helped to delineate low amplitude signatures more clearly where they are obscured by large amplitudes, low frequency anomalies and hence revealed more structural detail. 1VD in gray scale enhanced linear features in the area. The HD in a map form also helped in the identification of geologic boundaries in the study area.

- Tilt Derivative (TD): The TD brought out short wavelengths and revealed the presence of magnetic lineaments as well as boundaries of magnetic bodies within the study area using its zero-crossing.
- Rose diagram for lineament analysis: A rose diagram was used to display graphically the lineament distributions according to their length and orientation to add more meaning to the geological structures in the study area.

#### 5.1.3.4 Aeroradiometric Data

The Grid and Image tool was used to create single count images after which ratio enhancement techniques were applied. Gold deposits show increase in potassium (K) and thorium (Th), which indicate that, Th, which is generally considered very immobile, was harnessed in altered hydrothermal systems. To assist the identification of regions with high concentrations of Th and K, image maps were developed (Silva et al., 2003). An image map for uranium was also used to develop a ratio map of uranium and potassium (U/K). This can show granitoid rocks associated with low uranium and high K concentration. According to Boyle (1979), the low uranium concentration in such a process is as a result of pervasive hydrothermal alteration.

Other ratio maps were also created to take out lithological effects and differences in the data caused by changes in non-planar source geometry, soil moisture and errors associated with latitude correction. For example U/Th and U/K ratios were created to determine areas of high relative proportions of uranium.

#### 5.1.3.5 Other Data-set

Topographic data of the area was also made available in the form of a database.

# KNUST



## CHAPTER 6

### 6.1 RESULTS AND DISCUSSION

#### 6.1.1 Digital Elevation map

The digital elevation map (fig 6.1) of the study area showed both high and low lands with values ranging between 334.43 m maximum and 96.59 m minimum. High lands dominate the central, N-SW parts with values ranging between 334.43 m and 130.85 m. Low lands dominate the S-SW and S-SE parts of the study area with values between 130.85 m and 96.59 m.



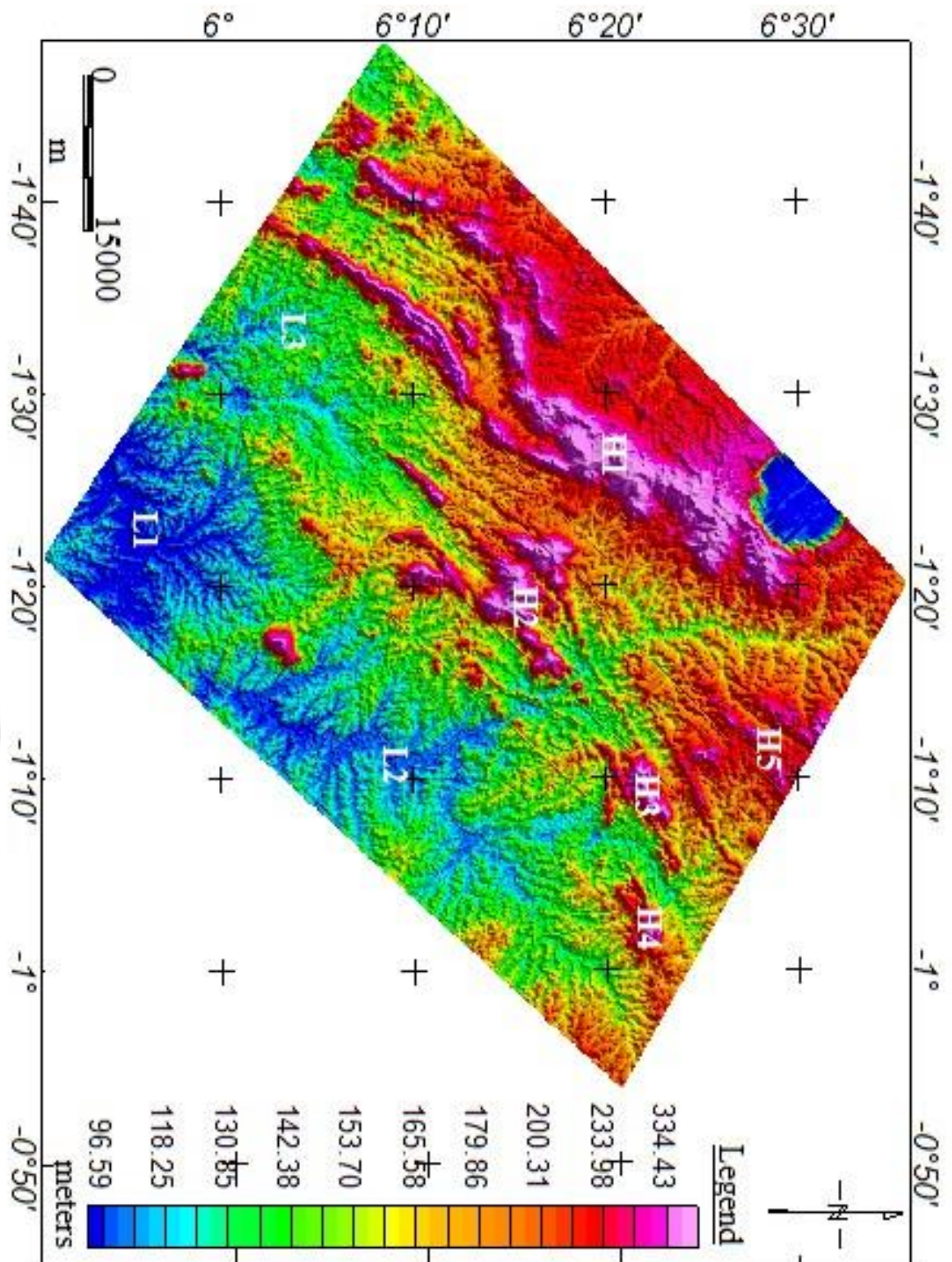


Figure 6.1: Digital elevation model showing high and low lands in the Beoso area Very high lands (H1) correlated with the Birimian meta-volcanics. Two of the belt type granitoids (H5) also correlated with a high lands. Very low lands (blue (L1, L2 and L3)) correlated with the areas which host River Pra and Ofin and lake Bosomtwe.

## 6.1.2 Qualitative interpretation of Airborne Magnetic Data

In order to carry out a qualitative interpretation of the airborne magnetic data, Residual Total Magnetic intensity (RTMI) map of the study area in colour aggregate was produced using Oasis montaj GeoSoft software. The Residual Total Magnetic Intensity map revealed variations in the magnetic intensity throughout the area.

### 6.1.2.1 Residual Total Magnetic Intensity (RTMI)

The RTMI (fig 6.2) was computed by subtracting the regional magnetic intensity from total magnetic response of the area. The area is marked by both high and low magnetic closures with total magnetic intensity values between -392.41 nT maximum and -608.43 nT minimum. Because the magnetic data was collected from areas near low geomagnetic latitudes, places expected to have low magnetic anomalies, have high magnetic anomalies and vice-versa. The Birimian meta-sediments (A1-B1, A3-B3) occupying the N-SW and S-SE part have high magnetic anomalies though low magnetic anomalies were expected. The Birimian meta-volcanics (C1-C4) which was expected to have a high magnetic anomaly, gave low Residual magnetic intensity values between -506.75 nT and -608.43 nT indicated by blue colour. Identified belt type granitoids (e.g. B2) showed fairly high Residual magnetic intensity indicated by green colour.

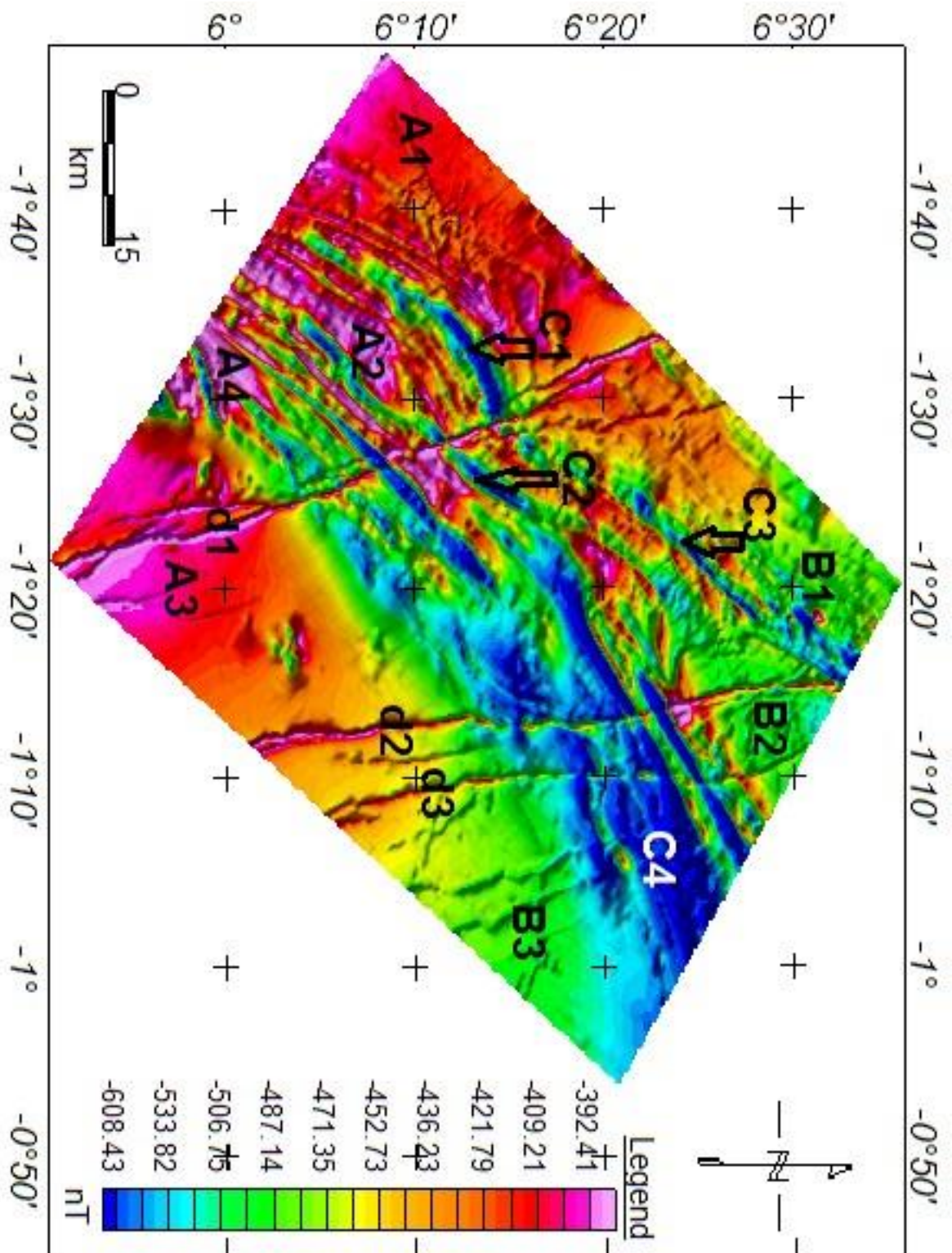


Figure 6.2: Residual Total Magnetic Intensity (RTMI) of study area showing Birimian meta-volcanics (C1-C3), Birimian meta-sediments (A1, A3, B1 and B3), some Tarkwaian sediments (A2 and A4) and identified dykes (d1, d2 and d3)

A fold trending NE with a syncline and an anticline was observed at the south western part of the Tarkwaian. The Birimian group and the Tarkwaian formation are trending in the NE

direction. Three major discordant linear structures, (known in the area as dolerite dykes) (d1-d3) of high magnetic intensity are trending N-S. The discordant nature of these structures show that, they were the last structures to form hence younger than the main formations in the area.

### 6.1.3 MAGNETIC ENHANCEMENT TRANSFORMS

Magnetic enhancement transforms used highlighted different properties of the magnetic field. The different enhancement transforms applied as part of the interpretation process for this study are discussed below:

#### 6.1.3.1 Reduction to Magnetic Equator (RTE)

The RTE shown in fig 6.3 removed asymmetries from the RTMI magnetic anomalies, caused by non-vertical magnetisations and regional field as indicated by (Blakely, 1995). That is, it calculated again the residual magnetic intensity, using an inclination of  $90^{\circ}$  for the magnetic field.

After application of the RTE, low (blue and green) areas in the RTMI showed as high areas in the RTE (fig 6.3) and high areas in the RTMI (magenta and red) showed as low areas in the RTE. The Birimian meta-volcanics which showed a low (blue)(C1-C4) in the RTMI(fig 6.2) now showed as a high (red and magenta) with values between 561.50 nT and 512.50 nT truncated with lows (green) at the northern area and (blue) south western part. The Birimian meta-sediments showed their true signature with high magnetic intensity at the N-NE part with values between 512.50 nT and 478.92 nT. This could probably be due to the

weathered materials from the Lake Bosomtwe impact crater and volcanoclastics from the Birimian meta-volcanics. It could also indicate less or no sediment cover (type of sediments that can give signatures such as in A1-A3).

# KNUST



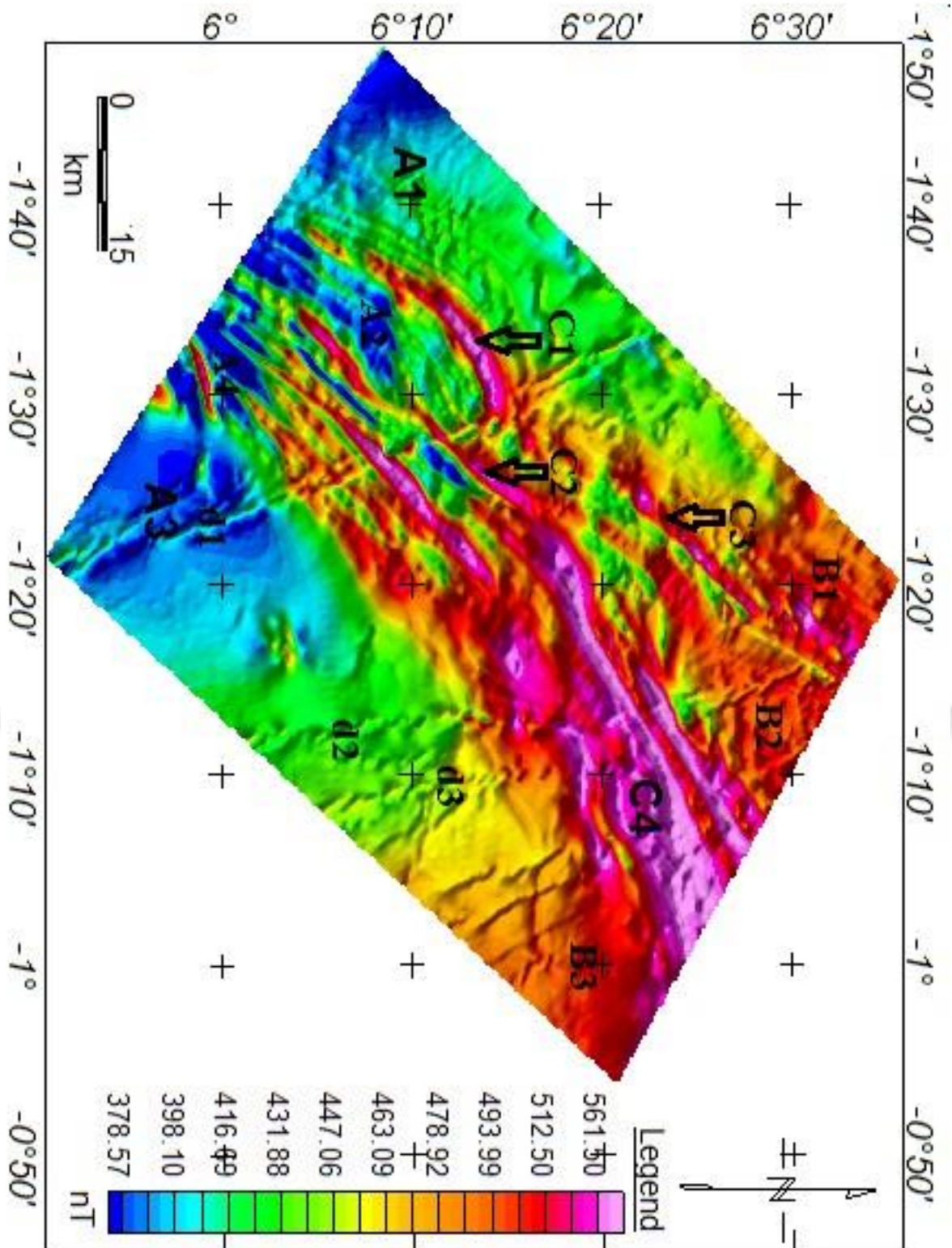


Figure 6.3: Reduction to the Magnetic Equator transform map of the RTMI (inclination =  $-12.790$  and declination =  $-4.620$ ) of study area

At the western and eastern part of the Birimian meta-sediments, moderately high magnetic closures were observed with values between  $478.92$  nT and  $416.69$  nT indicating the

presence of moderate thickness of sediment cover (type of sediments that can give signatures such as in A1-A3). Low magnetic closures in the whole of the S-SW part showed values between 416.69 nT and 378.57 nT indicating the presence of high thickness of sediment cover. Belt type granitoid showed high magnetic intensity with values between 512.50 nT and 493.99 nT indicated by red colour. Basin type granitoid were seen to be having a moderately high magnetic intensity values between 478.92 nT to 416.69 nT indicated by green colour. The three main formations (Birimian group, Tarkwaian group and the granitoids) observed in the RTMI could be seen also in the RTE trending in the north east direction with the three late major discordant linear structures (from fig 6.2) which trend N-S, showing high (red, yellow, green) to low (blue) magnetic intensity, not shown clearly.

#### 6.1.3.2 Analytical Signal (AS)

The analytical signal shown in fig 6.4 was calculated using the RTMI to remove asymmetries from the RTMI. It produced maxima directly over discrete bodies and their edges. The width of the maxima being indicative of the depth of the body (MacLeod et al., 1993).

Formations such as the Birimian sediments, the Tarkwaian formation and the granitoids (G) were depicted clearly with the exception of one of the belt type granitoid (one circled in black). The Birimian meta-sediments showed low magnetic anomalies as it should with values between 0.04 nT/km to 0.00 nT/km, indicated mostly by blue and green colour at the northern part. The Tarkwaian showed high magnetic anomaly fringes with values between

0.27 nT/km and 0.06 nT/km indicated by red/magenta to green colours and the Birimian meta-volcanics showed high magnetic anomaly with values ranging between 0.27 nT and 0.11 nT.

# KNUST



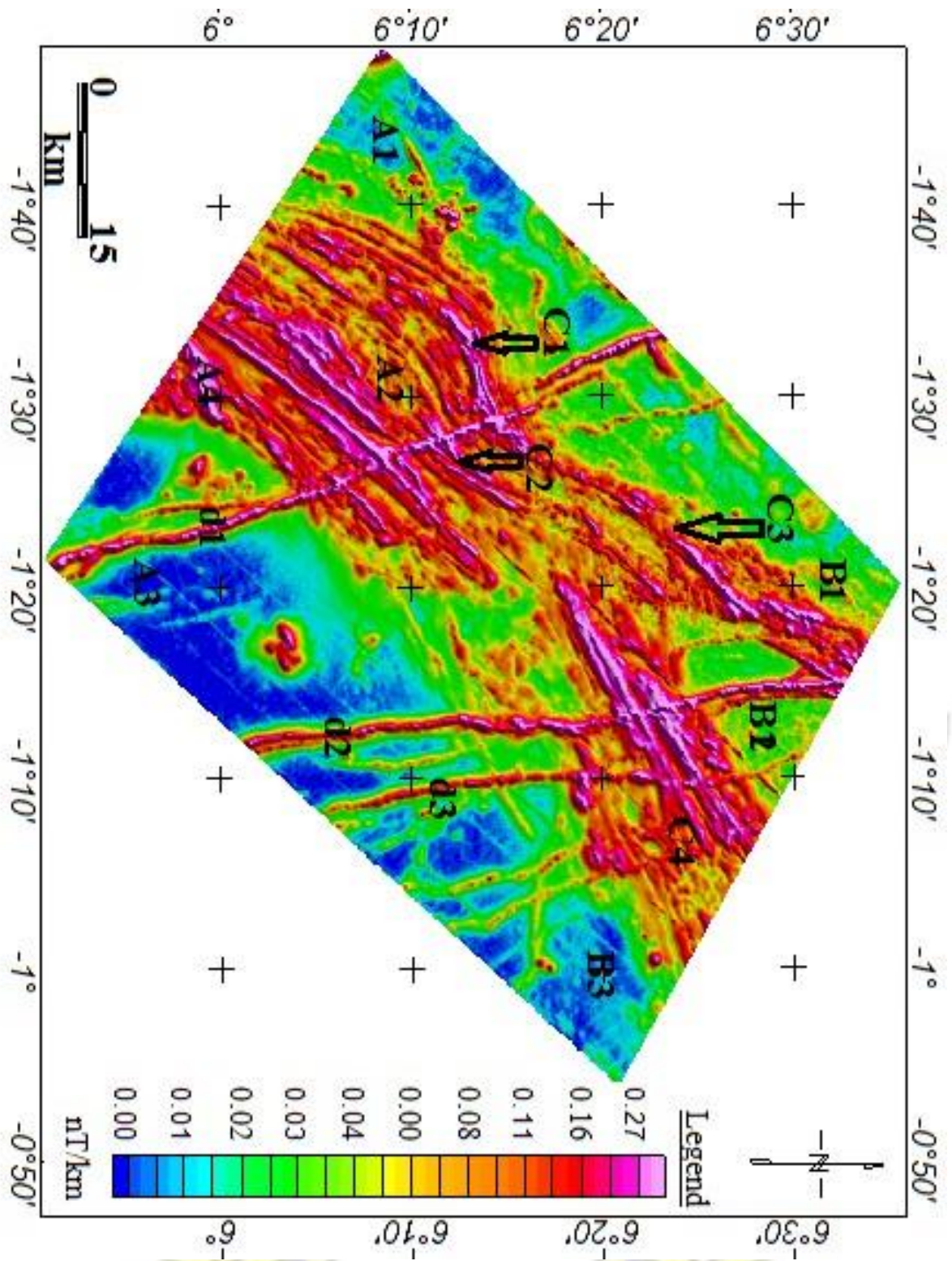


Figure 6.4: Analytical signal transform map of study area showing main lithologies (G, B and T) with the boundary of one circled in black not clearly shown

The thickness of the Tarkwaian (T) stripes showed that it is shallow seated than the Birimian sediments and additional offsets in magnetic highs showing breaks in source body were clearly shown. Main formations are trending NE-SW with the three major late discordant

structures (identified as dykes)(also in fig 6.2), having high amplitude signal with values between 0.27 nT/km to 0.16 nT/km, trending N-S. Generally the AS gave signatures similar to the RTE signatures but was more dependable than the RTE.

### 6.1.3.3 First Vertical Derivative (1VD)

The 1VD (fig 6.5) was calculated using the AS. 1VD showed shallow source anomalies, as well as deep source anomalies and contacts of magnetic sources. As magnetic sources get deeper, the magnetic anomalies associated with them became broader and less intense and decrease in the intensity of the magnetic anomalies indicated that source depth increase vertically or that they were uplifted and eroded (Blakely, 1995). Areas on map where magnetism has been destroyed revealed more structural details and the 1VD in gray scale also enhanced linear features in the study area. The decrease in magnetic intensity anomalies of the Birimian meta-sediments and the granitoids compared with the Tarkwaian indicates that the source depth increases vertically and also it indicates the fact that the Birimian meta-sediments and granitoids are deep seated than the Tarkwaian formation. Structures observed (fig 6.6 and 6.9) are trending NE- SW with the late dykes still trending in the N-S direction but of low magnetic signature with a value of -0.27 nT/km equal or more than the values of the high magnetic signatures (0.14 nT/km and above). This is probably a results of the highly depleted magnetite along these areas or reversed polarity.

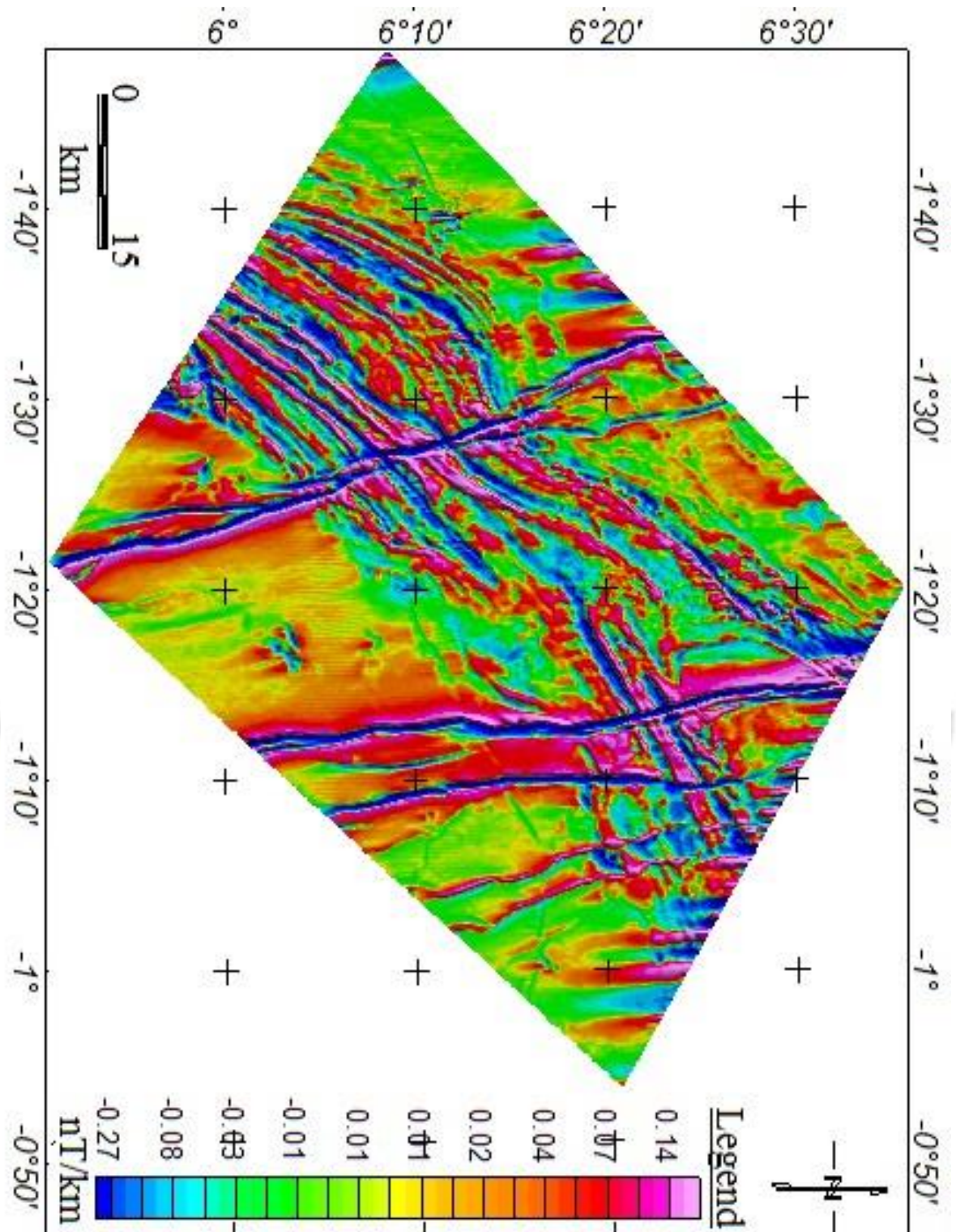


Figure 6.5: First Vertical derivative map (calculated on RTP) of study area, showing deep (the Birimian and granitoids) and shallow seated (Tarkwaian) features and also areas of magnetic reversal

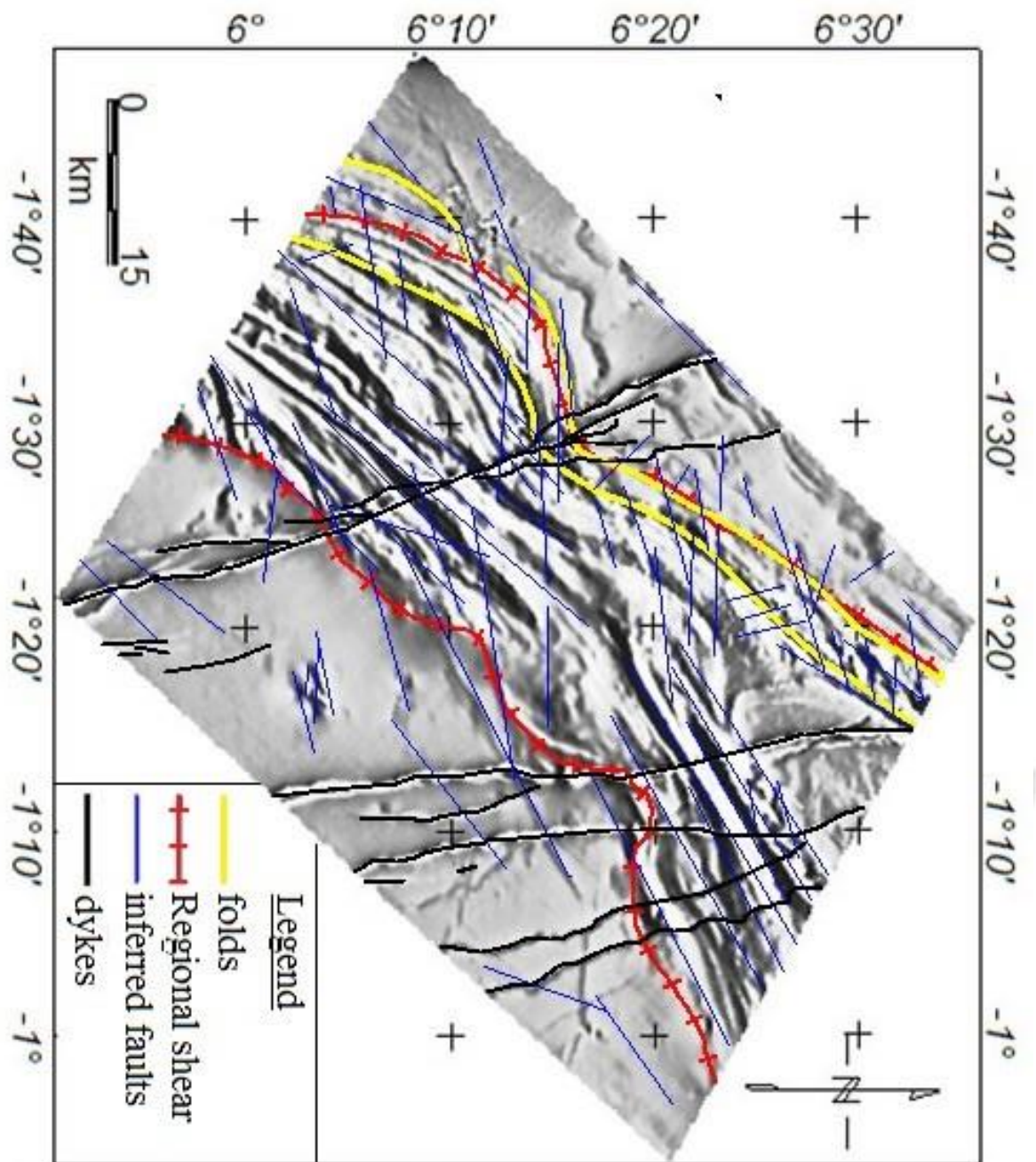


Figure 6.6: Interpreted geological structures overlain on FVD of the study area in grey scale to enhance geological structures in the study area

#### 6.1.3.4 Horizontal Derivative (HD)

After applying the analytical signal transform, the horizontal derivative was calculated to produce maximum ridges over the edges of magnetic basement blocks and faults or other magnetic bodies in the area. This highlighted linear features related to contacts in the data

sets. Structures as observed in Figures 6.7 are trending in the NE-SW direction with late dykes trending in the N-S. It also confirmed the fact that there is polarity reversal or complete depletion of magnetite at areas hosting dykes.

# KNUST



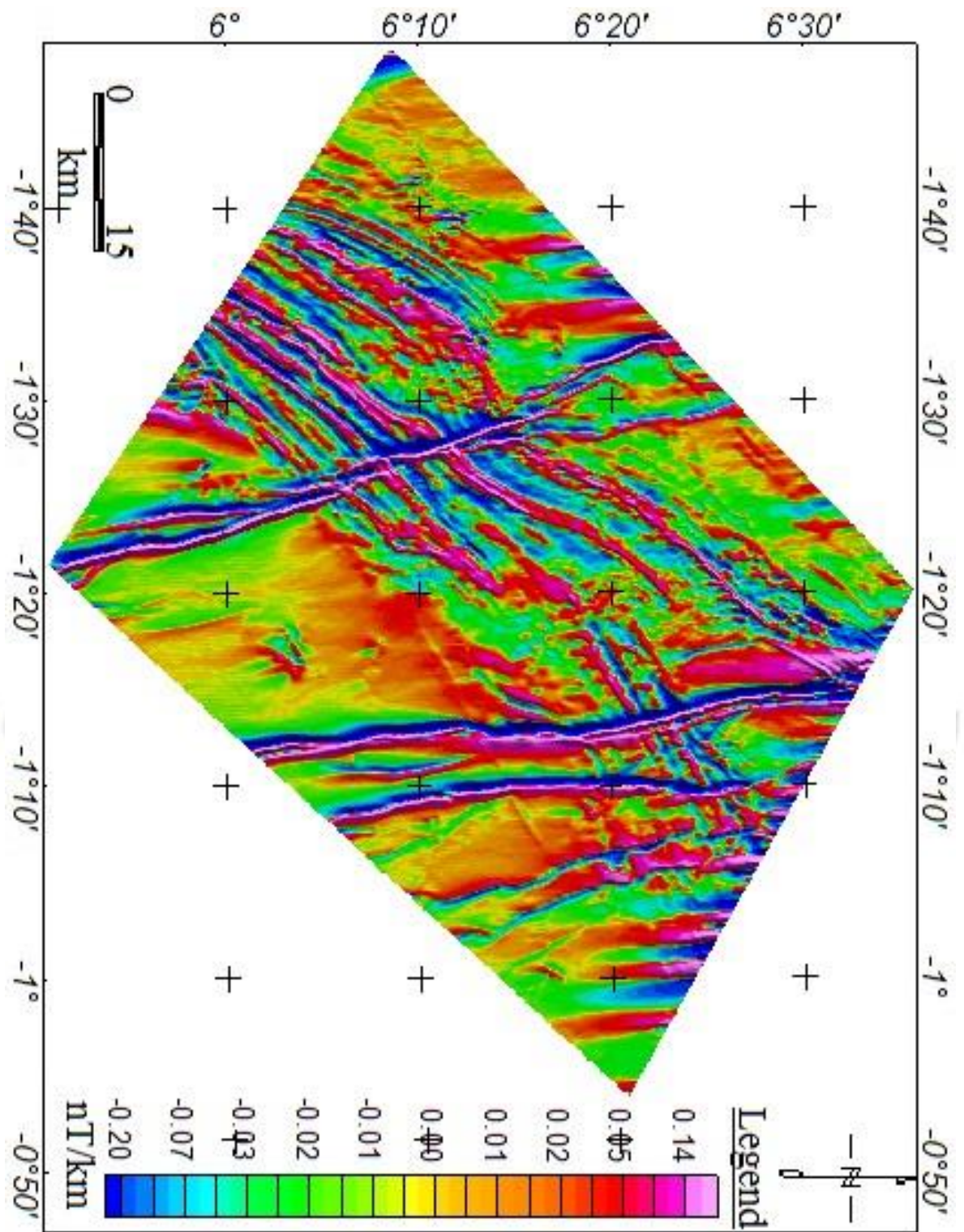


Figure 6.7: Horizontal derivative map (calculated using the RTE) of study area showing maximum ridge (magenta colour) over edges of magnetic basement blocks and linear features related to contacts in the data sets

#### 6.1.3.5 Tilt Derivative (TD)

Applying the tilt derivative highlighted signatures of shallow magnetic sources and so gave some guidance on interpreting known lineaments and zones. The TD (fig 6.8) of a residual magnetic field enhanced weak magnetic anomalies, otherwise overshadowed by stronger structures in the area improving subtle fabric.



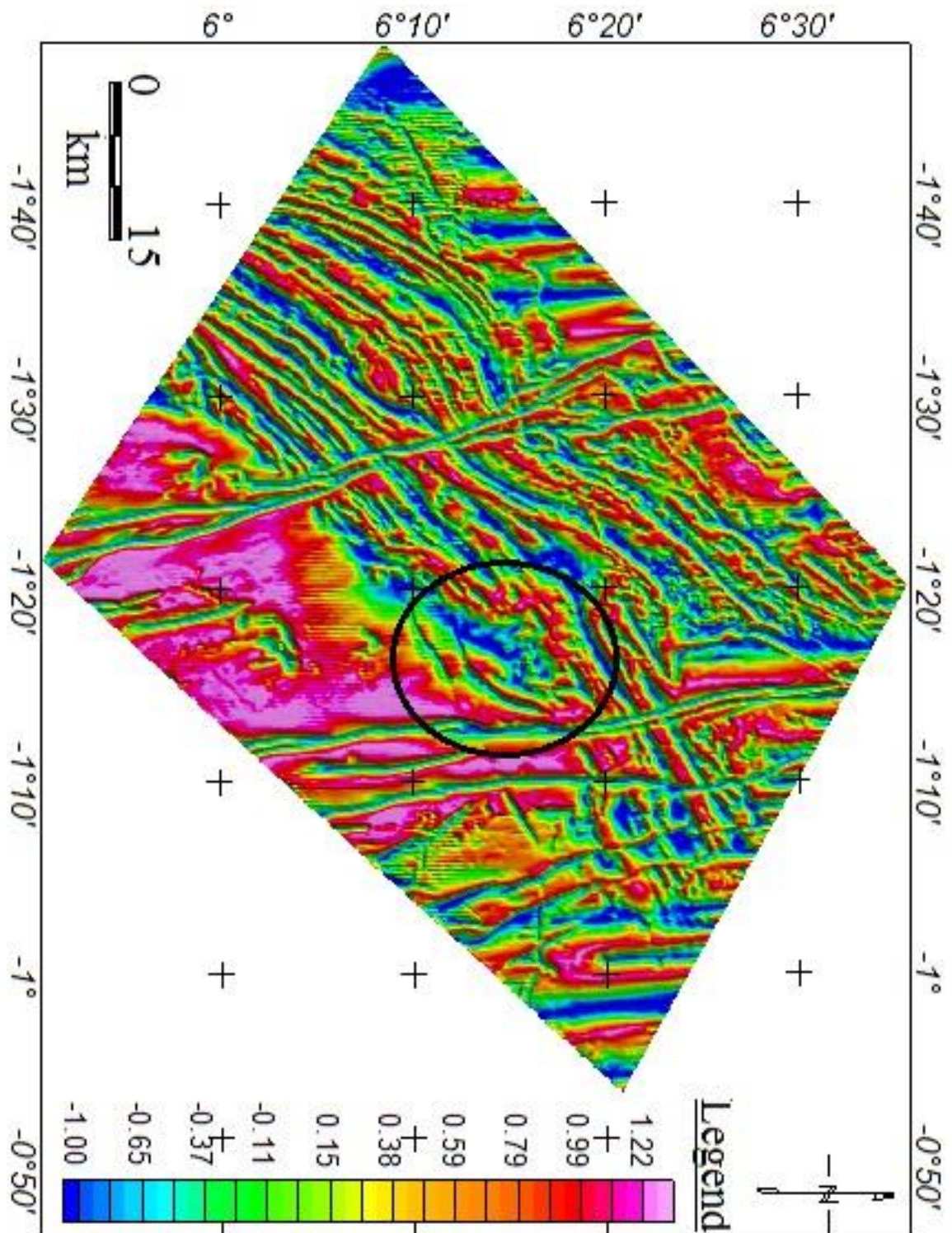


Figure 6.8: Tilt derivative map of the Beposo study area with improved fabric (e.g area circled in black compared with same area on Analytical Signal)

The area circled in black, with partly undefined boundaries in the AS map (fig 6.4) can now be seen clearly on the TD map (fig 6.8), indicating the effect of TD improving subtle fabric.

Again the late dykes trending N-S, are showing reversed polarity or indicating that there is a complete depletion of magnetite in areas hosting these structures. Structures are trending NE-SW direction (fig 6.9).

#### 6.1.4 GEOLOGICAL STRUCTURES

The structural interpretation was carried out using the analytical signal, first vertical derivative, horizontal derivative and the tilt angle derivative maps. Lineaments identified were then placed on a grey scale of the 1VD (fig 6.6). The major structural systems are well defined on the magnetics. The more outstanding features are:

- N-S dykes (fig 6.9) with some dipping to the west, having high analytic signal amplitude with highly depleted regions in areas hosting it as indicated by 1VD, HD and TVD.
- an important shear (fig 6.19) known in the area as the Regional /Ashanti shear lies at the contacts of main formations and trends NE-SW. The regional shear produced fuzzy or misty appearance with a weak trend along C3 of the Birimian meta-volcanics (fig.6.2). The shear system is known to host large amounts of deposits and operating mines such as the Prestea mine (6 million oz) and Bogosu mine (7 million oz).
- Set of NE trending major and minor faults (fig 6.9) which are interpreted as high reverse angle structures formed during the NW-SE directed regional compression, were defined. These are probably the principal fluid conduits during the mineralisation events.

- Set of major NE-SW trending folds which probably occurred during the Eburnean deformation, were also defined.

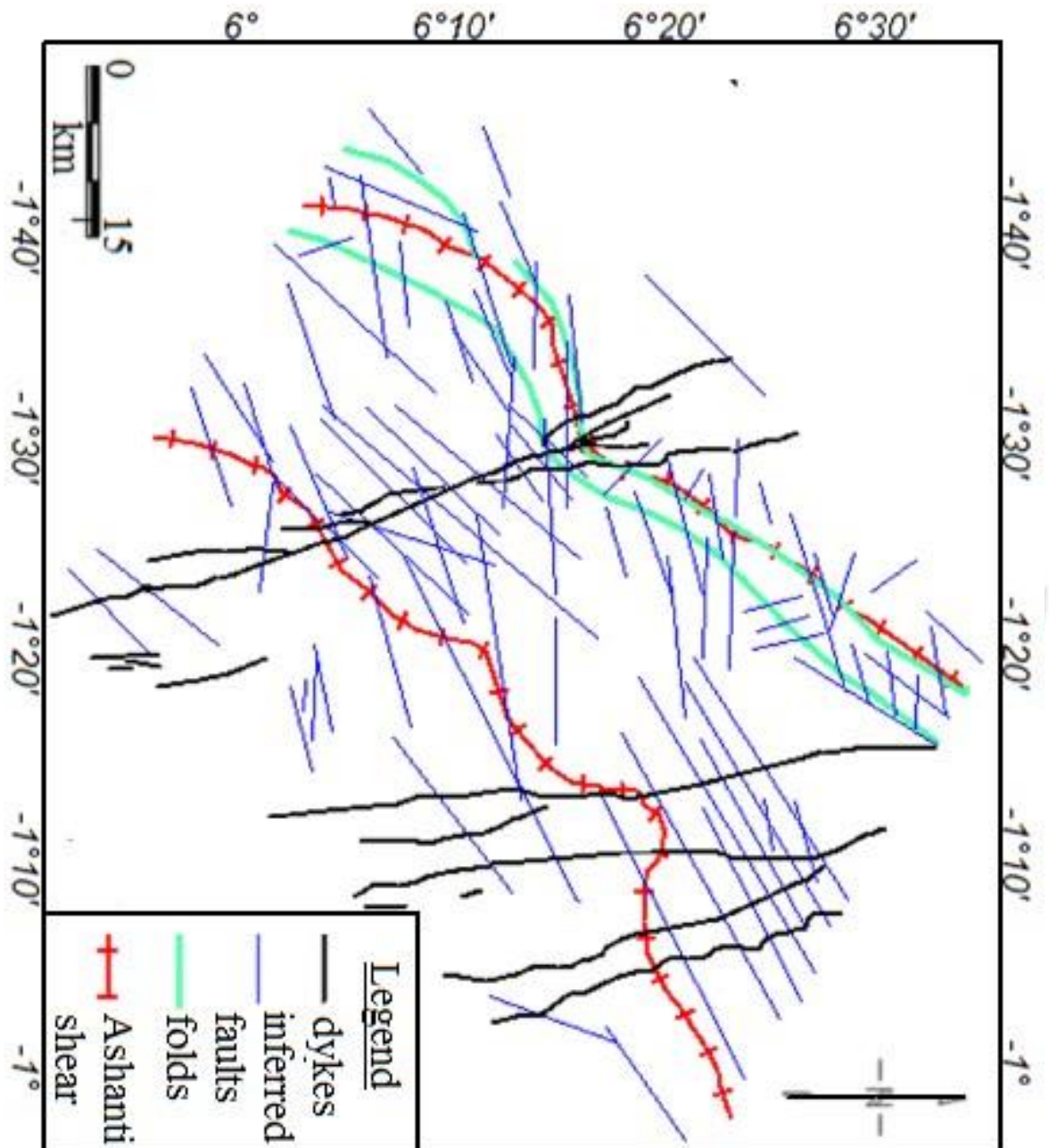


Figure 6.9: Interpreted geological structures of study area from aeromagnetic data

From rose diagram below, most structures in the area are striking between  $0^{\circ}$  and  $80^{\circ}$  (fig 6.10) NE- SW and dipping to the NE between  $30^{\circ}$  and  $90^{\circ}$ .

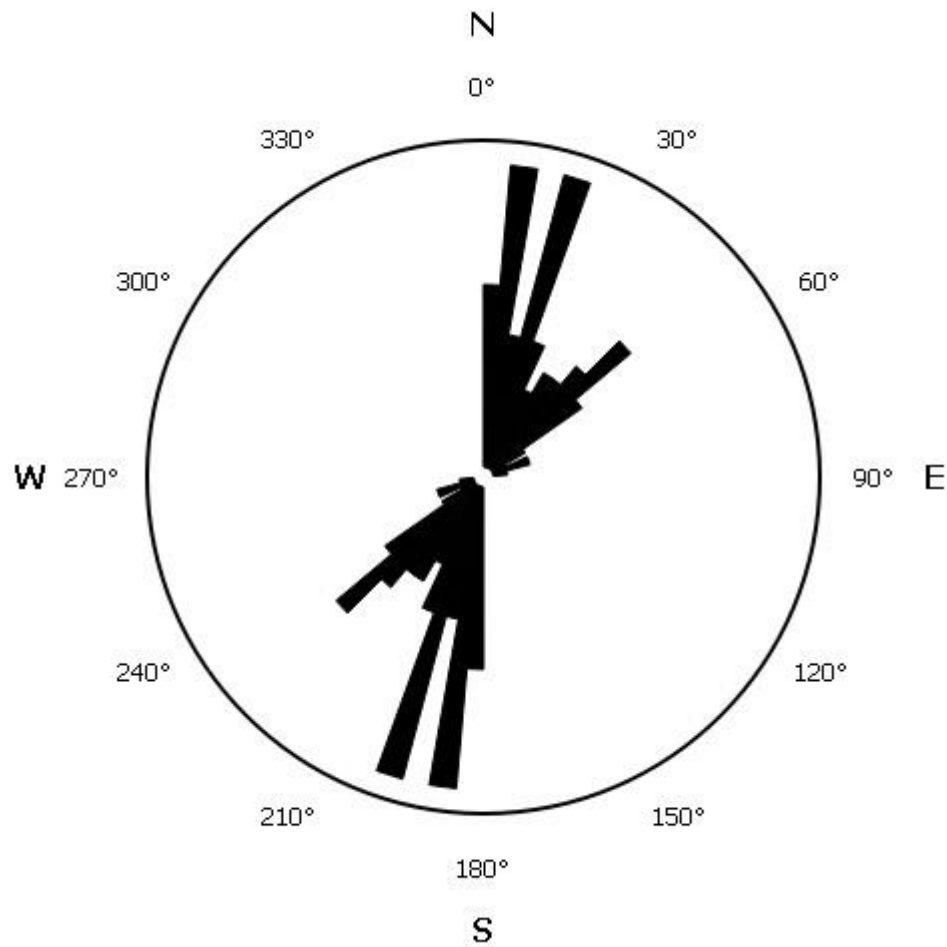


Figure 6.10: Rose diagram of geological structures in study area showing major strike direction and strike angles

#### 6.1.4.1 Deformation and Geological Structures

Geological structures depicted from the airborne radiometric and magnetic data-sets of the Beposo area include faults, folds, dikes and lithological boundaries. Though the meta-volcanics in the study area is prone to weathering, the sequence of deformation has been preserved in the geological structures and the geometry of the granitoid complexes. Observations from the data-sets, especially the magnetic data, showed that the geological structures were developed as a result of multiple deformations since they display faulted and tightly folded bands of Birimian series and Tarkwaian formation.

The trends of the inferred faults as well as the fold planes, dip steeply to the NW and strike to the NE. The area also featured a major, N-S trending, late-stage dolerite dike system that cuts across the Tarkwaian, Batholith and the basin type granitoid and splits up into at least three branches at the NW part of the study area. Different types of mafic intrusives also occur in most of the volcanic belts of Ghana, but they are particularly abundant in the Ashanti Belt and to a lesser degree in the Sefwi Belt. To date, very little attention has been paid to these intrusions and they are generally grouped under a common label. Griffis et al. (2002) noted that within areas dominated by mafic flows, there are numerous feeder dikes and sills with a common affinity to the tholeiitic basalts.

During airborne geophysical data study in the southern part of the Ashanti Belt, Perrouty et al. (2012) suggested five (5) deformational events. These five (5) deformation events, according to Perrouty et al. (2012), corresponds to a time of magmatism between 2200 and 2000 Ma. The first event is associated to a type of shortening called D 1, which occurred before the deposition of the Tarkwaian formation, followed by major tectonic sequence called D 2 -D 3, at around 2.1 Ga, characterised by NE-SW oriented, large folds in the Tarkwaian and Birimian formation. After D 3, two other deformation events D 4 and D5 occurred: D 4 is associated with recumbent folds and sub-horizontal cleavage and then, D 5 with a NW-SE shortening which produced km scale folds.

Sulphides and its associated Gold mineralisation can be correlated with D 1 , D 2 and D 3 deformations according to Allen (2011). From the interpreted structural map (fig. 5.9), three episodes of deformation D 1 -NE, D 2 -NNW and D 3 -NNE were observed. D 1 deformational event produced sets of NE-SW striking regional and local faults. D 2 deformational event resulted mainly in NNW-SSE and NW-SE faults, some of which crossed

earlier D 1 structures. The major thrust faults in fig. 6.9 are attributed to a second phase of deformation (D 2 ) that formed tight to isoclinal, gently and doubly plunging folds and a second cleavage. The D 3 event produced NNE-SSW set of faults and reactivated some D 1 and D 2 faults. Series of NE trending faults which are interpreted as high angle fault structures which formed during regional NW-SE compression dominates the area of study. These defined the lithological pattern in the area with all units striking parallel to these structures. However, there are a few N-S trending fault zones in the area. The mafic intrusions appear to be related to fairly late-stage dilational tectonics associated with regional transgressive shear systems that produced narrow basins filled with Tarkwaian molassic sediments (Strogen, 1991; Ledru et al., 1994). The dilational zones within the complex shear systems probably tapped deep-seated zones of mantle-derived mafic magma (Griffis et al., 2002). More recent work (Kiessling, 1997) which may well apply to most of the region, confirms that the Tarkwaian Formation/Birimian contacts are almost invariably sheared.

#### 6.1.5 LITHOLOGY FROM THE MAGNETIC DATA

The magnetic data defined major lithologic units and bodies under covered areas. The more outstanding signatures are:

- The central core Tarkwaian sediments of high and moderately fringed magnetic anomalies (figs 6.2 and 6.4) showed values that are higher than the underlying Birimian basement. According to (Perrouty et al., 2012), the Birimian should have lithologies with roughly 5 times greater susceptibility than the overlying Tarkwa group in order to visualise structural trends in the Buried Birimian basement. It is

possible therefore, that the magnetic data were not visualising structures in the Tarkwa formation but rather the structures in the underlying relatively Birimian series. So probably the Tarkwaian series was deposited as deltaic sediments in long intra-montane grabens coincident in part with the Birimian group. This observation was also seen by Feybesse et al. (2006).

- Granitoid intrusives have strong magnetic signatures where they outcrop or are close to the surface but low magnetic signatures where they are deep seated. The deep seated type correlated with a basin type granitoid whilst ones close to the surface correlated with the belt type granitoids.
- Birimian meta-sedimentary units were outlined according to their strong to moderate weak magnetic signatures (figs 6.2 and 6.4) since, magnetic mineral content has probably been oxidized to another mineral due to weathering (e.g magnetite oxidized to hematite). They are subordinate to the Birimian meta-volcanics and the mafic intrusive units.
- Birimian meta-volcanics was outlined according to their strong magnetic signatures (figs.6.2 and 6.4).

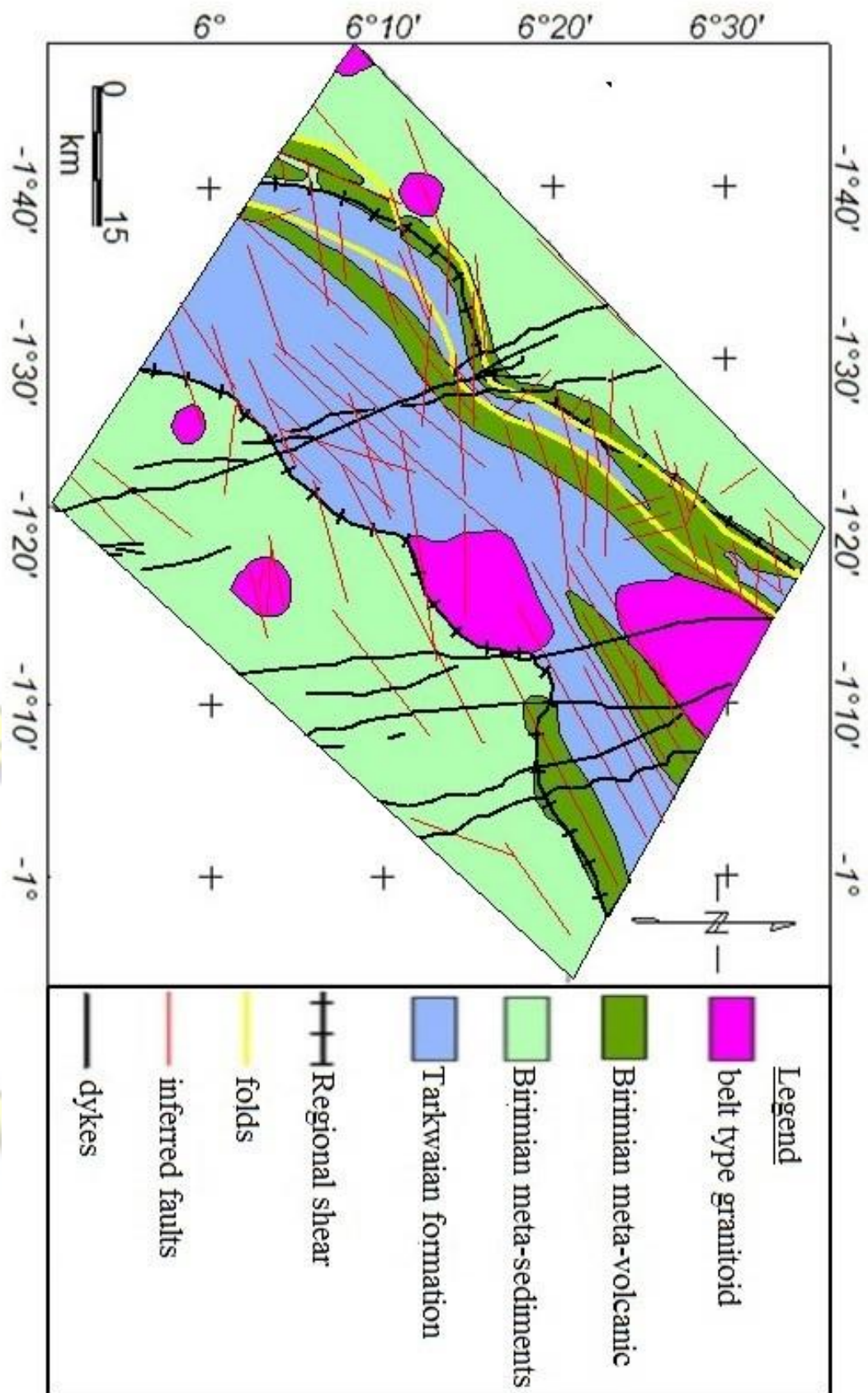


Figure 6.11: Interpreted geological structural map from aeromagnetic overlain with hydrothermal alteration zones

## 6.2 Airborne Radiometric Data Interpretation

Lithological units were discriminated based on the difference in radioelement signatures depicted by colour. Blue colours represent low and magenta represent high concentration of particular radio-elements. The ternary image was also used to display the distribution pattern of the three radio-elements (eTh, eU, K) in red (K), green (eTh) and blue (eU) respectively. Each radioelement was qualitatively classified into low and high concentration, according to the contribution in the ternary images, defined by image colour. Comparison of the enhanced images produced. The geological map produced by (Taylor et al., 1992) compared with the lithological map obtained showed generally good agreement except mismatching of lithological boundaries. In all thirteen lithological units were traced out.

### 6.2.1 Potassium map

The potassium map shown in fig 6.13 showed prominent lithologies which can easily be seen from the K grid. These include; the Basin type granitoid (11) (which intrudes the Birimian assemblage located in the NW part of the study area, bulky in mass and rich in aluminium, the belt type granitoid (1) (which occurs in smaller masses and relatively Na-rich) which according to (Eisenlohr and Hirdes, 1992) is emplaced in the volcanic belt and may be contemporaneous with volcanism of the Upper Birimian. This is located also in the Southern and Northern part of the study area), the Birimian volcanic belt (4) (that runs from the north to the west and also appearing at the south)), the Tarkwaian (5, 6, 7, and 13) (at the central portion which consist of the Huni sandstone (and Dompim phyllite) series made

of quartzites with bands, grits and sandstones of phyllites, the Tarkwa phyllites made of Huni sandstone, sericitic phyllites, greenish grey chloritic and schists, the banket series made of Tarkwa phyllite transitional beds and grits, quartzites, sandstones, breccia's and conglomerate, and the Kawere group made of quartzites, grits, conglomerates and phyllites) and the meta-sediments (2, 3, 8, 9, 10, 11, and 12) seen at the N-SW and S-NE areas.



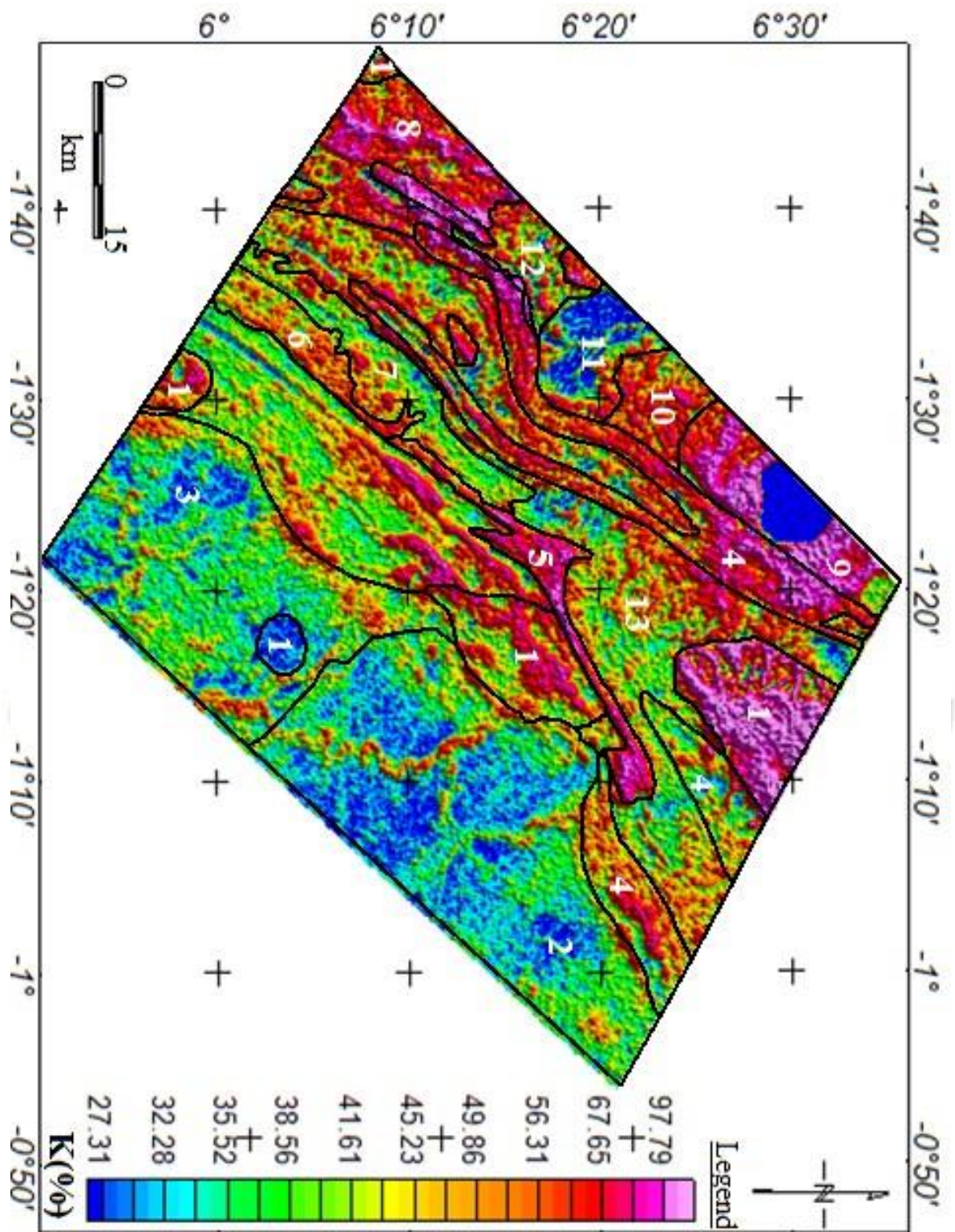


Figure 6.12: Potassium map of study area overlain with identified lithology The Birimian meta-volcanics (4) showed high potassium with values ranging between above 97.79 % to 49.86%. The belts type granitoids (1) also showed high potassium (with the exception of one at the southern part) with values ranging from above

97.79 % to 56.31 %. The belt type granitoid at the SE part of the study area have low potassium because it occurred in a highly sheared area. The basin type granitoid (11) also showed very low potassium with values 27.31% and below. The Birimian meta-sediments at areas near the lake Bosomtwe (9), Birimian meta-volcanics (8, 10 & 12), showed high potassium (red and magenta). These areas correlated with the fairly high lands in the area. The NW part of the area falls within the sheared zones hence has undergone more silification alteration as compared with the unshaped SE part of the study area. The tarkwaian also showed high potassium with values ranging from above 97.79% to 35.52 %.

### 6.2.2 Thorium map

Same distinct lithologies seen in fig 6.13 can be seen also from the eTh channel (fig 6.14). These include; The Birimian meta-volcanics (4) which showed low thorium with high Thorium intercalations. Values ranged between 22.05 ppm to 10.72 ppm. The belt type granitoids (1) showed fairly high Thorium (with the exception of one at the southern part) with values ranging from 18.89 ppm to 16.10 ppm. The belt type granitoid at the southern part of the study area have low thorium also because it occurred in a highly sheared area. The basin type granitoid (11) showed high thorium with values ranging from 27.36 ppm to 18.89 ppm.

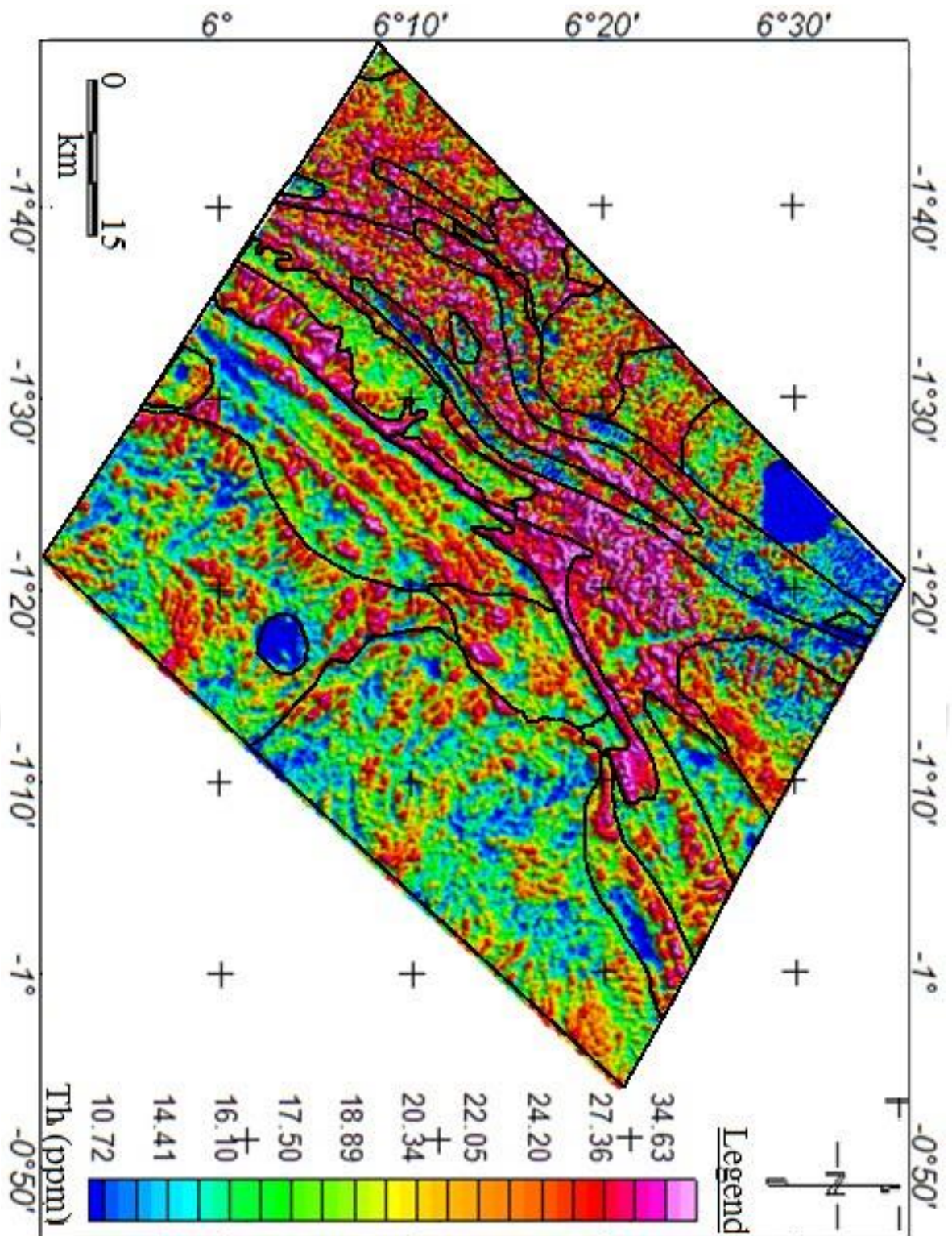


Figure 6.13: Thorium map of study area overlain with identified lithology The Birimian sediments at areas near the lake Bosomtwe (9) have low thorium probably because of silic alteration caused by the impact that created the lake Bosomtwe. Areas near the Birimian meta-volcanics (8, 10 & 12), showed high

thorium (red, magenta and green). These areas correlated with the fairly high lands in the study area. At units 1 and 2, at the right side of the study area, thorium was low with high (red) intercalations (caused by eroded sediments from high lands) probably because the whole of the area is covered with water and hence signal could not be recorded properly because they were attenuated by the water. The Tarkwaian also showed high potassium with values ranging from above 34.63 ppm to 10.72 ppm. Low thorium areas (blue) in the Tarkwaian correlates with areas which comes in contact with other formations.

### 6.2.3 Uranium map

Lithologies seen in fig 6.13 and 6.14 were again seen from the U channel (fig 6.15). These include; the Birimian meta-volcanics (4) which now shows low Uranium with high uranium intercalations. Values range between 14.87 ppm to 9.75 ppm and below. The belt type granitoids (1) showed fairly high Uranium (with the exception one at the southern part) with values ranging from 22.52 ppm to 14.87 ppm. The belt type granitoid at the Southern part of the study area have low uranium again because it occurred in a highly sheared area. The basin type granitoid (11) showed high uranium (with high uranium intercalations) with values ranging from 16.43 ppm to 14.87 ppm. The Birimian meta-sediments at areas near the lake Bosomtwe (9) have very low uranium probably because uranium is mobile and the area is a high land, hence might have been eroded to lower lands. Areas near the Birimian meta-volcanics (8, 10 & 12), showed high uranium (red, magenta and green). These areas correlated with the fairly high lands in the study area. At units 1 and 2, at the right side of

the study area, uranium was high (red and green) probably because the whole of the area is a low land covered with water, hence receives eroded sediments from high lands.

# KNUST



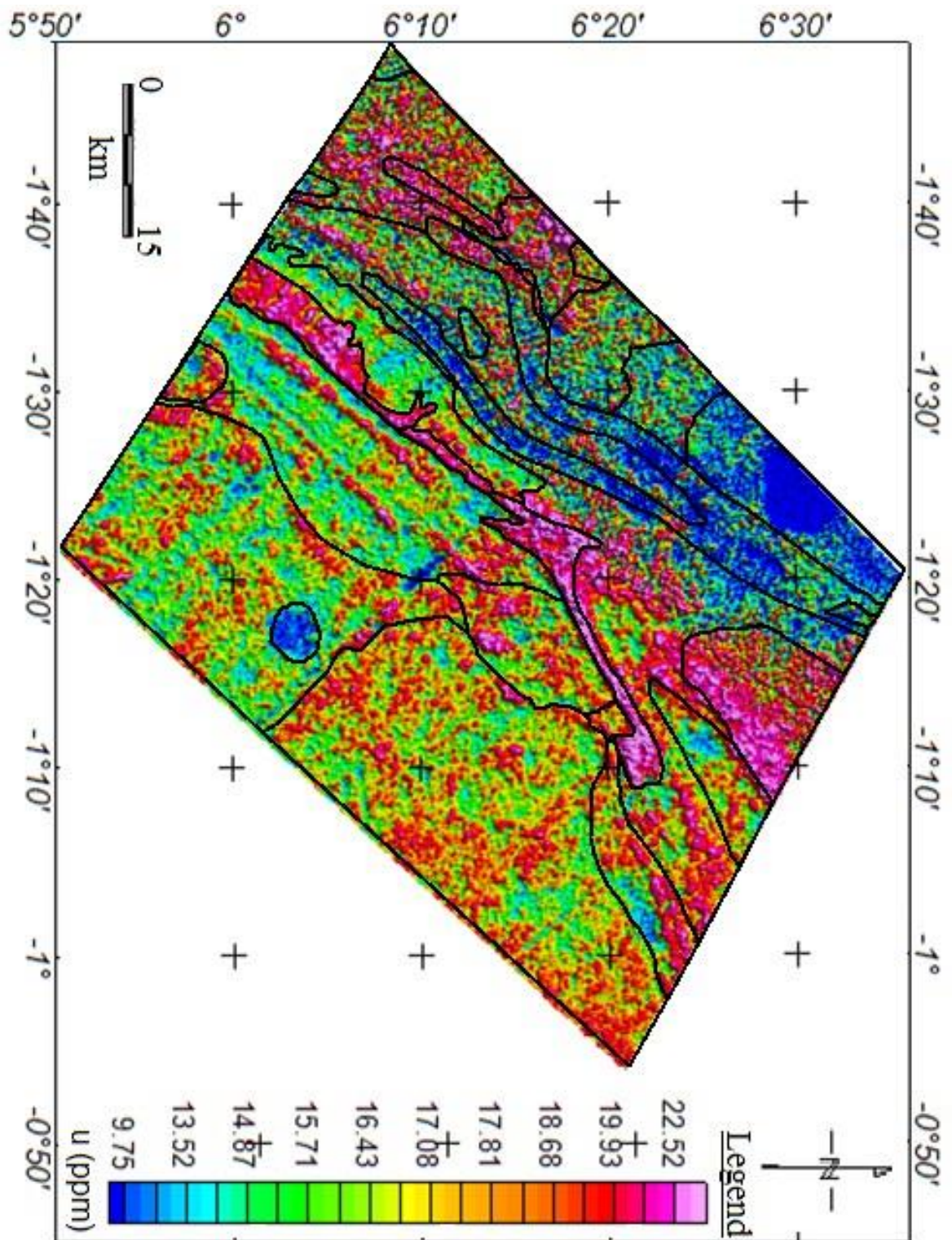


Figure 6.14: Uranium map of study area overlain with identified lithology The Tarkwaian also showed high uranium with values ranging from above 22.52 ppm to

14.87 ppm with the exception of areas that comes in contact with other formations.

### 6.3 RATIO MAPS

Captivating distributions were obtained from the ratio images of the radiometric grids, primarily eTh and eU enriched lithologies were clearly identified, from the eTh/K and eU/K ratios, with respect to K concentration. The Basin type granitoid located in the NW part shows a relatively high eTh and eU concentrations (fig 6.18), the Belt type granitoid located in the Northern part showed low eU and eTh concentration, the Birimian volcanic belt which traverse from the North to the West and also appearing at the South showed a relatively low eU and eTh concentration, the central core Tarkwaian showed relatively high eU concentration and high eTh concentration. The Birimian Sedimentary Basin at the eastern and western edge showed very high eU concentration and high eTh concentration. At the northern edge it showed low eU and eTh concentrations.



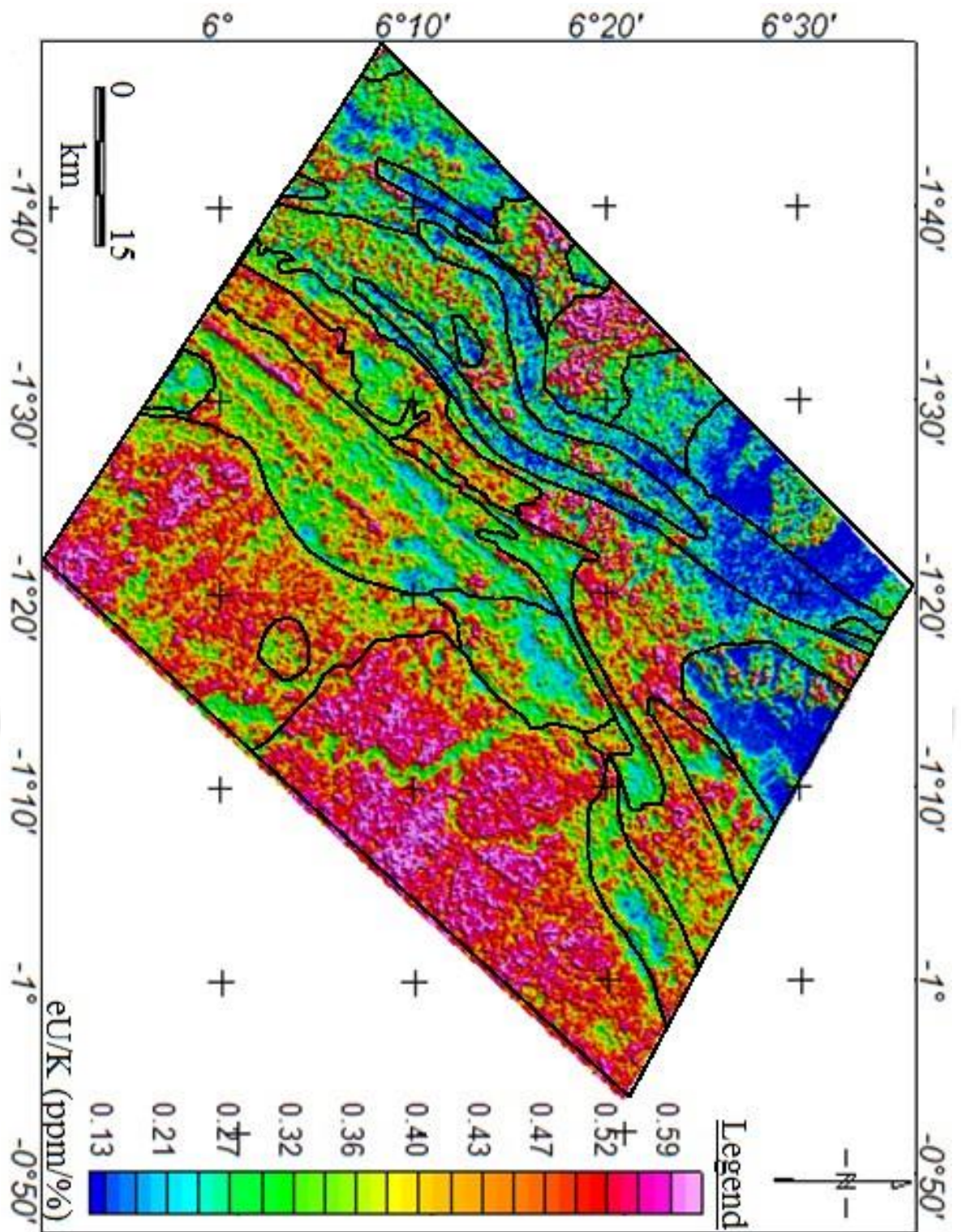


Figure 6.15: eU/K ratio map of study area overlain with identified lithology

### 6.3.1 eTh/K Ratio Map

Low eTh/K ratio (fig 6.17) can easily detect alteration zones because thorium, as a stable element, reflects original pre-alteration compositions (Airo, 2002). eTh levels permit easy field distinction of different granitic units mistakenly mapped as one type. While spectrometry cannot directly locate the base and precious metals, it can detect the K alteration associated with epithermal systems. K or potassic alteration typical of lode gold deposits (which shows elevated K) with anomalous K/eTh ratios along local shear or fracture zones may be indicative of gold bearing mineralisation (Airo, 2002).



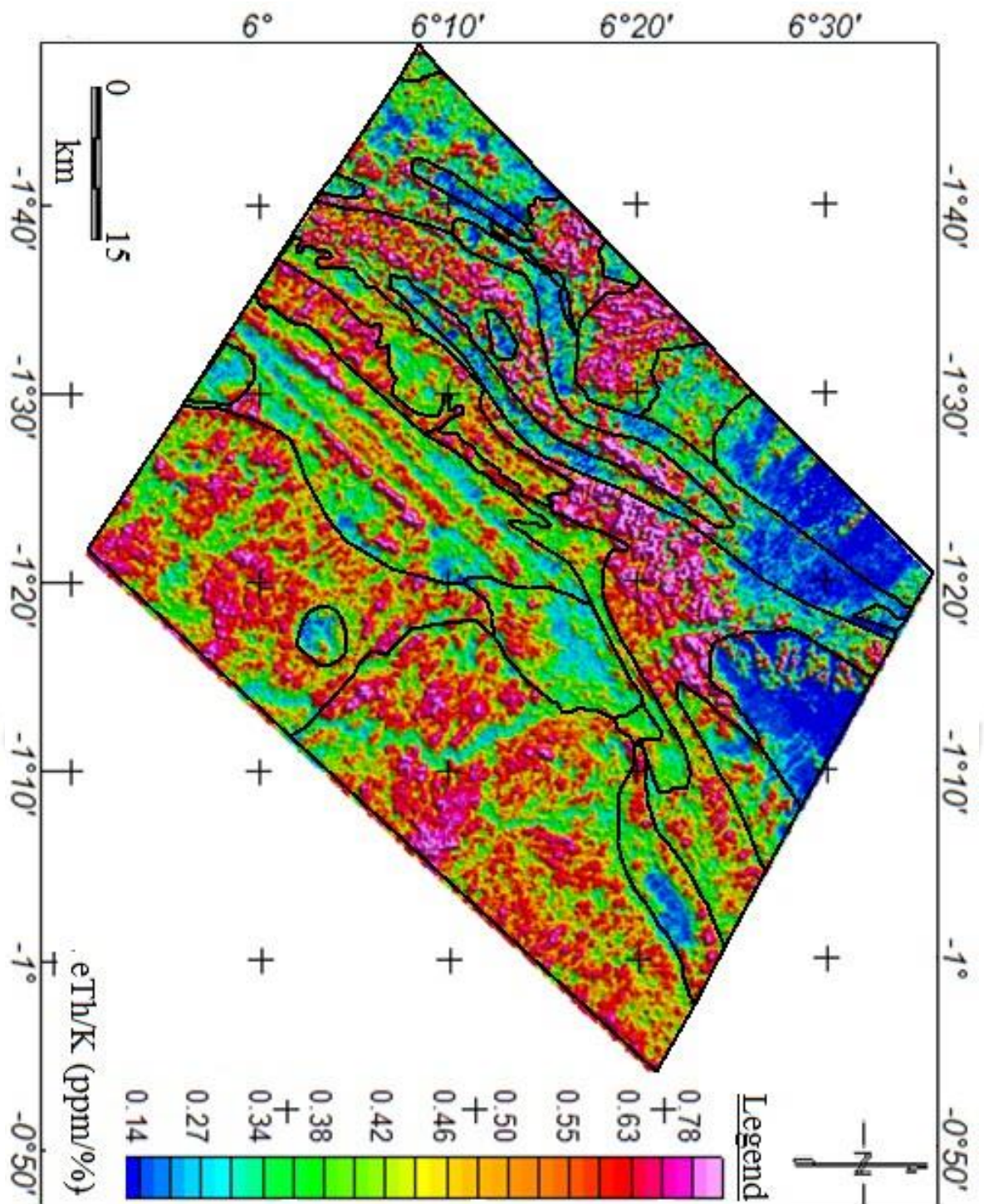


Figure 6.16: eTh/ K ratio map of study area overlain with identified lithology

### 6.3.2 eU/ eTh Ratio Map

Enhanced eU concentrations relative to eTh are characteristic in that their anomalous radio-element ratios are interpreted as partly due to chemical alteration of host rocks, and

partly due to the incorporation of easily eroded sulphide-bearing material into the surrounding till. High  $eU/ eTh$  within sedimentary units associated with locally depleted  $eTh$  points out prospects for sulphidization indicating alteration whereby  $eTh$  was leached out of the meta-sedimentary rocks (fig 6.18 on the right side). Gold and sulphide - bearing mineralisation is often closely connected to hydrothermal altered zones of bedrock and commonly controlled by  $K/eTh$  or  $eTh/K$  ratio.



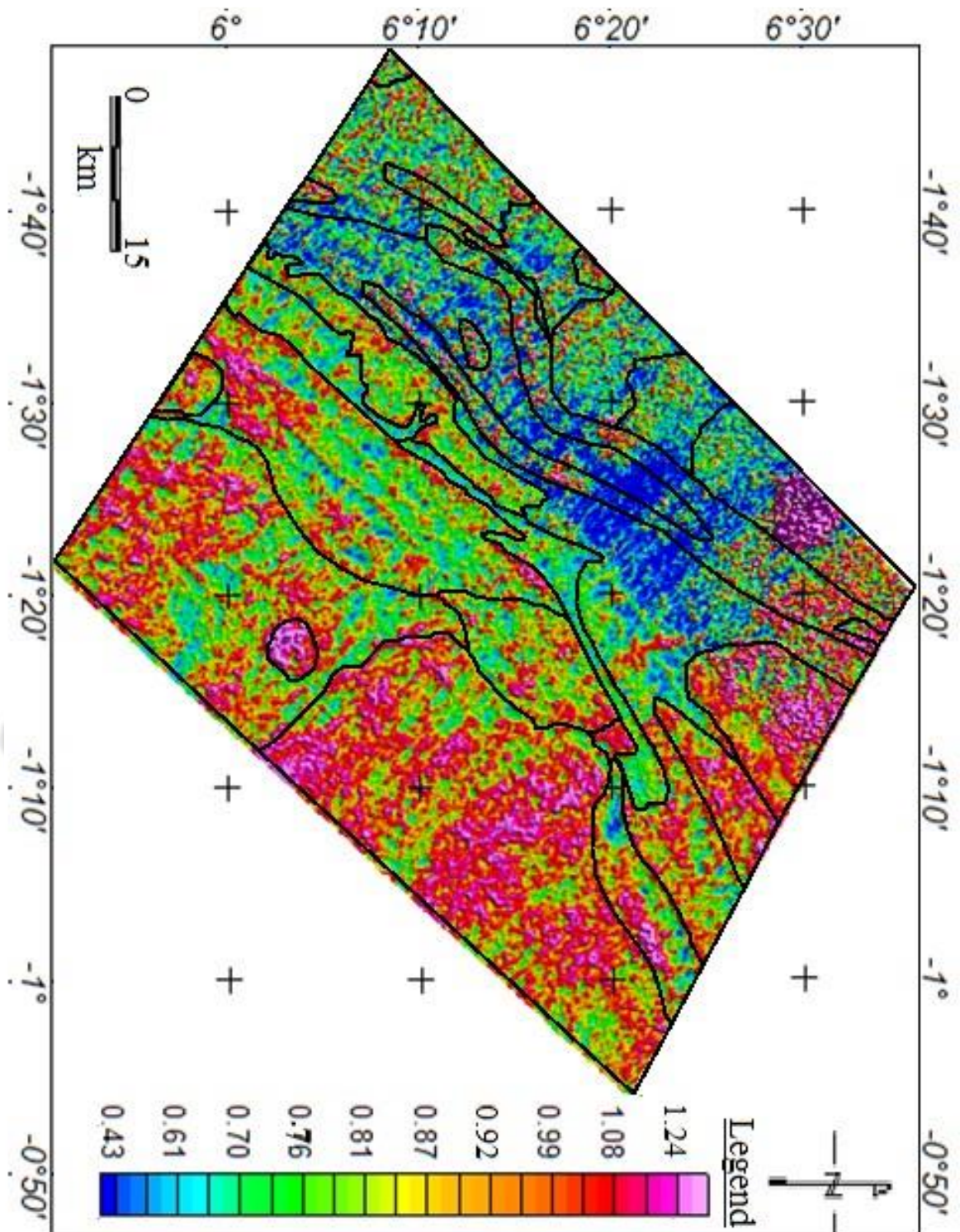


Figure 6.17: eU/eTh Ratio map of study area overlain with identified lithology  
 According to Clark (1997), the eU/eTh ratio equals about 0.33% in granitic rocks and most of the anomalous high ratios are related to two mica-granite.

## 6.4 LITHOLOGY FROM RADIOMETRICS

### 6.4.1 Ternary map

Thirteen gamma-ray spectrometric domains were classified based on the concentration of the radio-elements eU, K and eTh (fig 6.13, 6.14 and 6.15) and also the ternary image, since they allow visualization of the relative contribution of each radio-element. Unit 1 corresponding to the belt type granitoids showed magenta colour indicating high K and eU and low eTh. Unit 8 in the Birimian sediments gave similar signature. Unit 2 of the Birimian sediments was low in K and eTh but high in eU giving mostly blue colour. Unit 3 and 12 of the Birimian meta-sediments was low in K but high in eTh and eU giving mostly cyan colour. Also units 11 (basin type granitoid) and 6 (of the Tarkwaian) gave similar signatures. Unit 4 of the Birimian meta-volcanics was high in K but low in eTh and eU giving mostly red colour. Unit 9 of the Birimian meta-volcanics had a similar signature. Unit 5 was high in K, eTh and eU giving an anomalous bright section. Unit 6 gave low K, high eU and eTh. unit 7 showed high eTh and K but low eU giving a redish black colour. Unit 13 gave low K and eU, but high eTh indicated by the colour cyan to green. Unit 10 showed red to green colour indicating high K and eTh but low eU.

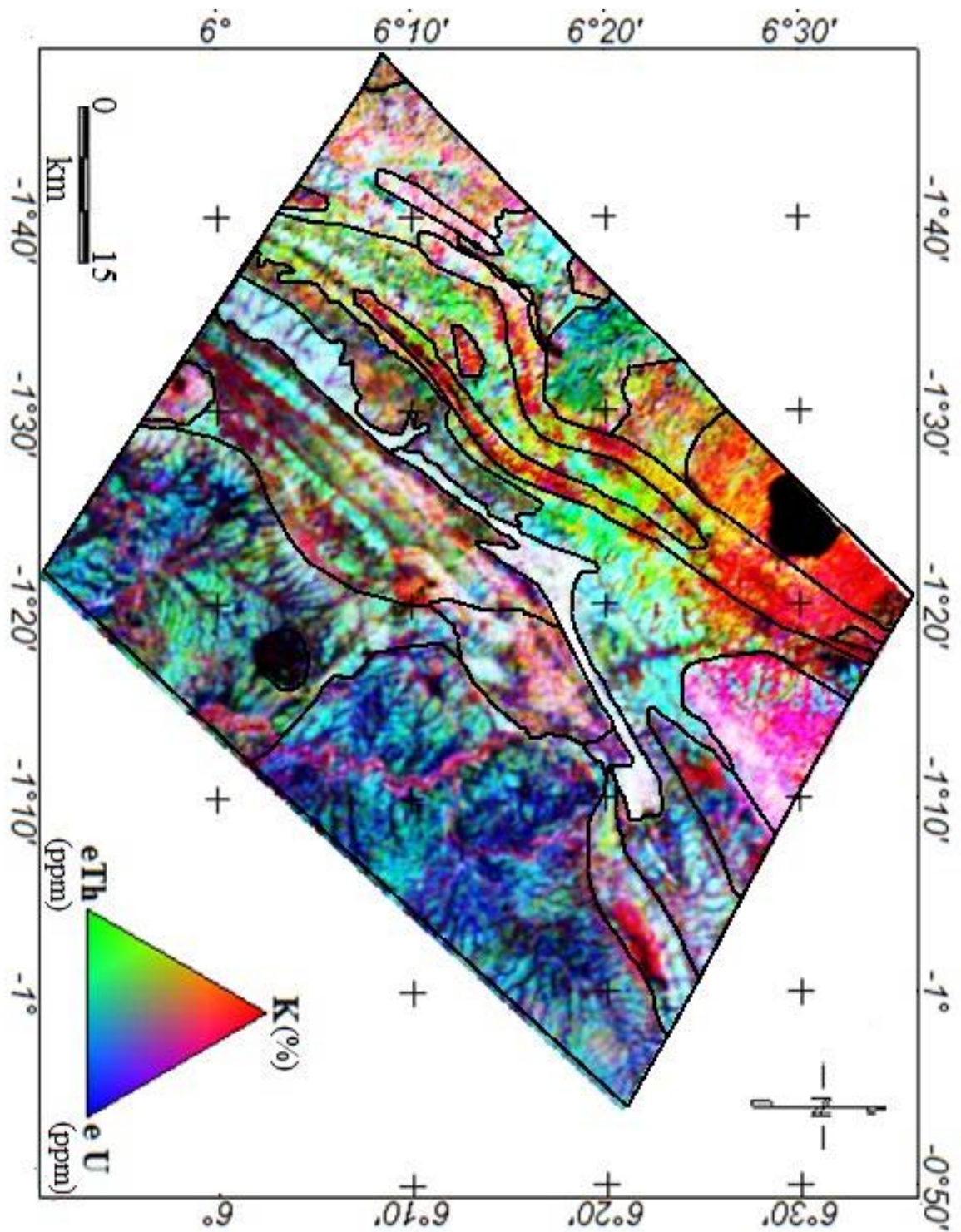


Figure 6.18: Ternary image map of study area overlain with identified lithologies

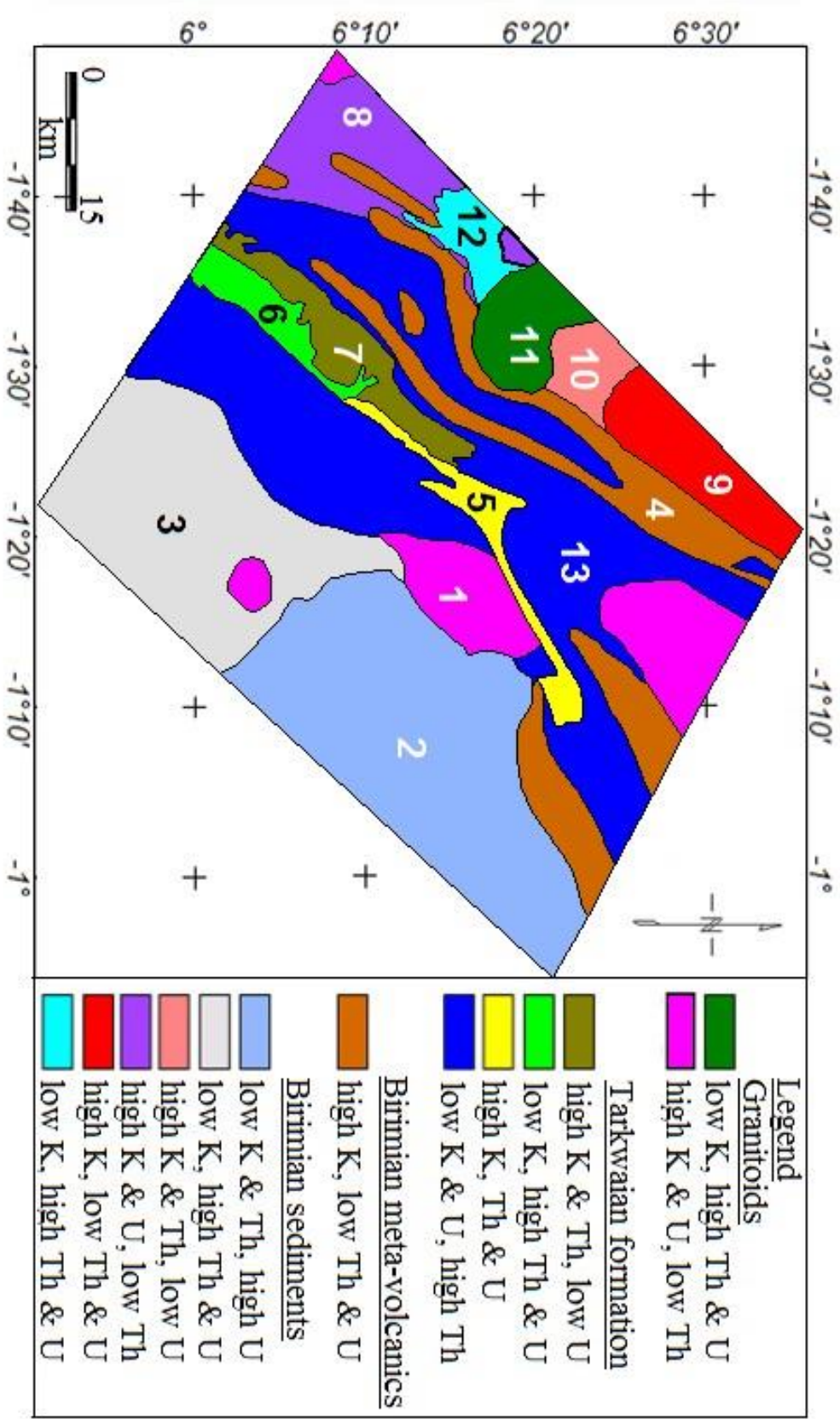


Figure 6.19: Interpreted lithology from radiometric data of the study area

## 6.5 Hydrothermal Alteration and Potential Metal Ore

### Mineralisation Zones

Alteration types were recognised according to the mineralisation zones and the different rock types in an area (Assie, 2008). Metal ore (gold) mineralisation in the area occurs principally by sulphide-sericite-quartz-carbonate (Silicic, phyllic alteration) alteration. In the ore zones, however, one notes in addition the presence of quartz veins, dolomite-ankerite-sericite, and sulphides (mainly pyrite and arsenopyrite). Propylitic alteration affects particularly the meta-basalt. The association of quartz veins and sulphides, however, is exclusively related to the hydrothermal alteration facies. In addition, in the study area, the hydrothermal alteration facies are commonly associated with highly-deformed zones (e.g. faults, shear zones). Nevertheless, it was generally difficult to distinguish the weak hydrothermal alteration from regional metamorphism. In summary, alteration in term of sulfidation, silicification, sericitization and carbonation occur particularly in the mineralisation zones. Comparison between aeromagnetic and radiometric data showed that addition of potassium correlates with a decrease in magnetite in alteration zones along faults zones whilst subtraction of potassium was associated to alterations along contacts. The addition of potassium is the most significant pointer of chemical alteration coupled with a decrease in the abundance of magnetite in mafic and ultramafic rocks. Post-metamorphic tectonic and hydrothermal processes tend to disturb or destroy the previously continuous patterns in magnetics. This resulted in offsets or terminations of magnetic signatures representing fault and fracture zones. Highly fractured regions are also affected by fluid injection and chemical alteration, which offsets the magnetic mineral. Partial destruction of magnetite grains resulted in a broken mineral

texture, such as shown in fig 6.21. Complete destruction of magnetite leads to loss of the magnetic anomalies or the formation of negative anomalies (e.g dykes in the study areas shown in fig 6.4). Based on the known information on alteration facies in the area, two alteration areas were defined: those along faults and those along contacts of main lithologies though there are other anomalous areas (bright sections (fig 6.19)). Of secondary importance are thrust faults which are potential structural traps for gold mineralisation (Thomas, 2010). So from the hydrothermal alterations, the areas with trust faults were delineated and as the potential metal (gold) ore mineralisation zones and overlain on the developed geological and structural map (fig 6.23).



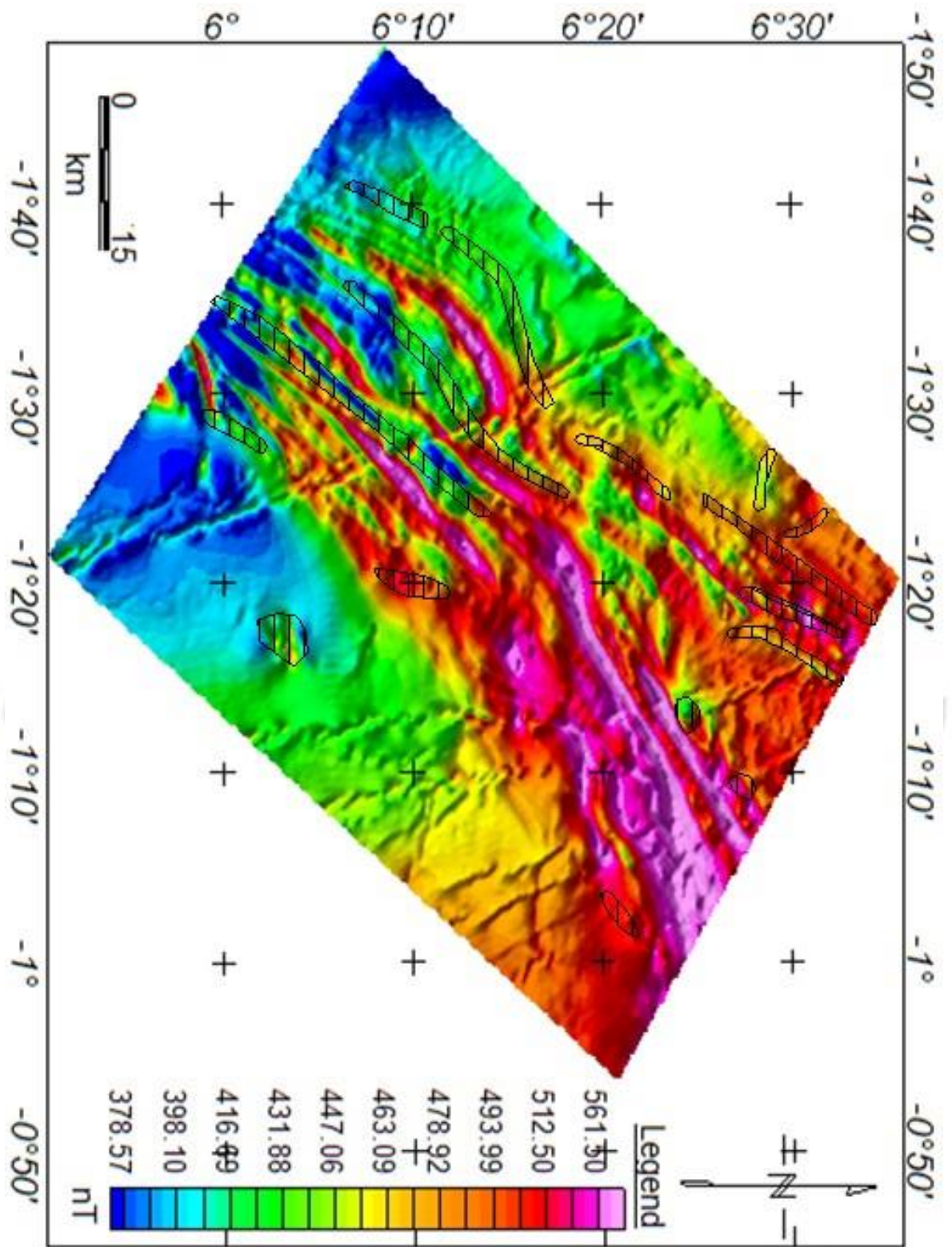


Figure 6.20: RTE of the study area overlain with hydrothermal alteration zones

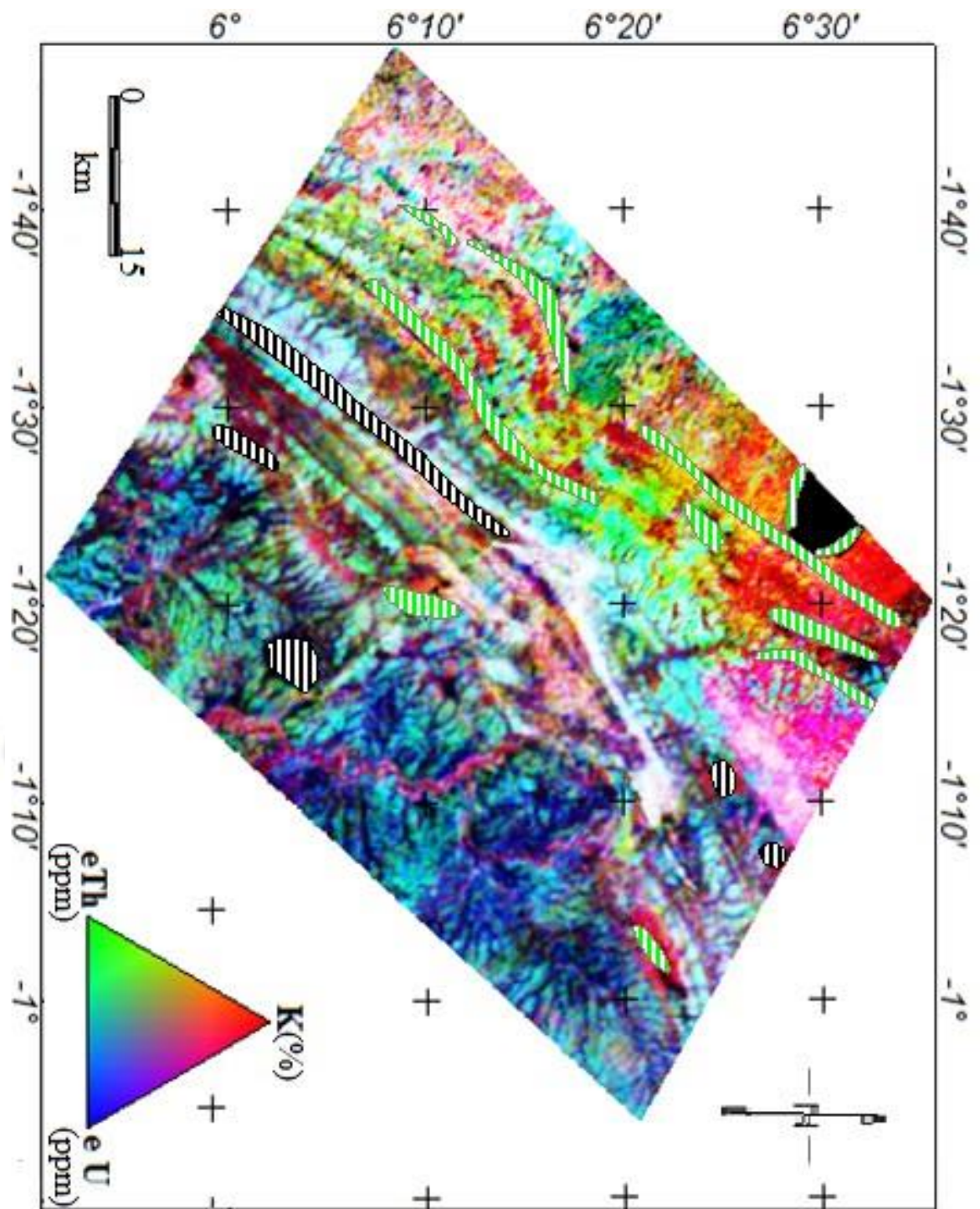


Figure 6.21: Ternary map of study area overlain with identified lithology and hydrothermal alteration zones

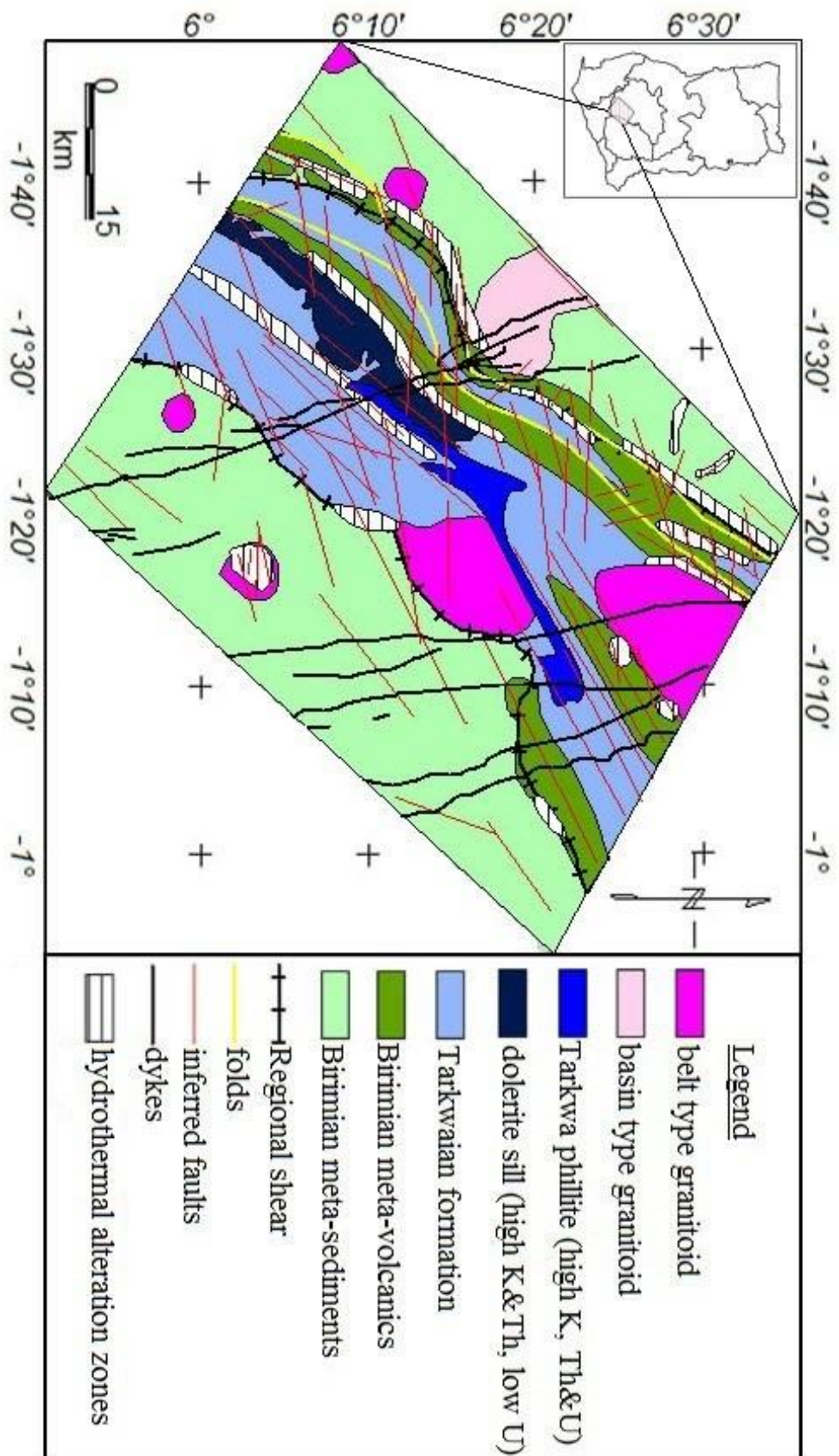


Figure 6.22: Proposed geological structural map of study area showing potential metal ore (gold) mineralisation zones

## CHAPTER 7

### 7.1 CONCLUSION AND RECOMMENDATION

#### 7.1.1 Conclusion

The work presented a new integrated geological and structural interpretation of the Beposo area through mapping the lithology, geological structures and hydrothermal alteration zones associated with possible gold mineralisation zones. Using observations from the magnetic and radiometric maps, five (5) new belt-type granitoids, one basin type granitoid and some Tarkwaian sediments were distinguished. Also utilising the magnetic maps, geological structures like folds, the Regional Ashanti shear, dykes and faults were delineated and also alteration zones found to be controlled by lithology and structure were also clearly identified.

#### 7.1.2 Recommendation

For a successful geological and structural interpretation of aerogeophysical data-sets (aeromagnetic and radiometric data), the following are recommended:

- Correlation with geological and geochemical facts should be coupled closely to the interpretation process-already at an early stage and background information on the influence of lithological variation and hydrothermally altered zones are necessary before estimating the reasons for the observed changes in radio-element ratios.

- The interpretation of the radiometric data was hindered by two main factors, though an effort was made to suppress the effects. These are topographic effects and vegetation cover. Therefore this study highly recommends that, similar studies in the area should consider the effects of vegetation.
- The tectonic setting of the Beposo area, was defined very well through the synergistic approach (that is subsurface and surface data) hence same combination is recommended for use in other areas of similar geological settings.
- Ground based geophysical surveys such as induce polarisation and resistivity should be carried out at the proposed delineated possible gold mineralisation zones.



## References

- Adadey, K., Clarke, B., Théveniaut, H., Urien, P., Delor, C., Roig, J., and Feybesse, J. (2009). Geological map explanation-map sheet 0503 b (1: 100 000), cgs/brgm/geoman.
- Airo, E. (2002). *Aeromagnetic and aero radiometric response to hydrothermal alteration*. Geological Survey of Finland.
- Allek, K. and Hamoudi, M. (2008). Regional-scale aeromagnetic survey of the South-West of Algeria: A tool for area selection for diamond exploration. *Journal of African Earth Sciences*, 50(2):67–78.
- Allen, D. (2011). Fahiakoba gold project Ghana, West Africa. Technical report.
- Allibone, A., McCuaig, T., Harris, D., Etheridge, M., Munroe, S., Byrne, D., Amanor, J., and Gyapong, W. (2002). Structural controls on gold mineralization at the Ashanti deposit, Obuasi, Ghana. *Special Publication-Society of Economic Geologist*, 9:65–94.
- Armstrong, M. and Rodeghiero, A. (2006). Airborne Geophysical techniques. 113–131.
- Assie, K. (2008). Lode gold mineralisation in the Paleoproterozoic (Birimian) volcano-sedimentary sequence of Afema gold district. Master's thesis, Technical University of Clausthal: Côte d'voire.
- Bahiru, E., Woldai, T., and De Smeth, D. (2011). Inter-relationship between lithology and structure and its control on gold mineralization in Buhweju area, SW of Uganda. Master's thesis, University of Twente.
- Bea, F. (1999). *Uranium*. *Encyclopedia of Geochemistry*, Marshall, CP and Fairbridge, RW (editors), Kluwer Academic Publishers, London.
- Bea, F., Pereira, M., Corretge, L., and Fershtater, G. (1994). Differentiation of strongly peraluminous, perphosphorous granites. the pedobernardo pluton. *Encyclopedia of Geochemistry*, 58:2609–2628.
- Blakely, R. J. (1995). *Potential theory in gravity and magnetic applications*. Cambridge University Press.
- Boadi, B., Wemegah, D., and Preko, K. (2013). Geological and structural interpretation of the Konongo area of the Ashanti gold belt of Ghana from aeromagnetic and radiometric data. *International Research Journal of Geology and Mining*, 3(3)((2276-6618)):124–135.
- Bodruddoza, M. and Fujimitsu, Y. (2012). Mapping hydrothermal altered mineral deposits using landsat 7 etm to image in and around Kuju volcano. *Indian Academy of Sciences*, 4:1049–1057

- Boher, M., Abouchami, W., Michard, A., Albarede, F., and Arndt, N. T. (1992). Crustal growth in west africa at 2.1 ga. *Journal of Geophysical Research: Solid Earth* (1978–2012), 97(B1):345–369
- Bonhomme, M. (1962). Contribution à l'étude géochronologique de la plate-forme de l'Ouest Africain. *Clermont-Ferrand Géol. Minéral*, 5:62
- Bowell, R., Foster, R., and Stanley, C. (1990). Telluride mineralization at ashanti gold mine, ghana. *Mineralogical Magazine*, 54:617–627
- Boyle, R. (1979). *The geochemistry of gold and its deposits (together with a chapter on geochemical prospecting for the element)*. Geological Survey of Canada
- Campbell, W. C. (1997). *Introduction to geomagnetic fields*. Cambridge University Press
- Chernicoff, C., Richards, J., and Zappettini, E. O. (2002). Crustal lineament control on magmatism and mineralisation in northwestern argentina: geological, geophysical, and remote sensing evidence", author = "chernicoff, c.j, richards, j.p, and zappettini, e. o. *Ore Geology Reviews*, 21(3-4):127–155
- Chopin, G. (1988). Humics and radionuclide migration. *Radiochima Acta*, 44/45:23–28
- Clark, D. A. (1997). Magnetic properties of rocks and minerals. *AGSO Journal of Australian Geology and Geophysics*, 17(2):83–103
- Cooper, G. and Cowan, D. (2006). Enhancing potential field data using filters based on the local phase. *Computers & Geosciences*, 32(10):1585–1591
- Cox, A. (1973). *Plate tectonics and geomagnetic reversal*. W. H. Freeman and Company
- Davis, D., Hirdes, W., Schaltegger, U., and Nunoo, E. (1994). U<sub>b</sub> Pb age constraints on deposition and provenance of birimian and gold-bearing tarkwaian sediments in ghana, west africa. *Precambrian Research*, 67(1):89–107
- Dickson, B. and Scott, K. (1997). Interpretation of aerial gamma-ray surveys-adding the geochemical factors. *AGSO Journal of Australian Geology and Geophysics*, 17:187–200
- Doell, R. R. and Cox, A. (1967). Analysis of alternating field demagnetization equipment. *Method in Palaeomagnetism*, 241–253
- Duodu, A., Loh, G., Boamah, K., Baba, m., Hirdes, W., Toloczyki, M., and Davis, D. (2009). Geological map of ghana 1:1000000
- Eisenlohr, B. and Hirdes, W. (1992). The structural development of the early Proterozoic Birimian and Tarkwaian rocks of South West Ghana, West African Earth science, 14(3):313–325
- Feybesse, J.-L., Billa, M., Guerrot, C., Duguey, E., Lescuyer, J.-L., Milesi, J.-P., and Bouchot, V. (2006). The paleoproterozoic ghanaian province: Geodynamic model and ore controls, including regional stress modeling. *Precambrian Research*, 149(3):149–196
- GETECH (2010). Advanced processing and interpretation of gravity and magnetic data.

- Ghazala, H. (1993). Geological and structural interpretation of airborne surveys and its significance for mineralisation, South Eastern Desert, Egypt. *Journal of African Earth Sciences (and the Middle East)*, 16(3):273–285
- Graham, K., Wemegah, D., and Preko, K. (2013). Geological and structural interpretation of part of the buem formation, ghana, using aerogeophysical data. Master's thesis, Department of Physics, Kwame Nkrumah University of Science and Technology
- Griffis, R., Barning, K., Agezo, F., and Akosah, F. (2002). Gold deposits of Ghana
- Gunn, P. (1997). Gunn, p.j, maidment, d, and milligan, p.r. *AGSO Journal of Geology and Geophysics*, 17:105–113
- Gunn, P. and Dentith, M. (1997). Interpreting aeromagnetic data in areas of limited outcrop. *AGSO Journal of Geology and Geophysics*, 17(2):175–185
- Harris, J., Bowie, C., Rencz, A., and Graham, D. (1994). Computer-enhancement techniques for the integration of remotely sensed, geophysical, and thematic data for the geosciences. *Canadian Journal of Remote Sensing*, 20(3):210–221
- Hirdes, W. and Nunoo, B. (1994). The proterozoic paleoplacers at tarkwa gold mine, SW Ghana; sedimentology, mineralogy, and precise age dating of the main reef and West reef, and bearing of the investigations on source area aspects. *Geologisches Jahrbuch D*, 100:247–311
- Hünken, U., Klemd, R., and Olesch, M. (1994). *Fluid inclusions in quartz pebbles of Proterozoic Tarkwaian conglomerates in Ghana*, volume 100.
- IAEA (2003). *Guidelines for radioelement mapping using gamma ray spectrometry data* (IAEA-TECDOC-1363)
- Jaques, A., Wellman, P., Whitaker, A., and Wyborn, D. (1997). High-resolution geophysics in modern geological mapping. *AGSO Journal of Australian Geology and Geophysics*, 17:159–174
- Jayawardhana, M. P. and Sheard, N. (2000). The use of airborne gamma-ray spectrometry-a case study from the mount isa inlier. *Australia Geophysics*, 65:1993–2000
- Johnson, S. S., Gathright, M. T., and Henika, S. W. (1979). Gamma-ray spectrometry and geologic mapping. remote sensing of environment. (25):17–24
- Junner, N. (1935). Gold in the gold coast. Gold coast geological survey. *Memoir*, (4):76
- Kesse, G. (1985). The mineral and rock resources of Ghana
- Kiessling, R. (1997). Sedimentation and structure in the tarkwaian group of the bui basin in west-ghana. *Geologisches Jahrbuch Reihe B*, 113–182
- Klemd, R., Hirdes, W., Olesch, M., and Oberthür, T. (1992). Fluid inclusions reequilibration and p-t-x constraints on fluid evolution in the ashanti gold deposit, ghana. *European Journal of Mineralogy*, 4:1017–1033
- Klemd, R., Hirdes, W., Olesch, M., and Oberthür, T. (1993). Fluid inclusions in quartz-pebbles of the gold-bearing tarkwaian conglomerates of ghana as guides to their provenance area. *Mineralium Deposita*, 28(5):334–343
- Krishnaswami, S. (1999). Thorium. *Encyclopedia of Geochemistry*. Marshall, CP and Fairbridge, RW (editors), Kluwer Academic Publishers, London

- Langmuir, D. and Herman, J. S. (1980). The mobility of thorium in natural waters at low temperatures. *Geochimica et Cosmochimica Acta*, 44(11):1753–1766
- Ledru, P., Johan, V., Milési, J. P., and Tegye, M. (1994). Markers of the last stages of the Palaeoproterozoic collision: evidence for a 2 Ga continent involving circum-south atlantic provinces. *Precambrian Research*, 69(1):169–191
- Luyendyk, A. (1997). Processing of airborne magnetic data. *AGSO Journal of Australian Geology and Geophysics*, 17:31–38
- Mackey, T., Lawrie, K., Wilkes, P., Munday, T., de Souza Kovacs, N., Chan, R., Gibson, D., Chartres, C., and Evans, R. (2000). Paleochannels near west wyalong, new south wales: A case study in delineation and modelling using aeromagnetics. *Exploration Geophysics*, 31:1–7
- MacLeod, I. N., Jones, K., and Dai, T. F. (1993). 3-d analytic signal in the interpretation of total magnetic field data at low magnetic latitudes. *Exploration Geophysics*, 24:679–687
- Merrill, R. (2000). The magnetic field of the earth: paleomagnetism, the core and the deep mantle
- Milési, J., Ledru, P., Ankrah, P., Johan, V., Marcoux, E., and Vinchon, C. (1991). The metallogenic relationship between birimian and tarkwaian gold deposits in ghana. *Mineralium Deposita*, 26(3):228–238
- Milési, J.-P., Ledru, P., Feybesse, J.-L., Dommange, A., and Marcoux, E. (1992). Early proterozoic ore deposits and tectonics of the birimian orogenic belt, west africa. *Precambrian Research*, 58(1):305–344
- Milsom, J. (2003). *Field Geophysics: The Geological Field Guide Series*. John Wiley and Sons Ltd
- Mittlefehldt, D. (1999). Potassium. *Encyclopedia of Geochemistry*.
- Mumin, A. H. and Fleet, M. (1995). Evolution of gold mineralization in the Ashanti Gold belt, Ghana: evidence from carbonate compositions and parageneses. *Mineralogy and Petrology*, 55(4):265–280
- Mumin, A., Fleet, M., and Longstaffe, F. (1996). Evolution of hydrothermal fluids in the Ashanti Gold belt, Ghana; stable isotope geochemistry of carbonates, graphite, and quartz. *Economic Geology*, 91(1):135–148
- Naude, C. (2012). Target selection from airborne magnetic and radiometric data in Steinhausen area. Master's thesis, Namibia: Rhodes University
- Oberthür, T., Vetter, U., Davis, D. W., and Amanor, J. A. (1998). Age constraints on gold mineralisation and paleoproterozoic crustal evolution in the ashanti belt of southern ghana. *Precambrian Research*, 89(3):129–143
- Oberthür, T., Vetter, U., Schmidt Mumm, A., Weiser, T., Amanor, J., Gyapong, W., Kumi, R., and Blenkinsop, T. (1994). The ashanti gold mine at obuasi, ghana: mineralogical, geochemical, stable isotope and fluid inclusion studies on the metallogenesis of the deposit. *Geologisches Jahrbuch*, 100:31–129
- Ostrovskiy, E. A. Antagonism of radioactive elements in wellrock alteration fields and its use in aerogamma spectrometric prospecting. *International Geological Review*, 17:8–461

- Perrotta, M., Almeida, R. I. T., Andrade, F. B. J., Souza Filho, R. C., Rizzotto, J., and Santos, M. G. M. (2008). Remote sensing geobotany and airborne gamma-ray data applied to geological mapping within terra firme Brazilian Amazon forest: A comparative study in the Guapore valley. *Remote Sensing and Spatial Information Sciences*
- Perrouy, S., Aillères, L., Jessell, M. W., Baratoux, L., Bourassa, Y., and Crawford, B. (2012). Revised Eburnean geodynamic evolution of the gold-rich southern Ashanti belt, Ghana, with new field and geophysical evidence of pre-Tarkwaian deformations. *Precambrian Research*, 204:12–39
- Pigois, J., Groves, D., Fletcher, I., McNaughton, N., and Snee, L. (2003). Age constraints on Tarkwaian palaeoplacer and lode-gold formation in the Tarkwa-Damang district, SW Ghana. *Mineralium Deposita*, 38:695–714
- Porwal, A., Carranza, E. J. M., and Hale, M. (2006). Tectonostratigraphy and basement mineralisation controls, Aravalli province (western India): New interpretations from geophysical data analysis. *Ore Geology Reviews*, 29(3):287–306
- Quadros, P. F. T., Koppe, C. J., Strieder, J. A., and Coats, L. C. F. (2003). Gamma-ray data processing and integration for lode-Au deposits. *Exploration Natural Resources Research*, 12:57–5
- Rajagopalan, S. and Milligan, P. (1994). Image enhancement of aeromagnetic data using automatic gain control. *Exploration Geophysics*, 25(4):173–178
- Reeves, C. (2005). *Aeromagnetic Surveys: Principles, Practice and Interpretation*. Netherlands. GEOSOFT
- Schetselaar, E. M. and Ryan, J. J. (2009). Remote predictive mapping of the Boothia mainland area, Nunavut, Canada: an iterative approach using Landsat ETM, aeromagnetic, and geological field data. *Canadian Journal of Remote Sensing*, 35(sup1):S72–S94
- Schmidt Mumm, A., Oberthür, T., Vetter, U., and Blenkinsop, T. (1997). High CO<sub>2</sub> content of fluid inclusions in gold mineralisations in the Ashanti belt, Ghana: a new category of ore-forming fluids? *Mineralium Deposita*, 32:107–118
- Sestini, G. (1973). Sedimentology of a paleoplacer: the gold-bearing Tarkwaian of Ghana. Ores in sediments. *International Union of Geological Sciences*, A 3:275–305
- Shives, R. B., Charbonneau, B., and Ford, K. L. (2000). The detection of potassic alteration by gamma-ray spectrometry-recognition of alteration related to mineralization. *Geophysics*, 65(6):2001–2011
- Silva, A. M., Pires, A. C. B., McCafferty, A., Moraes, R. A. V., and Xia, H. (2003). Application of airborne geophysical data to mineral exploration in the uneven exposed terrains of the Rio das Velhas greenstone belt. *Revista Brasileira de Geociências*, 33(2):17–28
- Strogen, P. (1991). The structural development of the early Proterozoic Birimian and Tarkwaian rocks of south-west Ghana, West African Earth Science. (3):3–39

- Taylor, P. N., Moorbath, S., Leube, A., and Hirdes, W. (1992). Early proterozoic crustal evolution in the birimian of ghana: constraints from geochronology and isotope geochemistry. *Precambrian Research*, 56(1):97–111
- Telford, W., Geldart, L., Sheriff, R., and Keys, D. (1990). *Applied Geophysics*. University Press Cambridge
- Telford, W., Geldart, L., Sheriff, R., and Keys, D. (1994). *Applied Geophysics*. University Press Cambridge
- Thomas, S. (2010). Case study of four vtem surveys for gold exploration in ghana. kegs gold workshop
- Tunks, A. J., Selley, D., Rogers, J. R., and Brabham, G. (2004). Vein mineralization at the damang gold mine, ghana: controls on mineralization. *Journal of structural geology*, 26(6):1257–1273
- Urquhart, D. (2003). *Geophysical Airborne Survey: Airborne Gamma-Ray Spectrometry Surveys*. Santiago Chile: GeoExplo Ltda
- Verduzco, B., Fairhead, J. D., Green, C. M., and MacKenzie, C. (2004). New insights into magnetic derivatives for structural mapping. *The Leading Edge*, 23(2):116–119
- Whitelaw, O. (1929). The geological and mining features of the tarkwa-abosso goldfield. *Memoir*, (1):46
- Wilford, J. (2002). Airborne gamma-ray spectrometry. *Cooperative Research Centre for Landscape Environments and Mineral Exploration, Commonwealth Scientific and Industrial Research Organization*, 144:46–52
- Yao, Y. and Robb, L. (2000). Gold mineralization in palaeoproterozoic granitoids at obuasi ashanti region, ghana: ore geology, geochemistry and fluid characteristics. *South African Journal of Geology*, 103:255–278
- Yao, Y., Murphy, P., and Robb, L. (2001). Fluid characteristics of granitoid-hosted gold deposits in the birimian terrane of ghana: a fluid inclusion microthermometric and raman spectroscopic study. *Economic Geology*, 96:1611–1643

## Appendix A

### A.1 Used Softwares

- L<sup>A</sup>T<sub>E</sub>X : typesetting and layout
- MapInfo 11.5
- Oasis Montaj (Geosoft): data processing and enhancement

